DOE FINAL REPORT
(Period February 1, 2010 – June 30, 2016)

WORK PERFORMED UNDER AGREEMENT

DE-OE0000244
Design, Test and Demonstration of Fault Current Limiting HTS Transformer

RECIPIENT

SuperPower Inc.
450 Duane Avenue
Schenectady, NY 12304-2631

PRINCIPAL INVESTIGATOR

Drew Hazelton
(518) 346-1414
dhazelton@superpower-inc.com

SUBRECIPIENTS

SPX Transformer Solutions, Inc
University of Houston

SUBMITTED TO:

U.S. Department of Energy
National Energy Technology Laboratory

David Szucs
david.szucs@netl.doe.gov

June 6, 2017

FCL Transformer Program
DE-OE0000244

Final Report
Table of Contents

Executive Summary

The Fault Current Limiting High Temperature Superconducting (HTS) Transformer project was initially awarded and undertaken in 2010 to design, build and test a 28 MVA next generation superconducting power transformer that had integrat3d fault current limiting (FCL) capability. The partners in the program were prime contractor SPX Transformer Solutions Inc. (formerly Waukesha Electric Systems), SuperPower Inc., Southern California Edison, The University of Houston and Oak Ridge National Lab. The project required the partners to develop new technology related to the HTS manufacturing and to tailor existing transformer design and cryogenic refrigeration technologies for this application. The project can be divided into ;three phases. Phase 1 is as described above, with SPX as the prime contractor. In late 2011, SPX did not wish to continue as the prime contractor and initially withdrew from the program. After a short hiatus and discussions between the partners and DOE, the program restarted (Phase 2) in 2012 with all of the above partners, except that now SuperPower assumed the role as the prime contractor.

Much of the technology was being perfected and the power transformer design nearly completed and prototypes started when in April 2014, the project's transformer manufacturer, SPX Transformer Solutions, Inc. decided to leave the program. SCE soon followed, as it was apparent that no transformer was to be built or tested in the SCE substation. ORNL also withdrew as they were a subcontractor to SPX. At that point, the project focus was re-scoped (Phase 3) to allow SuperPower to continue as Prime Contractor and fulfill the amended objectives of developing and proving the necessary technology to build an FCL superconducting transformer in the future.

The project developed new technology that enables the creation of a high temperature superconductor based FCL power transformer. SuperPower's research and development created new methods to bond HTS conductor to a supporting substrate, test and insulate the resulting bonded conductor, reduce winding ac losses, ensure FCL functionality during a transformer fault and build firm superconducting joints in the transformer harnesses and cabling. The bonded conductor in this program was shown to meet the critical operating parameters of providing the superconducting transformer operation while being able to meet the target normal state resistance required for FCL operation. The bonded conductor was also shown to be able to handle the fabrication stresses associated with the manufacture of the FCL transformer while also being able handle the high hoop stresses and axial forces during a fault transient. Much of the technology developed here is applicable to the broader applied superconductivity community. The ability to tailor the clad conductors performance characteristics gives the designer of devices utilizing HTS a broader capability to address the particular needs of an given application.

Combining these technologies into an operating power transformer would achieve the programs primary objective of demonstrating a smart grid transmission device that greatly reduces energy losses in the system, reduces greenhouse gases, improves power quality in the grid and eliminates the harmful effect of oil leakage and the risk of transformer fires.

1.0 **Introduction**

1.1 Project History

The original project proposal stated that the overall project objective was to design, develop, manufacture and install on a live grid utility host site a Smart Grid compatible Fault Current Limiting Superconducting Transformer. The Fault Current Limiting High Temperature Superconducting (HTS) Transformer project was initially awarded and undertaken in 2010 to design, build and test a 28 MVA next generation superconducting power transformer that had integrat3d fault current limiting (FCL) capability. The partners in the program were prime contractor SPX Transformer Solutions Inc. (formerly Waukesha Electric Systems), SuperPower Inc., Southern California Edison, The University of Houston and Oak Ridge National Lab. The project required the partners to develop new technology related to the HTS manufacturing and to tailor existing transformer design and cryogenic refrigeration technologies for this application. The project can be divided into three phases. Phase 1 is as described above, with SPX as the prime contractor. In late 2011, SPX did not wish to continue as the prime contractor and initially withdrew from the program. After a short hiatus and discussions between the partners and DOE, the program restarted (Phase 2) in 2012 with all of the above partners, except that SuperPower assumed the role as the prime contractor.

The originally proposed 28 MVA 3-phase FCL Transformer (69 kV/12.47 kV class) was to be placed within SCE' "2020 World – Integrated Systems of the Future" Smart Grid site located in Irvine, California. The project extended earlier work by a Waukesha Electric Systems (predecessor to SPX), SuperPower and Oak Ridge National Lab team work on the development of a 5 MVA. 25 kV/4.2 KV HTS power transformer carried out in an earlier Superconductivity Partnership with Industry (SPI) project [1,2]. As a significant and novel development, the device designed and technology demonstrated in this project had the added feature of integrated fault current limiting capability built into the windings of the transformer. HTS based fault current limiting technology is an area that SuperPower extensively studied under other projects [3]. The novel approach of incorporating fault current limiting capability in the superconducting power transformer provides significant advantages to the utility customer and helps meet many Smart Grid objectives without adding significant complexity aor cost to the device. By incorporating fault current limiting capability, the device is better able to handle fault transients and currents that may arise from the Smart Grid goal of accommodating new generation and energy storage options.

---

[1] SW Schwenterly, SP Mehta, MS Walker, RH Jones, "Development of HTS Power Transformers for the 21st Century: Waukesha Electric Systems/IGC SuperPower/RG&E/ ORNL SPI Collaboration", Physica C 32, pp 1-6 (2002).

[2] CS Weber, CT Reis et al, "Design and Operational Testing of a 5/10 MVA HTS Utility Power Transformer", IEEE Trans. Appl. Superconductivity 15, pp. 2210-2213 (2005).

[3] C Weber, D Hazelton, S Isojima, I Sauers, "Transmission Level HTS Fault Current Limiter", presentation, DOE 2007 Peer Review (2007).

Much of the technology was being perfected and the power transformer design nearly completed and prototypes started when in April 2014, the project's transformer manufacturer, SPX Transformer Solutions, Inc. decided to leave the program. SCE soon followed, as it was apparent that no transformer was to be built or tested in the SCE substation. ORNL also withdrew as they were a subcontractor to SPX. At that point, the project focus was re-scoped (Phase 3) to allow SuperPower to continue as Prime Contractor and fulfill amended objectives of developing and proving the necessary technology to build an FCL superconducting transformer in the future.

1.2 Project Partners

Over the course of the project, the various project partners provided the technical and program oversight as noted below in the following tables. The changes over the project are also noted in the tables.

Table 1.2.1: Initial (2010 – 2012 : Phase 1) Division of responsibilities between project partners. Note that ORNL was a subcontractor to SPX while UH was a subcontractor to SuperPower.

DOE – Program Oversight			
SPX Transformer Solutions (SPX)– Program Management			
SPX Transformer Solutions (SPX)	**ORNL experts)**	**SuperPower (SP) / University of Houston (UH)**	**Southern California Edison (SCE)**
Transformer Design and Fabrication Dielectrics Conductor Specs Testing Commercial Product Development	Cryogenics Conductor Specs Thermal Analysis of Design	Conductor Design and Production Fault Current Limiting Expertise Cryogenics Low ac loss conductor development (UH)	General Specifications Site preparation and field work Installation and Commissioning Host demo

With the initiation of Phase 2 (2012-2014) there was little change in project responsibilities between the partners other than change in project management and a change in ORNL's contribution due to retirement of key personnel that then became a consultant to SPX.

Table 1.2.2: Phase 2 (2012 – 2014) Division of responsibilities between project partners. Note that ORNL was changed to a former (retired) ORNL employee as a consultant to SPX while UH remained a subcontractor to SuperPower.

DOE – Program Oversight			
SuperPower Inc – Program Management			
SPX Transformer Solutions (SPX)	**Consultant (Former ORNL expert)**	**SuperPower (SP) / University of Houston (UH)**	**Southern California Edison (SCE)**
Transformer Design and Fabrication Dielectrics Conductor Specs Testing Commercial Product Development	Cryogenics Conductor Specs Thermal Analysis of Design	Conductor Design and Production Fault Current Limiting Expertise Cryogenics Low ac loss conductor development (UH)	General Specifications Site preparation and field work Installation and Commissioning Host demo

With the withdrawal of SPX from the program and subsequent withdrawal of SCE and former ORNL consultant, the Phase 3 participants are shown in the table below.

Table 1.2.3 Phase 3 (2014 – 2016) Division of responsibilities between project partners. Note that SCE and ORNL consultant withdrew when SPX withdrew from program.

DOE – Program Oversight
SuperPower Inc – Program Management
SuperPower (SP) / University of Houston (UH)
Conductor Design and Production Fault Current Limiting Demonstration / Expertise Cryogenics FCL Transformer Coil Module Prototyping and Testing Low ac loss conductor development (UH and SP)

1.3 Budgets

The total project budgets for the various participants during the different project periods are summarized in the table below. Both SPX and SuperPower provided 50% cost-share of the project funding. SCE participated in the project without receiving any DOE Smart Grid funding, opting instead to cover its costs internally and with other funding sources.

Table 1.3.1: Total project funding remaining for the various participants at the beginning of each of the Project Phases.

Project Phase	SPX Transformer Solutions / ORNL	SuperPower / UH[(1)]	Total Remaining Project Funding	Southern California Edison
1 (2010-6/2012)	$ 10.4 M	$ 11.0 M	$ 21.4 M	(3)
2 (6/2012-8/2014)	$ 9.0 M [(2)]	$ 10.1 M	$ 19.1 M	(3)
3. (9/2014-6/2016)	(withdrawn from proj)	$ 3.6 M	$ 3.6 M	(withdrawn from project)

(1) UH total funding during project ~ $0.6M

(2) ORNL withdrawal between Phase 1 and Phase 2 removed ~ $1.1M from budget

(3) SCE did not use any DOE funding for its part of the project.

2.0 Technical Discussion

2.1 Goals

The overall goal of the project during Phases 1 and 2 was to develop the technology required to build, test and install in a utility host site a fault current limiting high temperature superconducting (HTS) transformer. The target operating parameters of the transformer were 28 MVA (69 kV/12.47 kV) with the superconducting windings operating in a subcooled liquid nitrogen environment. The HTS windings would have an integrated fault current limiting (FCL) capability. These goals required the development of a specially designed HTS conductor in order to meet the parallel requirements of target normal state resistance required for FCL operation while being sufficiently mechanically robust to handle manufacturing stress and fault transient forces. The transformer design would have to be modified to handle the cryogenic environment. Standard transformer winding practices would be followed as closely as possible to minimize the impact on the manufacturing floor. Conventional insulation approaches would be applied using advanced insulation developed by SPX for standard transformers that had previously been shown to work well in a cryogenic environment[4]. Other systematic goals as noted below were targeted but could not be achieved with the withdrawal of SPX from the project. These additional project objectives included

- Quantify the benefits of superconducting transformers on lowering electricity cost and T&D costs through increased efficiency – conventional transformers losses are ~40% of total grid loss [4]

- Quantify the potential total ownership cost savings to the utility industry through longer life transformers, less frequent replacement of circuit breakers and downstream equipment (due to FCL functionality) and ability to reconfigure substation layout to take advantage of enhanced overcurrent capability and a smaller physical device size. This enables the utility to accommodate more substation power demand without adding costly (if even available) real estate.

- Demonstrate the practicality and benefits of the latest monitoring and control functions necessary for Smart Grid operations by integratingstate-of-the-art real time communication using the protocols and standards being developed by NIST and IEEE.

- Providing energy consumers tangible information about the environmental benefits of using superconductor devices in the Smart Grid through the active demonstration program. These benefits include reduction in flammability / oil leakage, reduced device size/weight and the opportunity for enclosed operation, reduction in green house gasses and improved power quality particularly as additional renewable power sources are added to the grid. This communication would be achieved through a public outreach program in conjunction with SCE.

---

[4] SW Schwenterly, E Pleva, “HTS Transformer Development”, presentation, DOE 2009 Peer Review (2009).

With the withdrawal of SPX in 2014, the goal of building a full three phase transformer and installing it in the SCE substation was deemed as being unachievable without a transformer manufacturer on the team. The goal of the modified project [Phase 3] was to demonstrate the key technical requirements needed in order to build a FCL transformer in the future. Long length conductor fabrication of an appropriate design would need to be demonstrated. Also, subscale HV module windings wound using the proposed FCL transformer winding approaches were to be used to demonstrate FCL functionality as well as quantifying the impact of ac losses on the operation of the device.

2.2 Task List / Lead organization

The functional SOPO task lists for the various phases of the project are listed below in Table 2.2.1. The lead organization(s) for each of the SOPO tasks are also listed,

Table 2.2.1 Listing of SOPO tasks with corresponding WBS# and lead organization along with applicability for the three project phases. An "X" indicates activity during that Phase, "C" indicates that that task had been completed in prior phases.

WBS #	Task Description	Lead Org	Phase 1	Phase 2	Phase 3
1.1	Update PMP	SPX/SP	X	X	X
1.2	NEPA compliance	SPX/SP	X	C	C
1.3	Develop interoperability and cyber-security plan	SPX/SP	X	C	C
1.4	Develop metrics and benefits plan	SPX/SP	X	X	X
2.1	Conceptual design	All	X	X	X
2.2	Utility survey	SPX	X	C	C
2.3	Key technology demonstration	All	X	X	X
2.3.1	FCL superconducting transformer design development	All	X	X	X
2.3.1.1	Development of 2G HTS windings for transformer	SPX/SP	X	X	X
2.3.1.2	Dielectric development for HTS transformers operation in a cryogenic environment	SPX	X	X	X
2.3.1.3	Bushing development for HTS transformers in a cryogenic environment	SPX	X	X	NA

2.3.1.4	Integration of a warm steel core in tho the overall transformer design	SPX	X	X	NA
2.3.1.5	Verification of fault current limiting with subscale windings	SP/SPX	X	X	X
2.3.2	HTS conductor development	SP	X	X	X
2.3.2.1	Conductor design for low ac losses	SP/UH	X	X	X
2.3.2.2	Conductor development for FCL operation	SP	X	X	X
2.3.2.3	Reliable long length 2G HTS manufacturing improvements	SP	X	X	X
2.3.3	Cryogenics development	All	X	X	NA
2.3.4.	Systems integration	SPX	X	X	NA
2.4	Project baselining	SPX	X	X	NA
3.1	Alpha (single phase) unit final design	All	X	X	NA
3.2	Alpha device fabrication	SPX	X	X	NA
3.3	Alpha unit test	SPX	X	X	NA
4.1	Beta (three phase) final design	All	X	X	NA
4.2	Beta device fabrication	SPX	X	X	NA
4.3	Beta unit test	SPX	X	X	NA
4.4	Installation of Beta demonstration unit in host utility switchyard	SPX/SCE	X	X	NA
5.1	Long term demonstration on the host utility grid	SPX/SCE	X	X	NA

2.3 Accomplishments

The overall project goal to develop the technology required to build a fault current limiting high temperature superconducting (HTS) transformer was partially met during the program in Phases 1 and 2. The requisite designs were developed and key technology demonstrations conducted. The target operating parameters of the transformer of 28 MVA (69 kV/12.47 kV) with the superconducting windings operating in a subcooled liquid nitrogen environment were incorporated into the design. Conventional transformer designs were modified to handle the cryogenic environment. Modeling of the heating due to ac losses in the windings

was challenging but a functional cooling approach was adopted into the design. In Phase 1 and 2, a conductor design for the HTS windings to have an integrated fault current limiting (FCL) capability were designed and developed. Long length production equipment was developed and long conductor lengths demonstrated. The specially designed HTS conductor met the parallel requirements of target normal state resistance required for FCL operation while being sufficiently mechanically robust to handle manufacturing stress and fault transient forces. Conventional conductor insulation approaches were demonstrated on the HTS conductor utilizing conventional transformer conductor insulating equipment. Initial work with SCE looked at the siting requirements for the transformer and a host site identified. Unfortunately, the goal of building, testing and installing a full scale FCL transformer unit in a utility host site was not met when SPX pulled out of the project.

In Phase 3, critical technologies required for a future design and build of a FCL transformer were demonstrated. Standard transformer winding practices were successfully followed in the winding of a subscale hig voltage (HV) coil module to minimize the future impact on the manufacturing floor. The same module demonstrated FCL functionality when tested under load. The issue of ac losses was addressed with methods for ac loss reduction in the windings demonstrated. Details of the technical accomplishments are given in the following sections.

2.4 Project activities

Project activities described below will be broken into two sections. The first section will cover Phases 1 and 2 and will include a summary of the SPX / ORNL activities and a more detailed description of the SP activities. The detailed SPX activities are included in Appendix 1 – SPX's Final Report prepared after they withdrew from the project. Similarly, UH's activities on the development of multifilament (MF) HTS conductors to reduce ac losses is summarized in this report with the details found in Appendix 2 – UH Final Report. The project activities will follow the SOPO listing and WBS numbering as shown in Table 2.2.1.

Task 1.1 – Update Project Management Plan (PMP)

The recipients routinely updated the PMP as submitted as part of the original application process. The PMP was used as a management tool and continually evolved through review and reassessment and was updated subsequent to any major/significant project revisions.

Task 1.2 – National Environmental Policy Act (NEPA) Compliance

The NEPA compliance report was completed early in the program and submitted for review in May, 2010,

Task 1.3 – Interoperability and cyber-security plan

This plan was developed in Phase 1 of the project by SPX and was submitted to DOE in September of 2011.

Task 1.4 – Metrics and benefits plan

The Metrics and Benefits Plan was updated quarterly over the course of the project.

Task 2.1 - Conceptual design

The team developed a conceptual design (Figure 2.1.1) for the superconducting fault current limiting (FCL) transformer that addressed the operational requirements of the proposed host site for the demonstration portion of this project. The team viewed the conceptual design as an iterative "living" design, evolving as input is received from other tasks and using the input from the broader market survey and the technical risk reduction studies. Multiple team design and readiness reviews were conducted in Phases 1 and 2 of the project.

The conceptual design procedure focused on the electrical and mechanical specifications which the transformer had to meet. The transformer has to function properly at the line voltages it is connected to and meet a specified reactance in the circuit. The system must have sufficient cooling to limit temperatures within a specified range and to handle the ac losses in the system due to stray magnetic field. In addition to steady-state normal operation requirements, the transformer must be designed to withstand without electrical breakdown surges appearing on the transmission lines from lightening or other causes. The transformer needed to be designed to withstand possible high fault currents such as short circuits on the terminals or the attached transmission lines without mechanical breakdown. Several modes of mechanical breakdown were addressed in order that the windings suffer no permanent deformation. The conceptual design studies used SPX standard design optimization software modified to take into account the presence of the superconductor and associated cryogenics systems. It was decided early on that the iron in the transformer would be kept warm due to the high losses experienced in the iron during operation that would overwhelm any cryogenic system. Calculations were made on the leakage reactance that would be developed in the system under the various operating conditions. Force and stress calculations were made as well as looking at the impact of impulses on the system. Estimates of the ac losses were made, particularly in the ends of the HTS coils in the transformer. Required normal state impedances were calculated for the FCL function leading to a target normal state resistance for the HTS windings. The impact on the fault current of the superconducting to normal state transition of the superconductor during a fault transient was also modeled. The details of these calculations and modeling are included in Appendix 1.

Early on in the conceptual design, the architecture of the HTS windings needed to be addressed. Since standard HTS conductors are very thin they lack adequate mechanical

support to withstand the short circuit forces. Thus it was necessary to develop a sturdier conductor architecture. The strength requirement had to be balanced with the need to meet a target normal state resistance in order to meet the FCL functionality requirements of the system. A composite architecture consisting of a modified HTS tape bonded to a backing material was chosen. of 1 mm thickness. The superconductor film itself is about 0.1 mm thick.

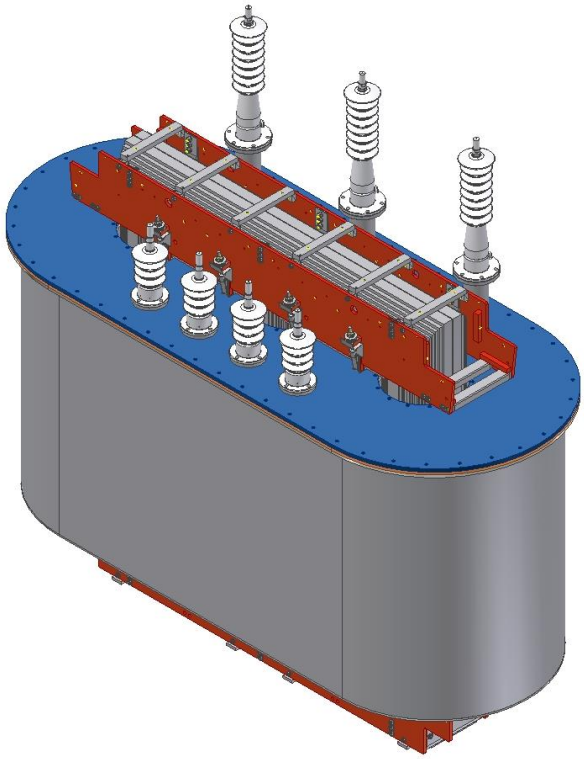

Figure 2.1.1 – Early conceptual design for the FCL transformer. HV bushings are on the right side, LV bushings on the left.

Task 2.2 – Utility survey

Early into the program, the team led by SPX and SCE conducted a survey of ~20 utilities on the needs and specification requirements they would like to see in a fault current limiting transformer. The majority of the respondents noted that high voltage (69 kV and above) transmission level FCL's would be of most interest to them and that they had sites within their system that could benefit from the availability of such a device. The responses received matched well with our initial design parameter space so did not result in any major impact on the evolving conceptual design.

Task 2.3 - Key Technology Demonstrations

The team conducted FCL transformer technology development by using second-generation high temperature superconducting (2G HTS) conductor optimized for a transformer application with fault current limiting capabilities.

Task 2.3.1 Fault current limiting superconducting transformer design development

The team conducted a series of demonstrations and risk reduction studies in certain key technical areas.

Task 2.3.1.1 – Development of 2G HTS windings for transformers

SuperPower completed the technology development of their proprietary conductor bonding process to enable superconducting transformer windings with fault current limiting capabilities. The final, insulated conductor configuration allowed the FCL transformer windings to use, as closely as possible, conventional winding techniques. The resultant bonded conductor is 14 mm wide and ~ 1.1 mm thick and consists of a modified 12 mm wide production conductor bonded to a 14 mm x 1 mm C715 CuNi alloy substrate. This conductor is then wrapped with six layers of a PPLP –like insulation developed by SPX to provide the insulated conductor that goes into the windings. SuperPower also worked on the development of HTS winding joining and termination technology for use in full-scale three phase FCL transformers.

Task 2.3.1.2 – Dielectric development for HTS transformers operating in a cryogenic environment.

In addition to the use of cryogenic compatible PPLP-like insulation on the HTS conductor, SPX verified that structural insulation materials used in transformer manufacture were cryogenically compatible. In instances where cryogenic compatibility was questionable, suitable replacement materials were identified.

Task 2.3.1.3 – Bushing development for HTS transformwersoperating in a cryogenic environment

SPX procured conventional resin impregnated bushing from a commercial supplier and tested them under cryogenic conditions. The results showed that these bushing were suitable to operate in the FCL transformer without any indication of degradation due to thermal cycling between ambient and liquid nitrogen (~77K) temperatures.

Task 2.3.1.4 – Integration of a warm steel core into the overall transformer design.

It was determined early on in the conceptual design process that the steel core of the transformer would need to be kept warm due to the thermal losses that were generated during operation. In order to handle this requirement, annular dewars would be used around the HTS windings. Studies were made at what air cooling would be required in the warm annular center through which the steel cores were placed.

Task 2.3.1.5 – Verification of fault current limiting with a sub scale winding

This task was accomplished in Phase 3 using a subscale winding of a high voltage module winding. The coil module was wound with long length, insulated bonded conductor using conventional transformer winding techniques (Figure 2.3.1.5.1). The measurements were conducted at the Center for Advanced Power Systems (CAPS) at Florida State University (FSU). The measurements were conducted in a LN2 bath (Figure 2.3.1.5.2). The test module was subjected to multiple fault current scenarios and demonstrated FCL capability without any indication of degradation of the windings or system.

Figure 2.3.1.5.1 Winding of HV module with insulated clad HTS superconductor.

Figure 2.3.1.5.2 FCL testing of HV module at CAPS(FSU)

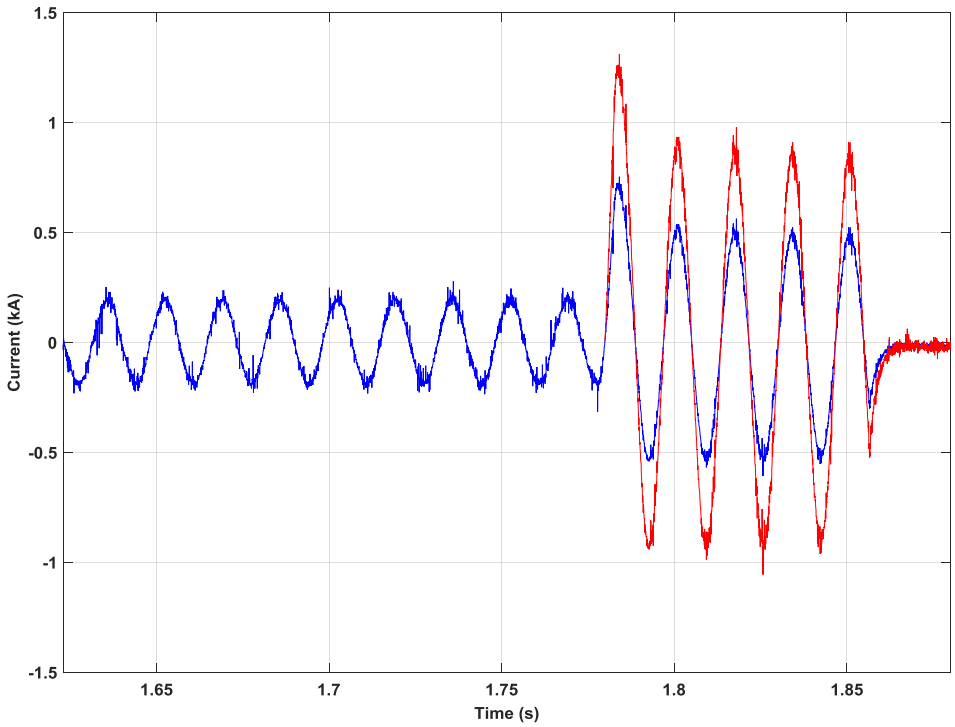

Figure 2.3.1.5.3 – Trace showing 5 cycle fault current limitation of HV module tested at CAPS (FSU). Red trace is calculated prospective current, based on empirical device impedance before current limiting effect. Blue trace is normal 360 Arms operating current (60Hz). First peak limitation is from ~1.3 kVpeak to ~ 0.65 kVpeak.

Task 2.3.2 – HTS conductor development

This task was a major SuperPower task in this program. The development of a bonded conductor with the correct normal state resistance (~ 25 mohm/m) coupled with mechanical strength sufficient to handle fabrication, winding and operational/fault transient stresses were successfully completed. The bonded conductor was developed in Phases 1 and 2 with the bonding and insulation lines fully operational in Phase 2.

Task 2.3.2.1 – Conductor design for low ac losses.

Work under this task had two components. The first of these focused on the development of striated MF conductors at the University of Houston and is described in detail in Appendix 2. An example of a striated MF HTS conductor is shown in Figure 2.3.2.1.1, This multifilament (MF) conductor would be bonded to the structurally supporting CuNi laminate. The composition of the MF conductor would have to be modified as described in Task 2.3.2.2 in order to meet the normal state resistance targets.

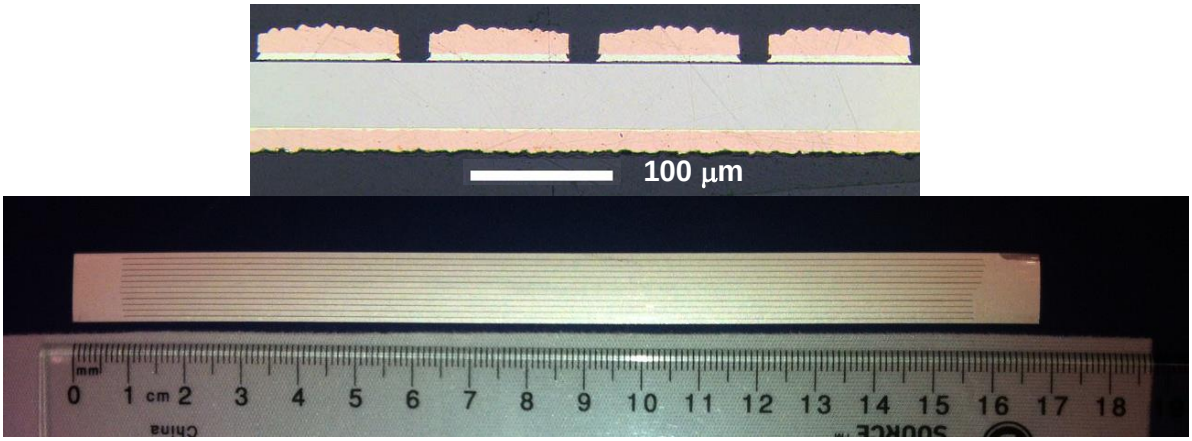

Figure 2.3.2.1.1 Example of multifilamentary HTS conductor evaluated in this program; (top) cross-sectional view; (bottom) top view.

Early on in the program, we recognized that the ac loss developed by the FCL transformer was going to be a major cost driver for production of this and future units. This would materialize in the size and capacity of the refrigeration systems needed to keep the LN2 cool. The higher the ac loss, the larger and more costly the cooling system would be. The initially proposed refrigeration system was costly, even using commercially available equipment, not requiring extensive development or prove out. Any reduction in ac loss almost direct correlates to money saved, as the system we were planning was a modular one with 6 cryo coolers, and we could reduce the number required accordingly as the anticipated load dropped yielding actual cost savings.

Another challenging issue was predicting what the ac loss for the transformer would be. There were numerous estimates, which all had uncertainties and assumptions, and would all greatly benefit from actual test and modeling to confirm or dispute. AC loss has multiple components, and we also needed to see which aspects were dominating, which ones were frequency or material dependent etc.

The major components of ac loss are:

- Hysteresis- First of 2 main drivers. A current that flows parallel to an electric field dissipates energy. Since this is time and position dependent, the total loss of energy can be calculated. Loss is generated by magnetic field perpendicular to the current flow and is highest in the end turns of a magnet.

- Coupling-Second of 2 main drivers we are looking at as it is the inter relational effect of each tape onto its above, below and adjacent neighbor – frequency dependent.

- Eddy Currents- Typically very low loss at the 50-60Hz frequencies the transformer would be operating at. For purpose of our study, can be considered negligible compared to the others

Our first step was to calibrate and validate test methodologies currently available. Florida State University (CAPS) has recognized expertise and an equipment base and is where we started. Our first tests were characterizing out existing HTS tape and trying a few variants of thickness, coatings, stacking and lateral spacing to see which aspects had an effect, A complete list of samples tested is shown in Table 2.3.2.1.1:

Table 2.3.2.1.1 List of samples and configurations subject to ac loss testing at CAPS(FSU).

Sample #	Sample Description	Surround Stabilizer	Dimension	Quantity	comments
1	SCS12050	Thin Cu - 10µ	6” x 12mm	3	M4-104-1 ~748-748.45
2	SCS12050	Cu - 100µ	6” x 12mm	3	M3-832-1 1540-1554
3	SF12050	Ag/Au - 2µ	6” x 12mm	2	M3-905-2 ~951.9-951.45
4	SF12050	Ag/Au with Bronze	6” x 12mm	2	M3-905-2 ~951.45-950.95
6	SCS12050	Cu -10µ	6” x 12mm	(1) 10 per stack	Stack of 10. No insulation / outer layer of Kapton insulation as wrap. M4-109-1 748-749.95
7	SCS12050	Cu -10µ	6” x 12mm	(1)10 per stack	Stack of 10. insulation on each conductor / outer layer of Kapton insulation as wrap. M4-109-1 745-748
8	SCS12050 laminated to Cu/Ni	Cu - 10µ	6” x 12mm	2	M4-104-1 ~750-754
10	SCS12050	Cu -40µ	12” x 12mm	(1) 10 per stack	Stack of 10. No insulation / outer layer of Kapton insulation as wrap. Caloremetric test

11	SCS12050 laminated to Cu/Ni	Cu - 40µ	12” x 12mm	(1)10 per stack	Stack of 10. insulation on each conductor / outer layer of Kapton insulation as wrap. Calormetric testing
13	Race track coil				
14	stack of 5 conductors x2 stacks				
14a	stack of 5 conductors x6 stacks				
15	SCS4050	Cu -40µ	12” x 4 mm	3	
20	12mm striated	single 12mm x 15 cm with 11 striations		3	

Our initial samples were 12mm wide (same as what would be used on project) HTS with various thickness and types of stabilizer. These were tested in a magnetic field with known induced currents, and the resulting measured voltage in the tape was them utilized to calculated a projected ac loss. This methodology had been used and calibrated against a calorimetric system also utilized at CAPS (more elaborate and 8x more expensive to run tests) and shown to have very reliable correlation. As seen in Figure 2.3.2.1.2, the measurement of ac loss in the conductor itself over a wide frequency range indicated that the losses were insensitive to frequency except at higher currents. This implies that coupling losses (frequency dependent) are a minor component in these measurements

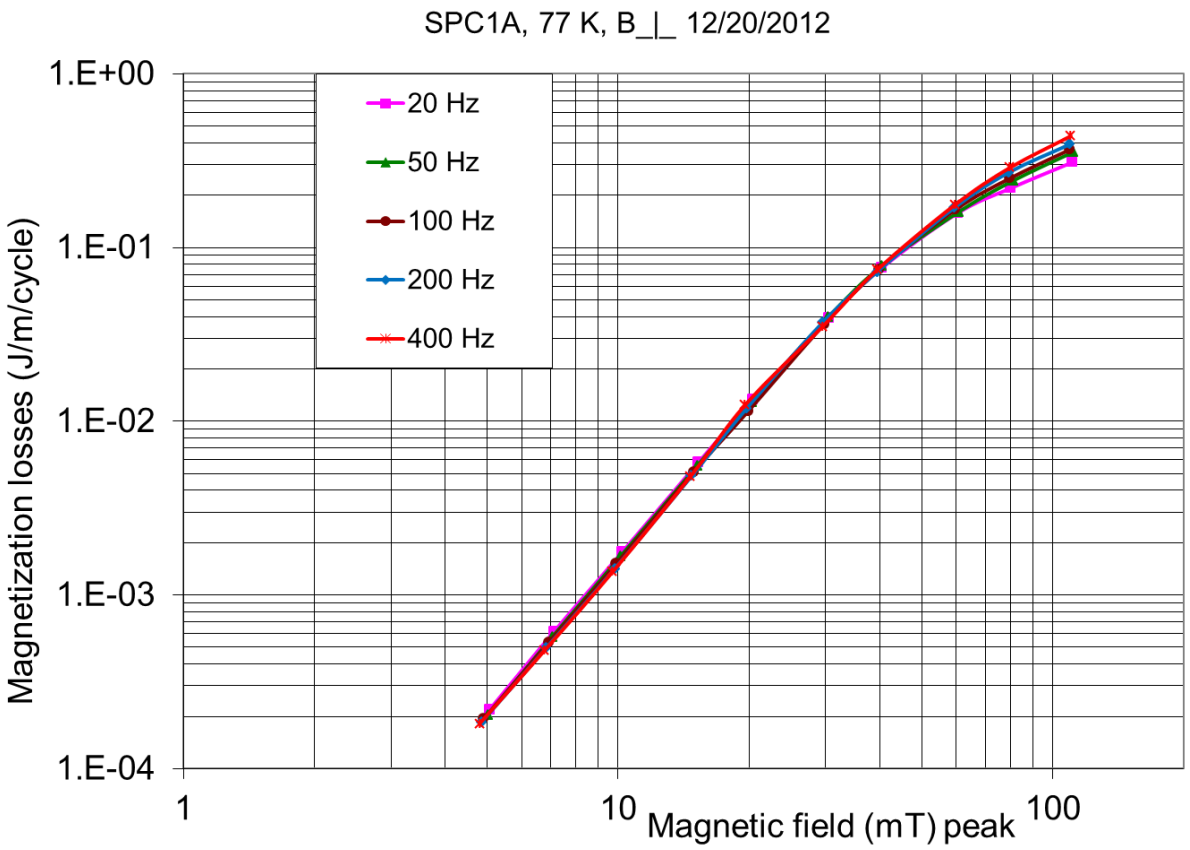

Figure 2.3.2.1.2 – AC loss measurement of Sample 1 over a frequency range of 20 – 400 Hz. Lack of frequency depence indicates that these samples are principally driven by hysteretic loss.

Conclusions from samples 1-4, 8 and 15 indicated that the type and thickness of stabilizer had no effect on AC loss for individual lengths of tapes. Also the addition of bonding a CuNi laminate to the HTS, also did not affect the ac Loss for a single sample.

The next batch of samples (6, 7, 10, 11, 13, 14,and 14a) were intended to more closely simulate the conditions the tapes would be seeing from their installed geometries in the transformer windings. We wanted to see what affect neighboring tapes (above and below, as well as adjacent) would have on the overall AC loss. Here we stacked numerous tapes atop one another using the same spacing as would be seen in the transformer. We also tested stacks side by side to mimic coil configuration both radially and axially.

The results of these tests came back with some unexpected (positive) results. 10 stacked conductors with representative spacing showed an AC loss equivalent to that of 110% of a single conductor. This indicated that a shielding effect was taking place, and that the inner stack of conductors was only contributing about 1% each (total of 10%) of the total loss. More testing, and verification was needed to validate this theory. It should also be noted

that this finding is just measuring the hysteresis loss, and not the coupling loss, however it still is a highly significant result.

Striated tape (sample 20) has long been recognized as one solution to reducing hysteric ac loss, and in this project we wanted to pursue multiple avenues as to how to get there, as well as determine just how much a benefit it would be. While the U of H team was working on 2 methodologies, a mechanical scribing method, and a sophisticated 11 striation laser technique (on a 12mm side substrate),

After completing this round of tests, the following conclusions were reached, directing us to the next steps :

- Bench" testing was limited to short samples or very small coils,
- Material content(Ag vs AgAu, Cu vs CuNi vs G10) proved to have no noticeable effect on results
- When testing multiple samples, whether one atop another, or side by side, the distances between the HTS layers had a direct impact on results. It did not matter whether spacing was a dictated by a void, or filler material
- When stacking conductors, there was a noticeable shielding affect taking place. Stacking of striated conductors did not give us expected results, but could not be easily determined as to how much was attributable to the small sample size and test conditions, vs interactions of shielding of stack and striated HTS layers.

Any further "bench" testing of short samples or small coils, while interesting and potentially enlightening, was not going to give us the type of data we required for a larger scale. At this point , we made the decision to pursue a large scale ac loss test system in house at SP, which would give us the ability to model scaled versions of the transformer coils, as well as give us a platform to make smaller version of representative wound coils more quickly and interpolate data with confidence.

In order to measure the losses in the actual windings, a large diameter dewar calorimetric ac loss test system was developed (Figure 2.3.2.1.3). Measurements of ac losses were then made on the HV module that was used for the FCL functionality test. First step was to characterize the dewar's thermal performance, in order to judge it's stability and baseline the parasitic heat leak. Once established, this would then be a simple offset into our overall calculation for ac loss. Then HV test module was then utilized for the ac loss measurements (Figure 2.3.2.1.5) with results shown in Figure 2.3.2.1.6 showing a frequency dependence indicating the presence of some coupling losses in addition to hysteretic losses. These results enabled us to estimate full system ac losses in a FCL transformer.

Figure 2.3.2.1.4 – Calorimetric ac loss test system for coils consisting of a double wall non-metallic vacuum insulated dewar (right) and a gas warming / mass flow meter system (left).

Figure 2.3.2.1.5 - Top plate of dewar with transformer HV scaled coil module in place for ac loss testing

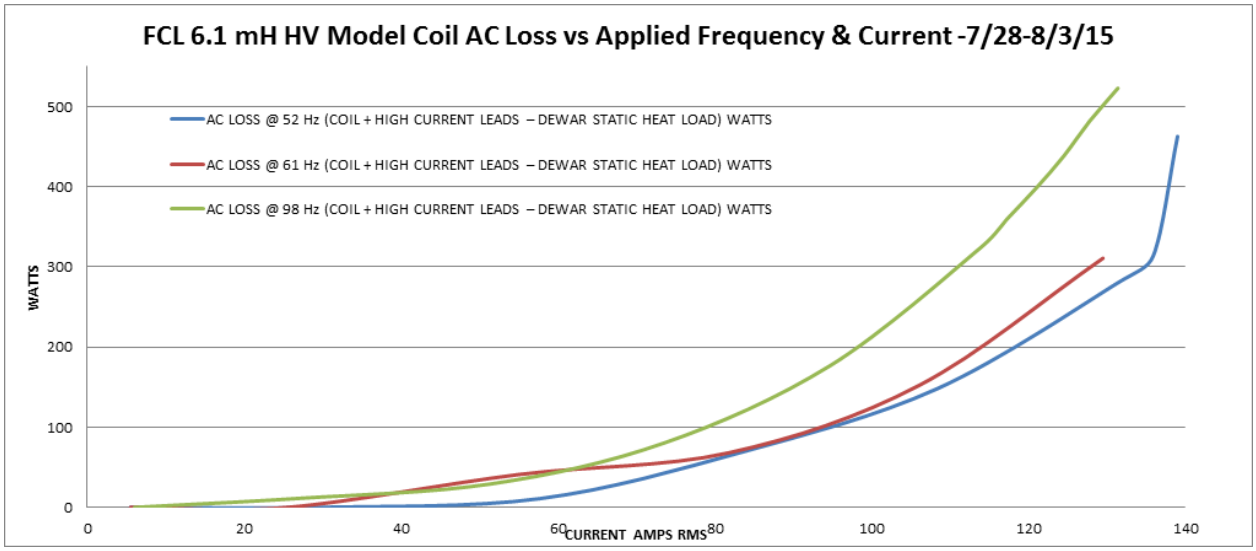

Figure 2.3.1.1.6 – Results of calorimetric ac loss measurements on the HV test module indicating a frequency dependence from a coupling loss component.

Task 2.3.2.2 Conductor development for FCL operation

The conceptual design studies indicated that a normal state resistance of ~ 25 mohm.m for the clad conductor would be required to meet the FCL operating conditions. Coupled with the mechanical requirements needed to handle the fabrication and faultcurrent stresses, these requirements drove the design of the conductor. Multiple conductor architectures were examined for the normal state resistance varying both the laminate thickness and conductor components such as Ag and Cu thickness. The HTS tape architecture for standard production material through the silver sputtering step (SF designation) is shown below in Figure 2.3.2.2.1. The typical thickness of the component layers are as follows:

Hastelloy C276 substrate:	0.0500 mm
Buffer stack	0.0003 mm
YBCO HTS film	0.0016 mm
Ag cap layer	0.0038 mm total

Mechanical considerations indicated that the thickness of the laminated structural element would need to be on the order of 0.8 – 1 mm thick. A review of available alloys for the structural laminate led to the decision to use alloy C715 70:30 CuNi. This alloy provided the requisite mechanical strength, was easily soldered to and had sufficient resistance. Initial analysis was done with a 12 mm wide laminate which was later changed to a 14 mm wide laminate. The resistance of the HTS conductor itself was driven by the resistive contributions of the Hastelloy and Ag layers. The normal state resistance of the YBCO film is very high while the buffer stack is insulating.

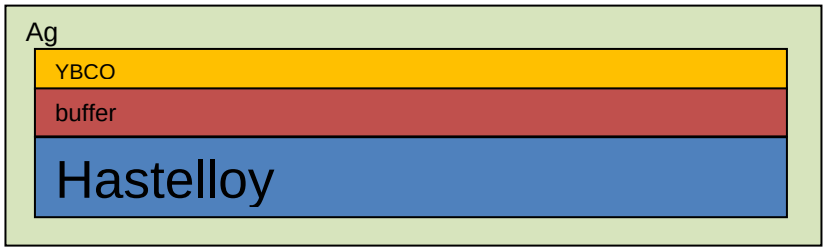

Figure 2.3.2.2.1 – Standard production HTS conductor architecture through Ag cap layer (SF designation)

The Ag thickness of ~ 0.002 mm is difficult to solder to as the Ag layer is readily gettered by the molten Ag. Therefore, in order to have a structure that can be soldered to, we would have to add a solder compatible layer on the Hastelloy side of the HTS conductor. Initially we looked at a thin copper layer or a thicker Ag layer. In both cases, the resultant normal state resistance was too low since both Ag and Cu have very low resistance at 70K. This can be seen in the plot below in Figure 2.3.2.2.2. Even reducing the total Ag thickness from 0.0038 mm to 0.002 mm and keeping a copper thickness to 0.001 mm, the resulting normal state resistance would require a reduction of the CuNi laminate to ~0.5 mm which would not meet the mechanical requirements.

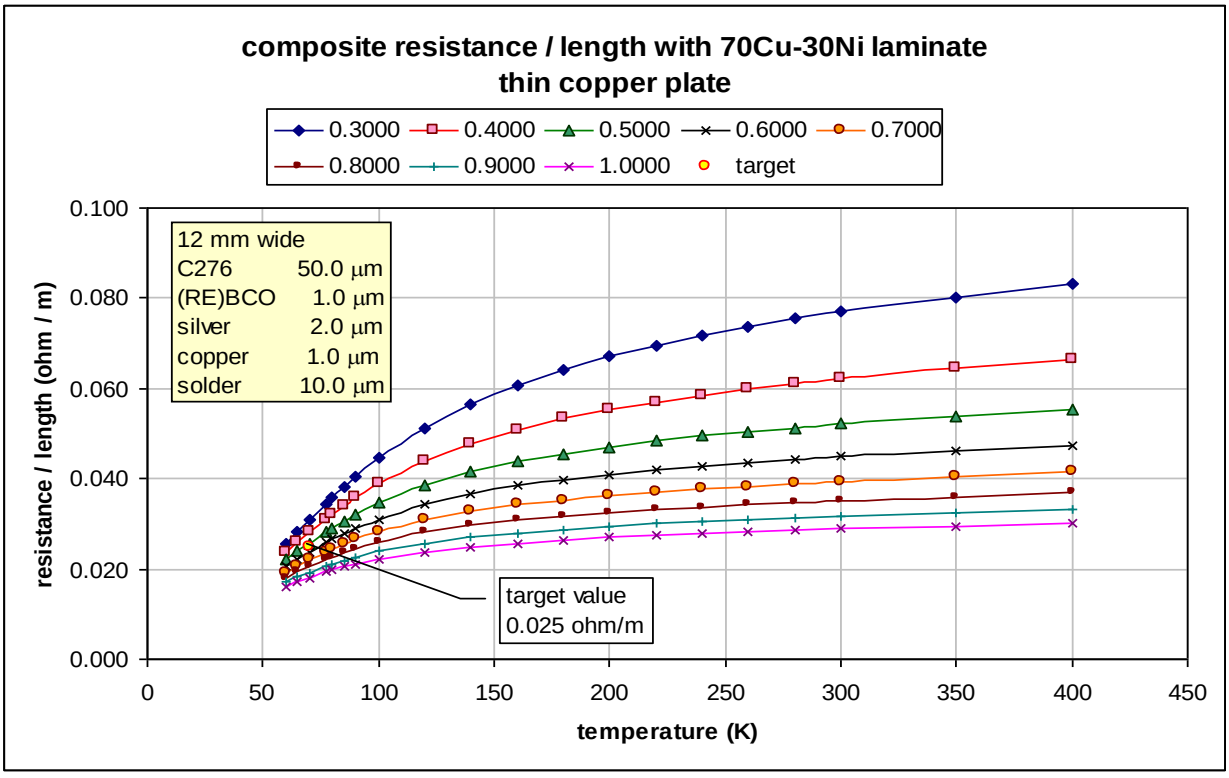

Figure 2.3.2.2.2 – Analysis of normal state resistanceof clad composite with 50 μm Hastelloy C276 substrate, 2.0 μm Ag and 1 μm copper. Target normal state resistance implies that a ~0.5 mm CuNi laminate would be required.

Analysis of multiple configurations indicated that even with thin 0.002 mm thick Ag, the target normal state resistance would be difficult to achieve. The decision was then made to switch to a AgAu alloy instead of the Ag. This alloy was known to be compatible with the YBCO film and had been used in the fabrication of HTS tapes for current lead applications. The increase in resistance of the AgAu alloy when compared to pure Ag was sufficient to open up the design space to achieve the target normal state resistance. This can be seen in Figure 2.3.2.2.3 below.

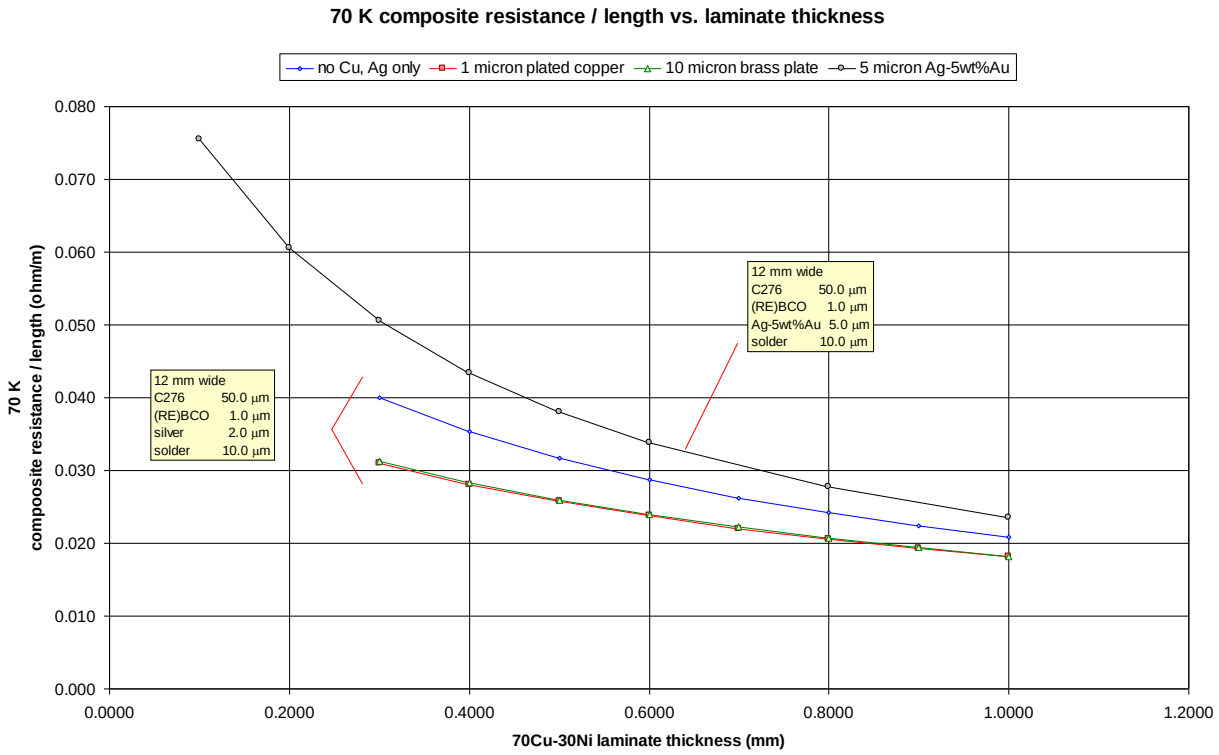

Figure 2.3.2.2.3 – Clad composite normal state resistance comparison between Ag and AgAu options.

The next decision was which process to use to apply additional material (either plated or sputtered) to give a sufficient surface to solder to without gettering the Ag /Au layer .Plating was the preferred method based on process costs, however, we needed an element or alloy that:

- is resistive enough for FCL function
- is cost effective
- was commercially available or could be made to be commercially available
- environmentally friendly product as well as process and by products
- chemically compatible with HTS (needed to be acid based solution so as not to poison HTS layer)

Sputtering, while a more expensive process, is more flexible in the alloys that could be applied. Major issues here were controlling and expelling the heat generated during processing so as not to affect superconductivity of the HTS by overheating it and improving efficiency of operations (lowering cost) . We pursued both processes, had samples made and tested, and came up with the following conclusions:

Plating:

Most plating is done with singular metals, i.e. Cu, Ag, , Au to name a few which all were too conductive to meet the FCL function and requirements. The challenge was to find compounds that can be plated and are more resistive for FCL.operation. White Bronze or Nickel were two of the most promising candidate choices. Sn flash plate with White Bronze of 2 micron was initially tried. Initial FCL testing acceptable but solderability at higher temperatures failed due to bubbling of the Sn. We then attempted replacing the Sn with palladium, however issues with the caustic chemistry of the Pd plating solution (although only pH of 7.5) poisoned the HTS. We then looked at plating the white bronze directly but were unable to procure acidic based solution from any major suppliers. Two more options were attempted using caustic solutions. Flash coating of a leveling Cu(Cu with organics) layer then plate tri-metal white bronze or a flash coat of matte Sn then plate tri-metal white bronze. Both of these approaches consistently showed damage to the HTS layer and thus deemed unacceptable.

Sputtering:

Overall confidence was low to be able to meet the project timetable with reliable plated product, so the attention was focused on sputtering the solder contact layer. Two options were considered. The first of these was to use a AgAu sputtered layer with known good solderability and FCL characteristics, but expensive and required a thick layer so as not to getter during soldering. The second option was to use a brass or bronze alloy. These would be less expensive but would need to be tested to determine the optimal alloy choice for solderability and FCL functionality. The two configurations would look like those below.

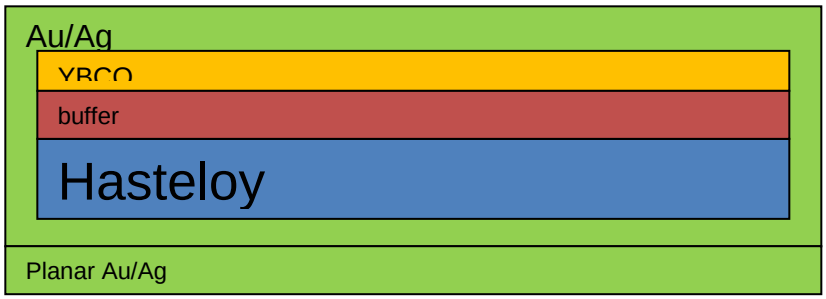

Figure 2.3.2.2.4 – Composite conductor configuration with planar sputtered AgAu layer

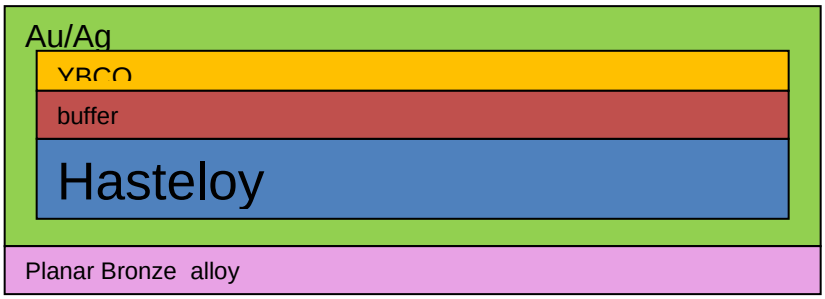

Figure 2.3.2.2.5 – Composite conductor configuration with planar sputtered bronze alloy

Next challenges were to quickly decide which alloy to use and what thickness and configuration (single sided or encasing). The alloys evaluated are listed below in Table 2.3.2.2.1. We also needed to arrange machine availability for short run samples of 100mm-2m, mid length samples of 10-30m and production samples of up to 400m. We also needed to conduct temperature studies of the process in order to protect the HTS film from overheating leading to oxygen loss and critical current decrease.

From the initial trials summarized in the table below, we narrowed choices to three alloys and ran sputtering trials for temperature as seen below in Figure 2.3.2.2.6. Based on these trials, and compatibility with the CuNi laminate, we opted to pursue CuNi as the bronze alloy choice. The following steps were performed with both AgAu and CuNi.

> Initial runs of short lengths were conducted

> Longer length runs of various thickness (2.0,2.2,2.4,2.6,2.8,3.0 microns) were run and then bonded with 1 mm thick CuNi laminate.

> Focus was to first get process that works, then work to cost reduce

> Preference was to use Cu alloy resulting in a huge cost advantage

> Trials were conducted using a cooling helix in order to minimize heating during deposition

> 0.5 microns/pass deposition showed no degradation of Ic

> 2 microns/pass showed degradation of Ic (too much heat buildup)

> Ran additional trials to find crossover point

> Ran multiple passes to get sufficient material (1.5micron)

The final configuration decided on-is shown below in Figure 2.3.2.2.7 consisting of HTS tape with 1.5 microns sputtered CuNi, soldered to 1 mm thick x 14 mm wide CuNi

laminate. We arranged for samples to be made on prototype machines, while obtaining a used "production capable" machine. This was a 5 strand helix design planar sputtering system. We ran additional temperature profiles, and then designed , built and installed a cooling helix which was added to the machine to insure temperatures would remain within the "safe" operating range for the HTS

Table 2.3.2.2.1: Table listing various alloys evaluated for the solder bond surface and conclusions. Based on these trials, down select to three alloys was made.

	Composition	Resistivity ($\mu\Omega-cm$)	Thickness (nm)	Simple test with solder iron			Splice test	Result	Remarks	Conclusion
				In	SnPb	SnSb	SnSb			
AgAu		2.297	5	NG	NG	NG	NG	NG		
Alloy510	95Cu 5Sn	11.5	1	NG	NG	NG	-	NG		Pursue further with bonding tests
			2	Good	Good	NG	NG	NG		
			3	Good	Good	NG	OK	OK		
			4	Good	Good	NG	OK	OK		
			5	Good	Good	OK	Good	Good		
Alloy260	70Cu 30Zn	6.16	1	Good	Good	NG	-	-	Wettability in splice test seems worse than that of Alloy510.	No further action at this time
			2	Good	Good	OK	OK	OK		
			3	Good	Good	OK	OK	OK		
			4	Good	Good	Good	OK	OK		
Alloy464	60Cu 39Zn 1Sn	6.63	1	Good	OK	NG	NG	NG		Pursue further with bonding tests
			2	Good	Good	NG	OK	OK		
			3	Good	Good	NG	Good	Good		
			4	Good	Good	NG	-	Good		
			5	Good	Good	Good	Good	Good		
Alloy220	90Cu 10Zn	3.92	3	Good	Good	Good	OK	OK		Pursue further with bonding tests
			4	Good	Good	Good	Good	Good		
			5	Good	Good	Good	Good	Good		
Alloy360	61.5Cu 31.5Zn 3Pb	6.63	3	Good	Good	OK	OK	OK	Easy to peel off from hastelloy, and also from inside of the chamber	No further action at this time
			4	Good	Good	NG	OK	OK		
			5	Good	Good	Good	Good	Good		
C715	70Cu 30Ni	38.71	3	Good	Good	Good	OK	OK	Easy to peel off from inside of the chamber	Pursue further with bonding tests
			4	Good	Good	Good	Good	Good		
			5	Good	Good	Good	Good	Good		

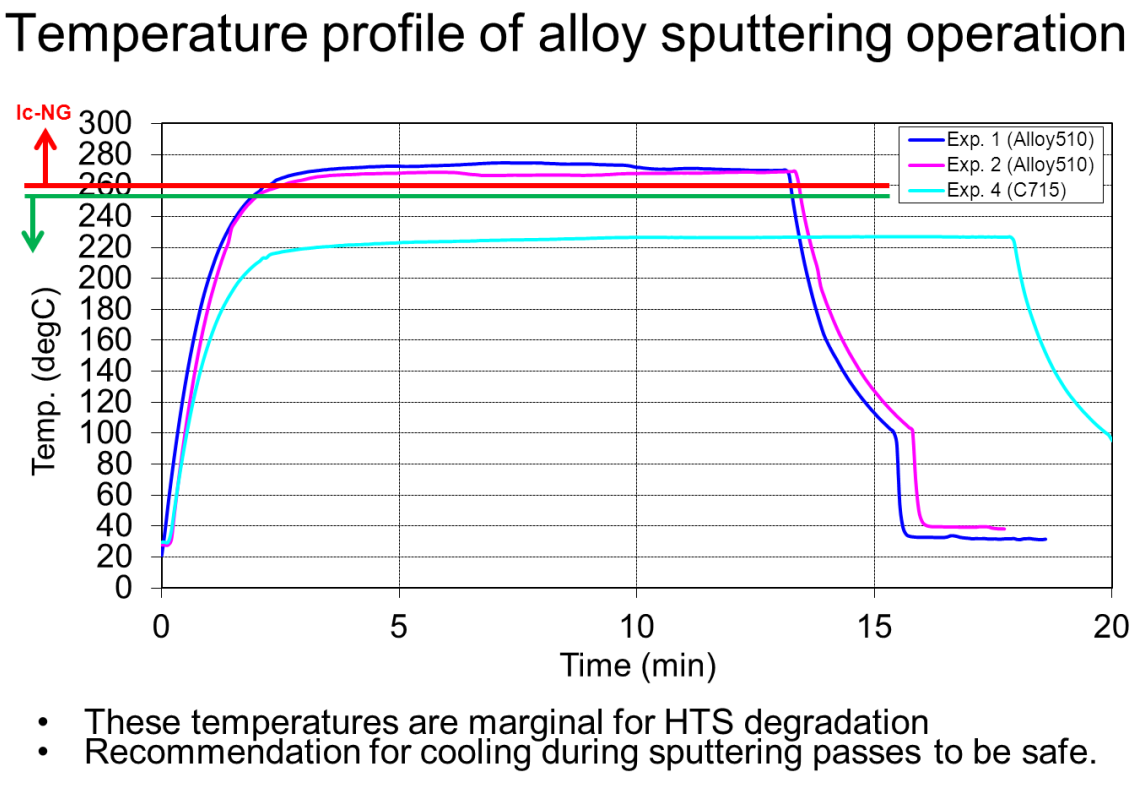

Figure 2.3.2.2.6 –Data from sputtering trials looking at the impact of temperature rise during processing on critical current (Ic)

Figure 2.3.2.2.7 – Final configuration of the bonded conductor to be used in the project

2.3.2.3 Reliable long length 2G HTS Manufacturing

The overall objectives in this task included the following:

A. In Phases 1 and 2, supply SPX with 15.5km of, 325A HTS conductor bonded to a substrate with sufficient strength for transformer winding application, having FCL material characteristics, tested and insulated.

B. Develop methodology and associated tooling for creating terminations of bonded HTS for attachment to conventional copper terminals and wires

C. In Phase 2, supply SPX 5.2Km of insulated copper tape to facilitate a single phase winding and testing coil (both HV and LV).

D. In Phases 1 and 2, work with SPX to develop and coordinate tooling for receiving, loading, unwinding and winding of conductor.

E. Optimize and balance technology vs. cost, to support commercialization of product

The following 3 major categories, will be further broken down to explain each of individual issues, tasks, and accomplishments within each of the above listed overall objectives

- Product Engineering challenges and accomplishments
- Process Engineering challenges and accomplishments
- Logistical Challenges and accomplishments

A. Supply SPX with 15.5km of, 325A HTS conductor bonded to a substrate with sufficient strength for transformer winding application, and FCL material characteristics, and insulated.

Product Engineering challenges

Within the HTS manufacturing process develop/determine a high resistivity stabilizer (to enable FCL function) for HTS in lieu of Ag. This challenge was resolved with the selection of AgAu alloy as the stabilizing cap layer.

- Must protect HTS layer
- Must be permeable to allow oxygenation of HTS
- Must be able to be soldered to, or receptive to interfacial layer for soldering to
- Must be able to be applied “economically” within existing HTS manufacturing processes or with minimal impactful changes
- Must be able to withstand cryogenic temperatures with no degradation (such as tin pest)

- Develop product structure to allow for bonding HTS with stabilizer to laminate. Key required attributes included:
    - sufficient strength to withstand conventional transformer winding techniques
    - sufficient strength to handle a transformer fault event
    - ability to function as FCL
    - bonding process must not getter stabilizer layer during bonding process.

This last set of requirements was resolved with the structure developed as described in the above section and shown in Figure 2.3.2.2.7.

The overall process for fabricating the HTS conductor is shown below in Figure 2.3.2.3.1. The processes shown in yellow below were proposed to be modified, vetted and accepted as minor deviation to the existing HTS manufacturing, allowing for a cost effective method for "screening" the HTS prior to adding stabilizer to insure that wire slated for the FCL program met the specific criteria required, before adding the Ag/Au cap layer stabilizer. Green processes are those that were then done to fabricate the final bonded conductor and are described in more detail below

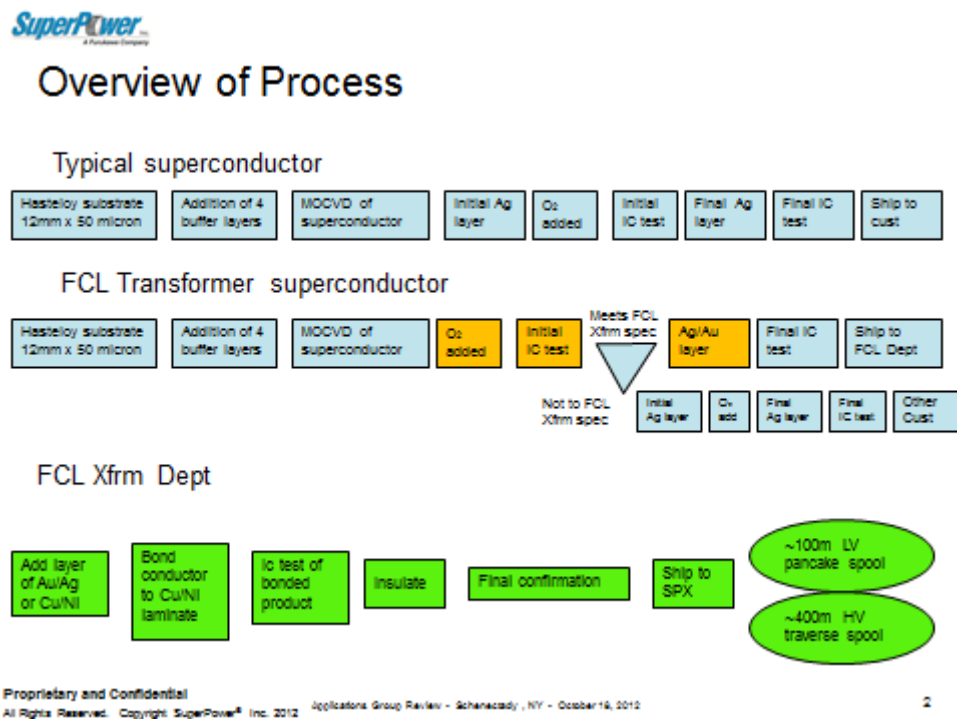

Figure 2.3.2.3.1 – Overview of production process used to fabricate HTS conductor for this project. The yellow squares are modifications made to the process. Green processes are those that were then done to fabricate the final bonded conductor.

Add layer of CuNi by planar sputtering to HTS conductor.

The CuNi layer was applied by using a planar sputtering system as shown below in Figure 2.3.2.3.2 using deposition parameters developed in earlier trials. Lengths of up to 400 m were processed without degrading the critical current of the HTS film.

Figure 2.3.2.3.2 – Planar sputtering equipment used to deposit ~1.5 micron thick CuNi bonding layer on the Hastelloy side of the HTS tape.

Bond the conductor to the CuNi laminate

Process challenges-production bonding tooling

Superpower had a small prototype bonding system for adhering HTS tape to various substrates, however due to the nature of the FCL transformer requirements; this system was not a consideration for the project. A new integrated system of machines and processes was designed, and built in a green field environment to meet the needs of the program. The system utilized some existing technology as well as many new or modified technologies to achieve the final goal.

Everything including the feed and take up reels, cleaning (pre and post) fluxing soldering, inspection etc. had to be built for the scale of the project. For perspective, SuperPower's standard HTS tape is 12mm wide and 55-100 microns thick. A rell for holding 300m of

tapel is ~ 0.25m diameter and weighs ~5 kgs. The FCL program larger HV reels would need to hold just over 300m's of 1.06 mm thick material. This would require reels in excess of 1 meter diameter that weighed in excess of 200 kgs.

We decided on building the system in modules and testing them independently and then integrating them into the overall system. We viewed this as the only viable method to meet our timing and quality objectives

Highlights of the equipment and process are detailed below. Table 2.3.2.3.1 below is a subjective ranking used to determine which method of bonding to pursue for production. After cost and performance consideration, moving belt on arc method was chose

Table 2.3.2.3.1 Summary of bonding processes considered early in the project.

– Bonding Process Development Status
  - Moving forward with 2 of 4 concepts in parallel to maximize probability of success
  - Developing design of 3rd concept

			Subjective rankings- 10 good /1 bad				
	Pros	**Cons**	**Productivity**	**Confidence**	**Expected Reliability**	**$$**	**Combined A x B x C x D**
Flat Die (existing) Pressure or height control	• Simple tooling • Easy to modify • Already built • Least $ tool • Can apply findings to other concepts	• Highest Friction • Wire is stressed in application due to flat bond	5	7	7	9	2205
Large Wheel Tension control	• Large space • Neutral stress in application	• Expensive to build • Expensive to prototype	8	7	8	5	2240
Modified Belt Sander concept Tension control	• Advantages of wheel design with less cost and space	• More complex design	8	7	8	7	3136
Tractor drive with silicon belts Pressure control	• Low friction • Conforms to tape shape	• Expensive • Highest # of unknowns	9	5	9	6	2430

Bonding process development

For the bonding process itself, we estimated the temperature profile for the bonding process based on trials and had success establishing basic parameters for dwell time and speed. If too short, desirable intermetallics do not have a chance to form.If too long, can start to degrade AuAg layer or affect Ic. The elements being bonded must be maintained under correct tension and force during the bonding process. The HTS tape and laminate

must be correctly aligned prior to reaching the position with the melt point of the solder. Tension or pressure must be applied before the solder reaches the melting point. The temperature must be sufficiently high to fully melt the solder but can not exceed the critical temperature that results in a degradation of Ic. The distance of the heated zone must be sufficient to heat, liquefy, dwell, and then solidify. An example of a successful temperature and dwell cycle is given below in Figure 2.3.2.3.3. The solder "suite" decided upon for the project were: solder for bonding,(SnPb eutectic), terminations (SnSb), and bonded conductor repair (InAg).

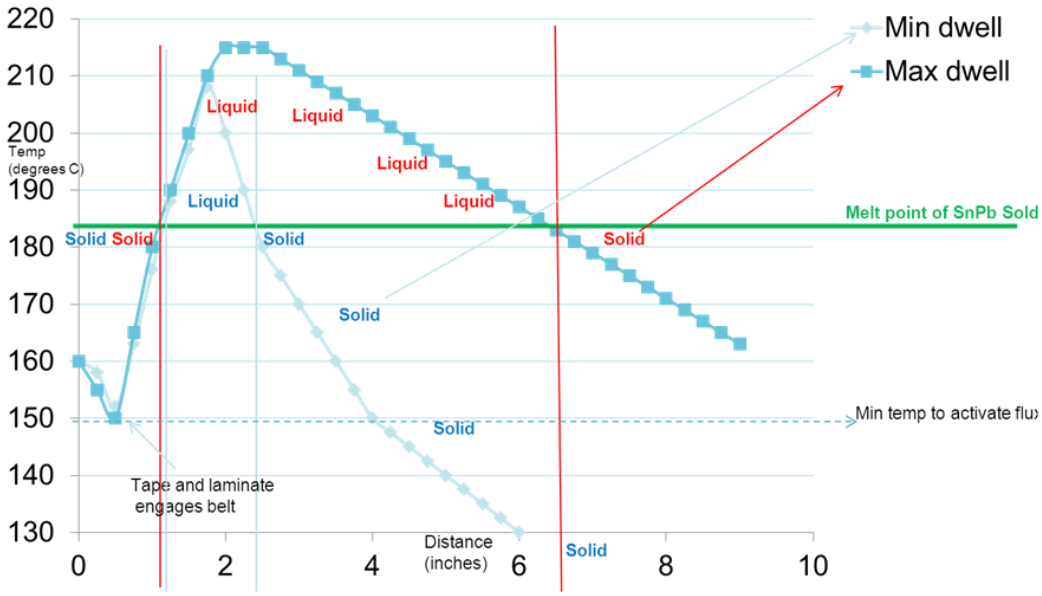

Figure 2.3.2.3.3 -Temperature and swell cycle for bonding process using SnPb eutectic solder with 183 deg. C melting point.

The overall bonding tool concept is laid out in Figure 2.3.2.3.4 including general system requirements. Some considerations for the design included:

- Straightening the laminate (may not be a necessary operation, but needed to be planned for). Would use commercially available equipment and be able to move in and out of machine easily.
- Pre solder cleaning using Potassium Hydroxide (KOH). Since KOH has a high pH (13.5), safety systems for chemical dispensing, collection, plans for neutralizing and disposal would need to be implemented. The ability to monitor and add make up to keep solution correct was included. Sufficient rinse and ability to monitor rinse tanks was included in the design. Testing was conducted to ensure no adverser effects on Cu, Ag and YBCO.
- Bonding of conductor to substrate –Three methods were considered and trials conducted for application of solder:
-

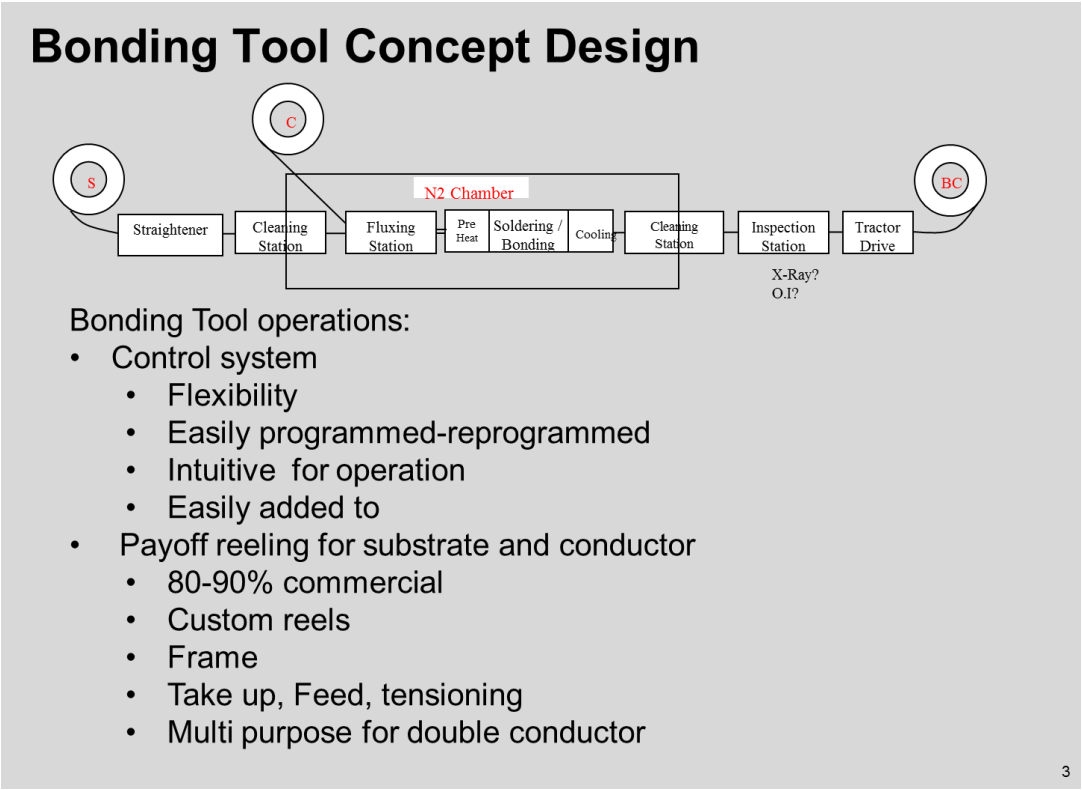

Figure 2.3.2.3.4 – Bonding tool concept design and considerations.

- Continuous flow of solder paste
- "Replowed" and skived solder preapplied on the laminate
- Clad solder preapplied on the laminate

Paste solder was utilized in early development trials and deemed too inconsistent for long runs production. Reflowed and skived laminate/solder was used in early runs on the production system: The process provided an acceptable product except excess solder was an ongoing headache regarding removal. Also, variation was noted in the skived height of solder throughout the run. The laminate clad with solder had very tight controls on thickness and consistency of solder layer. During the bonding process, much less overflowing solder was experienced and the cost was less than "reflow" and skived. Based on above, laminate clad with solder became the clear choice for moving forward.

Pay off eequipment for the laminate was designed. The large diameter (~1 m) was utilized to ensure no additional preset was induced in the 1 mm thick CuNi laminate. In addition, a pay-off station was developed for the HTS tape. More than one payoff spool was provided for flexibility in future bonding applications. These two pay-off stations are shown below in Figure 2.3.2.3.5.

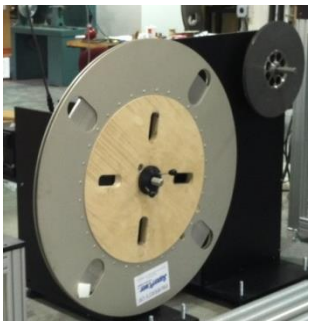

Figure 2.3.2.3.5 – Pay-off equipment for laminate (left) and HTS conductors (right).

The pre-cleaning station utilized a commercial unit modified to handle parallel tapes (laminate, HTS) in its various cleaning sections. Development of the ultrasonic KOH based cleaning system to successfully remove solder "smut" from the solder clad laminate in line as we prepare to solder. The use of KOH necessitated the use of safety features such as overflow containment and proper ventillation. A similar type station was utilized for post cleaning of flux (although not with KOH). The cleaning stations are shown below in Figure 2.3.2.3.6.

Figure 2.3.2.3.5 – Pay-off equipment for laminate (left) and HTS conductors (right).

The heart of the bonding line is the bonding station. The general concept of the bonding station is shown below in Figure 2.3.2.3.6 consisting of a reel that takes cleaned solder clad laminate and feeds it to a preheat wheel. The preheat-takes place prior to entering the solder melt zone. Pre-heat temperature is optimized using an optical pyrometer for preheat wheel control. The laminate then enters a laminate alignment adjustment block. In

parallel, cleaned HTS tape is fed through a superconductor alignment adjustment block. The combined solder clad laminate and HTS tapes are then fed over the belted heated arc where the solder is melted, joined to the HTS tapes and the final bonded composite cooled. The production design of the heated arc provides 30" (750mm) of working area from where tape contacts to exit point. Space for up to 12 heaters and 6 thermocouples is provided on the arc for fine resolution and control. Active cooling in the latter stage of the arc ensures solidification while on radius. Excess solder is handled by a heated vacuum baffle installed to minimize overflow solder spatter. An N2 gas enclosure is provided to mitigate if necessary against excess oxidation.

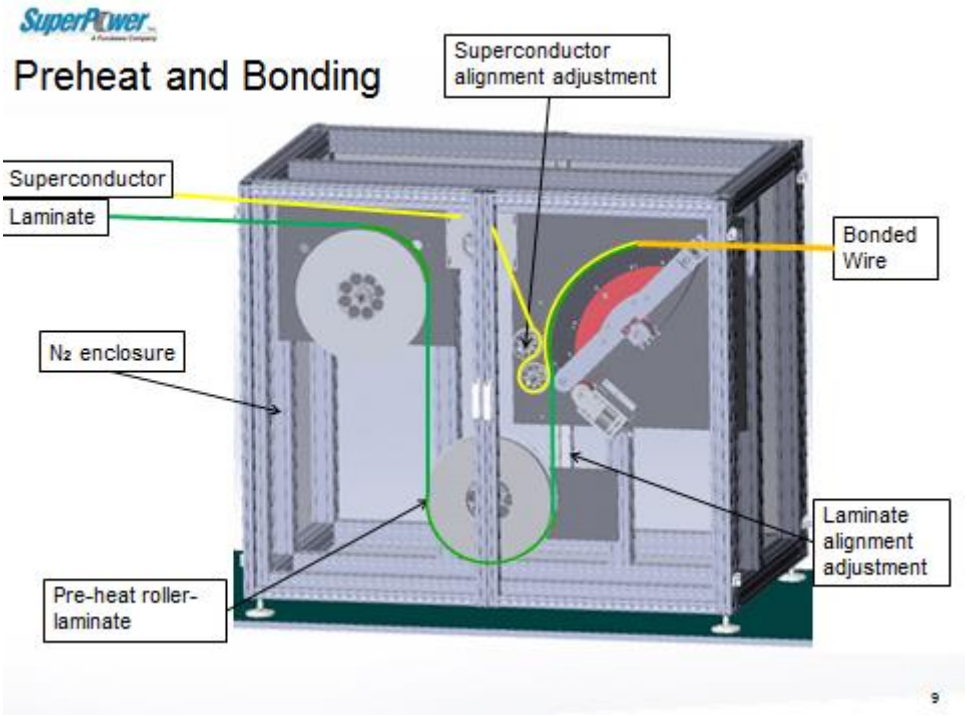

Figure 2.3.2.3.6 – Layout of solder bonding station.

The methodology for bonding HTS tape to the CuNi substrate required the creation of a custom flux application system for the laminate just prior to bonding. We tried multiple drip, spray, brush application systems and settled on pressurized drip system feeding absorbent felt pads under clamped pressure. This allowed us to control the fluxing rate and optimized line speed. We also created a custom heated "smoothing" device for the heated arc to work on top of the arc and help heat and smooth the flow of solder on the top side of the HTS. Challenges here were finding a low friction material, able to withstand the heat of the soldering process, and not damage the HTS surface which is facing out. We were able to utilize a Teflon coated fabric belt (same as what we used for our drive belt on arc)

Design of Experiments tests were conducted for the bonding arc and included heater response and control tests, heated belt temperature profiling, multi zone tension testing and individual module testing. Additional Design of Experiments tests on the bonding function were conducted on the temperature profile, tension(bonding force), flux or no flux: before or after pre-heat and tape speed.

Deburring of excess solder to prevent sharp points later penetrating the insulation after the bonding application was evaluated. Both deburring by mechanical slot or hot wire deburring. The deburring by mechanical slot used a "mail slot" physical deburr feature to be used directly after bonding when the solder was still warm (but solidified). This tended to clean up the majority of remaining bulk solder. To address the finer solder tips, that could potentially poke through the insulation and create a short at high voltage, we developed and employed a hot wire deburr. We bought off the shelf units, and then customized them to our specific shapes and sizes. After running numerous trials to insure they were not imparting additional heat and affecting the Ic of the tape, we were able to dial in the process and successfully produce tape with variation of less than .002"(verified by our laser detection system on bonding and our mechanical burr detection system on our insulating line – see Figure 2.3.2.3.7). Tension for consistent tape movement is provided by a tractor drive (Figure 2.3.2.3.8) and the finished product taken up on large diameter take up spools (Figure 2.3.2.3.9). An overall view of the bonding line is provided in Figurer 2.3.2.3.10.

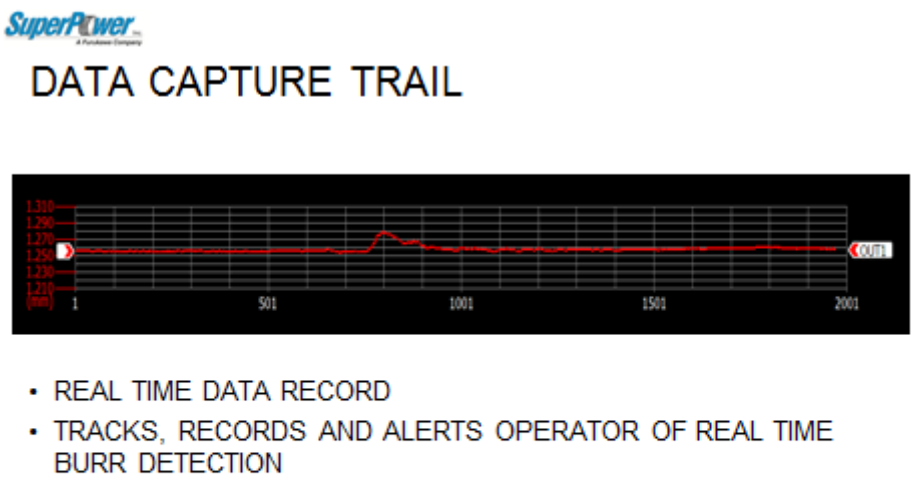

Figure 2.3.2.3.7 Example of burr detection signal included on insulating line.

Figure 2.3.2.3.8 – Tractor drive used to provide tension in the line.

- 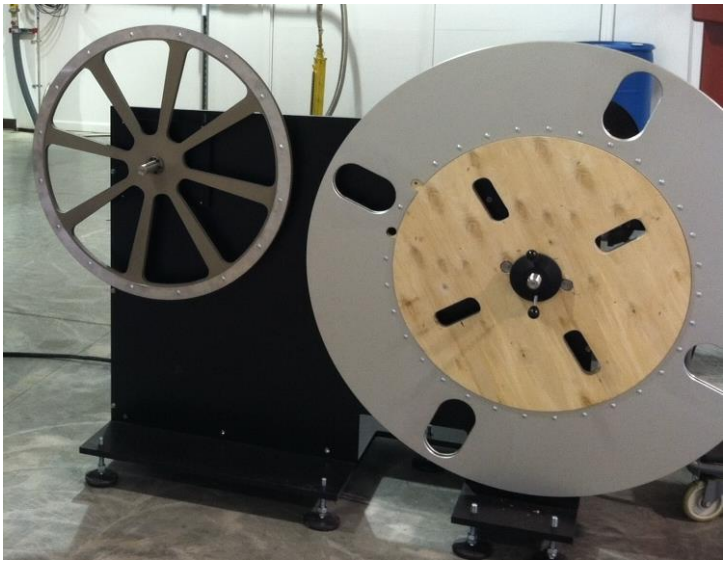

Figure 2.3.2.3.9 Take-up guide spool and product spool

Figure 2.3.2.3.10 - Overall view of finished process line

Bonded conductor quality assurance systems include dimensional testing via laser and testing of the integrity of bonding via x-ray. Laser inspection for dimensional stability enables us to ensure there would be no burrs that would adversely affect the insulating process. We were most concerned with sharp points, but were also able to measure slight variations of width or thickness. The most complex aspect of this was that we were measuring a moving tape, that also flexed, and so our laser system had to float and measure a target that constantly was shifting up and down and side to side, yet we wanted an absolute result. The software was able to be programmed to take a measurement not from an absolute origin, but instead from side to side, or top to bottom of the part, even if that was shifting. An example of the type of image available is shown in Figure 2.3.2.3.11.

Early on in the program, it was determined we needed to have a way to inspect and verify the quality of the bond between the HTS and the laminate. In this FCL transformer application, it was unknown what would be an acceptable level required, therefore we had to develop, test and create a spec, while simultaneously find a non-destructive way to measure what we specified. Early testing was done by bonding, testing FCL characteristic, then tearing off HTS to verify percentage of bonded surfaces. While this

was a crude method, it got us into the ballpark of what we needed. In conjunction we evaluated multiple non-destructive test methodologies – eddy current and x-ray. An example of the results from the eddy current system is shown in Figure 2.3.2.3.12. It was difficult to correlate the results from the eddy current detection system with the solder quality and this approach was abandoned.

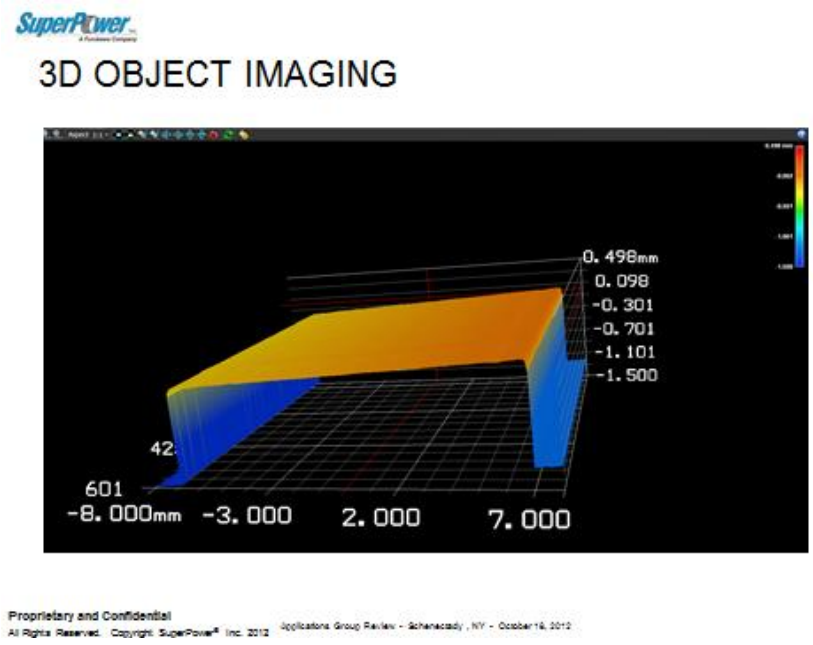

Figure 2.3.2.3.11 – Example of laser dimensional measurement of as bonded product

- Quality Systems
  - One manufacturer successful with eddy current detection
    - Able to detect "presumed" good, marginal and defective samples
    - Will do an autopsy on samples to confirm above status
    - Complete System is in $30-$50K range
    - Need to provide with additional "Production" samples
  - Initial Samples provided to 2nd supplier for similar evaluation

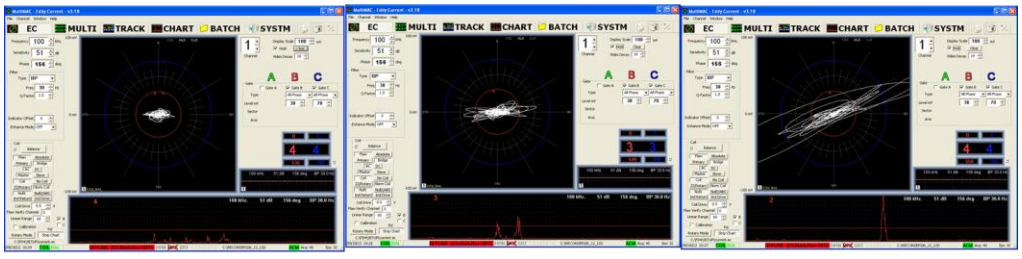

12

Figure 2.3.2.3.12 – Examples of eddy current trials on solder quality

After trials and considerations, we chose to go with an x-ray system produced by Glenbrook Products (Figure 2.3.2.3.13) gave us good resolution and could be adapted to accept a constantly moving tape.. Unlike conventional x-ray systems, this unique x-ray camera technology captures x-ray images with relatively low kV x-ray emissions. Next steps were to study voids (Figure 2.3.2.3.14), and determine what would be acceptable, and then develop algorithm to process this data on the move.

Figure 2.3.2.3.13 – X-ray system incorporated into the bonding line to evaluate solder voids in bonded product.

We engaged a vision system company to help build us bridge software that would analyze the output of the x-ray camera and then give us a usable format to judge the product based on the specification we chose. This was a very iterative process as the software had to to read the snapshot camera image, average multiple images over a specified distance, assign each void on each snapshot a size,sort each of the voids into pre-determined groupings based on size, and count them for a given distance. The software would then do a calculation of overall bonding coverage, as well as having specific rules such as no single void shall be larger than A x B . The software would then give us a go/no go signal of the bonding integrity for that distance based on the supplied acceptance criteria we derived from our functional testing.

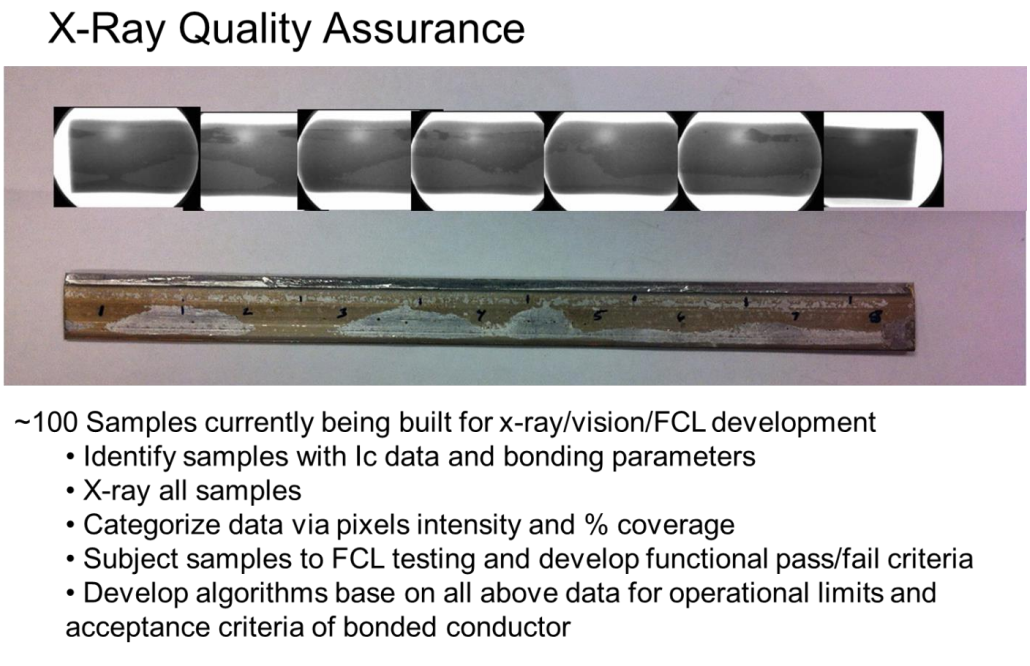

Figure 2.3.2.3.14 – Example of x-ray images of a poor solder quality sample. Data such as this would be fed into the analysis software to produce a go/no-go result.

Since the final product tape (14 mm x 1.06 mm is much stiffer than standard product, we needed to develop a reel to reel critical current test system for this larger conductor. The system developed was based on a dynamic concept of critical current testing measuring Ic while moving over Cu wheels immersed in LN2 bath. Initial trials applied these concepts and tried components to eventually build the production setup with larger current wheels and utilize trial wheels for voltage readings. We then constructed the tank and cold enclosure and integrated electronics and programming to control the measurements and tape drive system. The concept of the system is shown below.

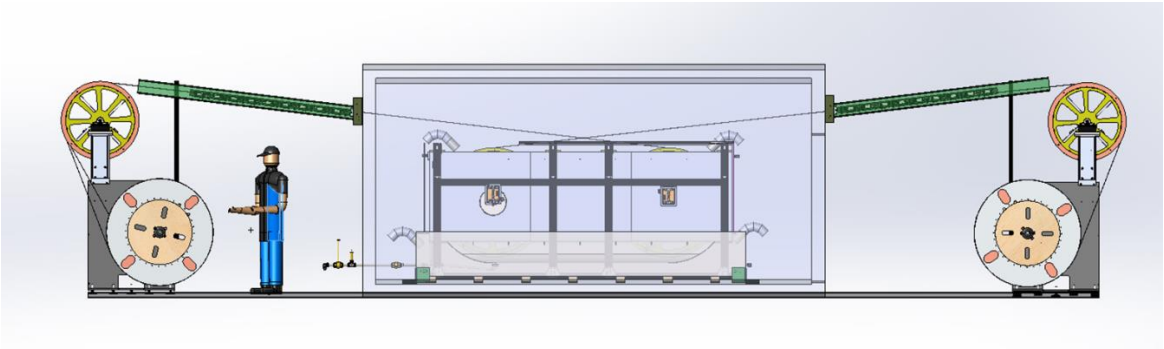

Figure 2.3.2.3.15 – Conceptual design of reel-to-reel Ic test system for thick clad product.

The reel-to-reel Ic test system was constructed (Figure 2.3.2.3.16) and initial trails conducted. Ic measurements were successfully taken although further refinements will be needed to put the system into full production.

Figure 2.3.2.3.16 – Photo of reel-to-reel Ic test system for thick clad product.

Insulation of the clad conductor used the same process and equipment that SPX has used to insulate their copper wire for decades. All new development was around handling of the bonded conductor and payoffs / takeups. US Machinery, the original manufacturer refurbished SuperPower's unit that it had acquired from SPX. Polyester based insulating tape supplied by SPX is used. The tape has a porous construction to allow N2 to pass through it to the conductor. The machine was installed at SuperPower (Figures 2.3.2.3.17, 2.3.2.3.18) and personnel trained \(by SPX trainer) and unit debugged for production use. Payoffs and Takeups were built (or ordered) to accommodate the large diameter spools. Long lengths of both copper strip dummy and clad HTS product were successfully insulated using this equipment.

Handling and shipping of the large diameter spools (28" ID minimum, 50" (1.27 meter) OD to hold 400 meters) required the development of special handling equipment and shipping containers. Examples of this equipment are shown in Figure 2.3.2.3.19 and a typical shipping container is shown in Figure 2.3.2.3.20. Multiple spools would be inserted into each of these boxes.

Figure 2.3.2.3.17 – Photo of reel-to-reel insulation system used to insulate thick clad product.

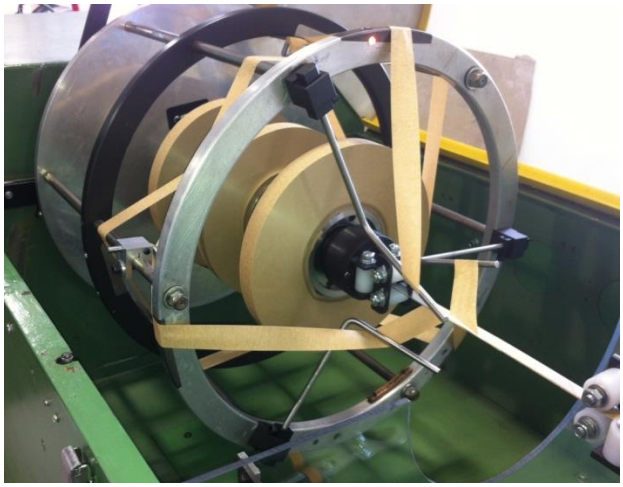

Figure 2.3.2.3.18 – Photo of taping head applying three of total six insulation layers on clad conductor.

Figure 2.3.2.3.19 – Photo of handling equipment developed for the large spools carrying final insulated, clad product. \

Figure 2.3.2.3.20 – Photo of large diameter spool with final insulated condicutro in shipping box. Up to 6 spools could be shipped per box.

In order to use the conductor in the coils, we needed to develop methodology and associated tooling for creating terminations of bonded HTS for attachment to conventional copper terminals and wires. For the terminations, we needed to enable two conductor pigtails to be joined and secured outside of the winding. These would be soldered together to obtain good electrical connection. These pig-tails were then encased in a jacket to maintain joint strength and allow the jacket to be secured to the transformer support structures.. After multiple iterations, the design was proven, including design adjustments with SPX involvement, and then integrated with the transformer support structure and manufacturing processes. Examples of the termination design are shown in Figures 2.3.2.3.21 a/b

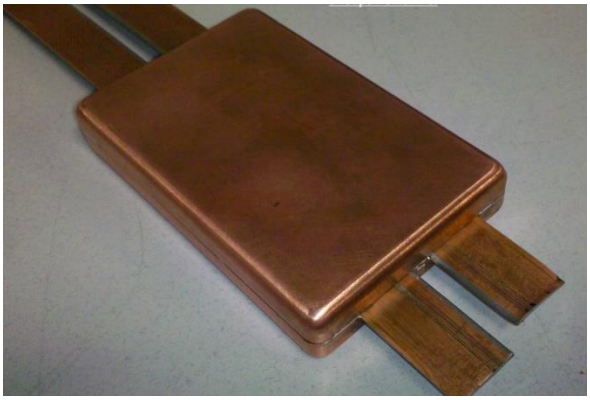

Figure 2.3.2.3.21 – a) Prototype termination, b) examples of terminations incorporated on test winding.

Improving Ic and lengths of run of HTS conductor

Development and utilization of premixed liquid precursor

The process for creating the critical HTS layer at SuperPower is done using metal organic chemical vapor deposition (MOCVD) processing. Current methodology for preparing the precursor was to mix the combination of ingredients by weight which are purchased in the powder form together in a solvent (THF) at SuperPower. This process was typically performed just prior to the production run, and the precursor was kept in an agitated state until utilized. The batches are 3-4 liters each and during the course of a typical 1000 m production run, multiple batches would be consumed depending on the type of product being processed. Some of the perceived opportunities for improvement to this process were to have the vendor pre-mix the precursor at its facility, in a N2 environment, and sample and adjust content according to desired ratio of chemical, instead of by weight of dry powders. This could be done by using ICP to analyze the large batch, and then add small amounts of required chemical to bring batch into overall specification The quantity/batch would be in the range of 250 liters. This was hoped to give a far more consistent ratio of chemical from batch to batch, and also eliminate any possible contamination from atmospheric air.

In order for Superpower to implement this technology, a couple of changes were also required on the precursor delivery system to the production machine. Present methodology is to pump precursor into the evaporator chamber, via mechanical pumps. The premixed liquid precursor was shipped in pressurized vessels, and thus could be transferred to the evaporator by means of pressurized gas.

Other issues which required attention were handling systems for the larger bulk vessels and creating a methodology for purging the system with pure THF at completion of runs. These were relatively straight forward task, but never the less were needed in order for the system to operate.

During the project (Phase 3) 750 liters of liquid precursor were order and evaluated. Based on typical usage, this would equate to ~ 6km of finished product. Multiple scenarios were set up to evaluate the performance of it compared to the traditional method, and spread out over a 4 month time span to insure we had representative data, and were not influenced by singular events.
Since the overall HTS manufacturing process is heavily influenced by each of its core processes, it was not reasonably feasible to create a Design of Experiments (DOE)to cover all eventualities. Therefore an abridged approach was taken, and many characteristics and influencers were considered in when, where and how much to use in comparing the liquid to our traditional approach.

Results showed slight, but unremarkable improvements. Statistically insignificant is the mathematical term for the outcome of the overall study compared to existing process and methodology. We did however make the following gains in output based on the study:
Were able to see noted improvement from going from pumped liquid to pressurized fed liquid, and have since adapted that as our primary conveyance method. We were able to see more consistency in select runs (even though there may not have been improvement due to other factors outside of the precursor) The data showed only a minor improvement, however there was an overall sense that the process was better using the liquid and with more time and samples, we feel we could show this. Lastly cost must be considered in this equation. There is extra cost associated with having our vendor prepare and ship the product in this manner. When you factor in this added cost, versus the minor improvement, it would tend to favor our traditional method for the most cost effective solution.

Development and implementation of 30 micron Hastelloy substrate as the base material for the HTS tape (currently using 50 micron Hastelloy)

In order to process longer continuous length of HTS, one of the limiting factors at SuperPower is reel size capacity within its IBAD system. As this is a key operation, and also has a substantial setup and pump down cycle that must be amortized into the cost of the operation, the ability to process more tape in one set up gives us multiple advantages. Moving from 50 micron to 30 micron thick Hastelloy substrate allows us to run 40% more tape/setup, as well as having 40% more tape/reel. During finishing operations, the likelihood of having longer lengths available to the final operations goes up significantly, thus improving yield lengths of final product. The challenges of going to a 40% reduction in substrate thickness are many fold and the major ones are listed below:

- Handling and tension studies needed to be performed at each operation, with operational characteristics (heating temperatures) factored in
- The very first operation, electropolishing is key to establishing a good foundation for the rest of the subsequent processes.

- Trials with the 30 micron tape required multiple iterations of metallurgical and process changes from our vendor, and then evaluation through our processes, to narrow in on what would be an acceptance criterion that would yield good product.
- In some cases, the vendor did not have the capability to measure the specific attributes that we required,and necessitated SP doing the analysis and feeding it back real time, while the vendor held their processing line until they received the information from us. This proved to be costly and time consuming, but in the end has shown tremendous promise.
- After 10+ iterations of vendor process tweaks, we have been getting solid results (as good and better than our standard 50 micron tape), and are pursuing offering this a commercial product.
- Subsequent process development trials on every process were required to establish optimized process parameters with the thinner tape.

Besides giving us the added length and capacity improvements, in certain applications, where current density (Je) is critical, this product offers a significant improvement over our standard 50 micron offering. The FCL transformer in this project is not an application who would readily benefit from this attribute due to the 1mm thick bonded substrate, which would overshadow the difference between 30 and 50 microns of HTS, however future transformers with a different design could potentially take advantage of this characteristic.

2.3.3 Cryogenics development

The development of the cryogenic system was a SPX lead item and is described in more detail in Appendix 1. In Phase 3, work was conducted at SuperPower looking at the cooling structure required in the windings to provide sufficient LN2 flow through the windings, particularly during fault conditions. An example of the resulting winding structure is shown in Figure 2.3.3.1. The windings contained a corrugated support structure that provided cooling channels along the axis of the coil.

2.3.4 Systems integration

Initial trials of winding a full size coil with dummy conductor were initiated at SPX with input from SuperPower towards the end of Phase 2. These winding trials were proceeding well when SPX pulled out of the Project. Figures 2.3.4.1 and 2.3.4.2 show the progress on the initial winding trials before they were halted. Prototype LV windings were being trialed with 10 conductors being used in parallel.

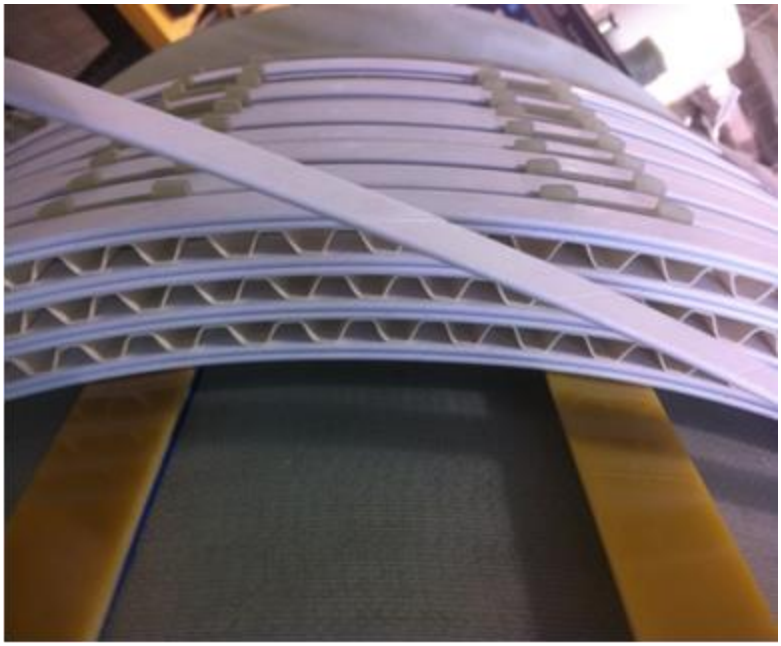

Figure 2.3.3.1 – Prototype HV coil module using spaced windings to enhance LN2 cooling of the FCL transformer windings.

Figure 2.3.4.1 – Prototype LV windings being conducted at SPX with dummy conductor insulated at SuperPower. Photo shows the payoff system for the 10 tapes being wound in parallel.

Figure 2.3.4.2 – Prototype LV coil former on winding machine at SPX ready for winding trials using 10 parallel tapes. Inset shows an LV interconnect attached to the conductor.

2.4 Project baselining.

This was an SPX centric task and is covered in their report in Appendix 1.

3.1-3.3 Alpha unit final design, fabrication and test

Other than some initial SPX final design work (see Appendix 1), these tasks were not completed in the project due to the withdrawal of SPX from the program.

4.1-4.3 Beta unit final design, fabrication and test

Other than some initial SPX final design work (see Appendix 1), these tasks were not completed in the project due to the withdrawal of SPX from the program

4.4 Installation of Beta demonstration unit in host utility switchyard.

Initial meetings and installation plan discussions culminated in a meeting in late March, 2014 with SCE on the placement and cooling support systems for the eventual 3-phase beta unit install. Members of the team from SPX and SuperPower toured the SCE MacArthur substation (Figure 4.4.1) and identified the location where the device would be placed and the refrigeration support requirements (Figure 4.4.2). This included discussions with a local Praxair representative. The team also discussed the electrical connection, communication and construction requirements. The team participated in an SCE project planning meeting and discussed schedule. SCE had initiated the construction plans for final bids for the rerouting of primary and secondary circuits, trenching for cable and refrigeration piping and the pouring of concrete pads.

SPX pulled out of the project a few weeks later obviating the need for further work in this area.

Figure 4.4.1 – Members of the SCE, SuperPower and SPX teams touring the SCE MacArthur substation during March, 2014.

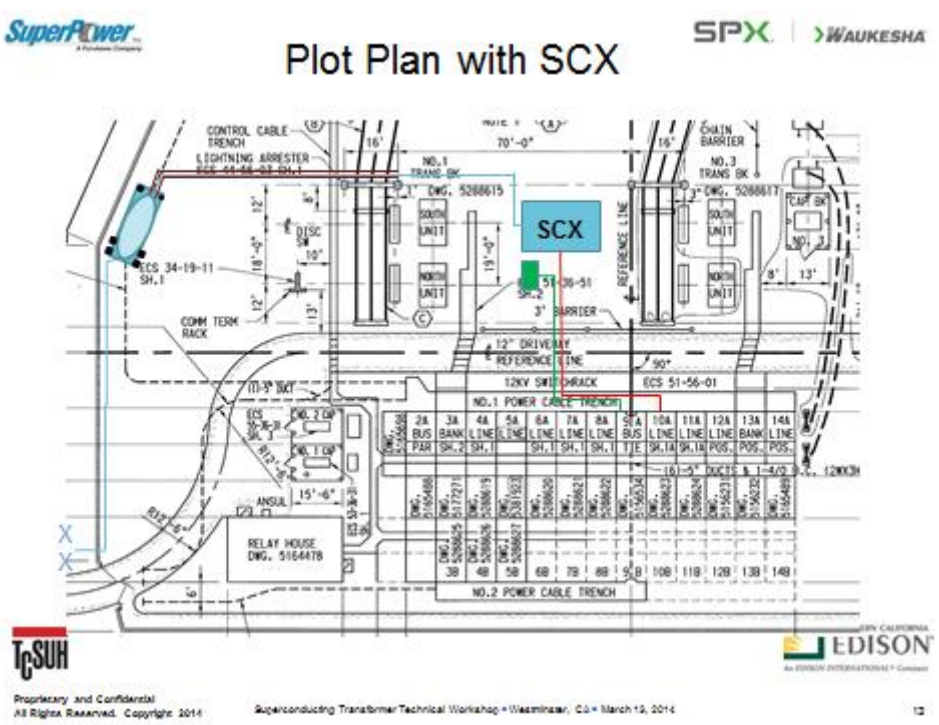

Figure 4.4.2 – Plot plan of the SCE MacArthur substation showing the proposed placement of the 3-phase beta prototype and location of auxiliary LN2 trailer.

5.1 Long term demonstration on the host utility grid.

This task was not completed with the pull out of SPX from the program.

3.0 Publications / Conferences / Awards

- Work on the bonding line was presented at the 2016 Applied Superconductivity Conference (ASC 2016 - Sept 2016 / Denver, CO) as presentation 4LPo2K-06 [Development of 2G HTS conductor for a FCL Transformer]. Copies of the presentation are included in Appendix 3.

- Work on the bonding line and thinner substrates was presented at the 2016 Coated Conductors for Applications (CCA 2016 – Sept 2016 / Aspen CO) workshop as presentation IO-14 [.2G HTS Wire Development at SuperPower]. Copies of the presentation are included in Appendix 3.

- In September 2015, SuperPower announced the availability of a large coil ac loss test facility based on technology developed under this program. See [http://www.superpower-inc.com/content/superpower-adds-new-ac-loss-coil-test-facility].

4.0 Conclusions

Critical conductor technologies have been demonstrated towards the future use in FCL transformers. It has been demonstrated that a clad conductor architecture can provide the mechanical strength and target normal state resistance required in order to operate in the FCL transformer and cryogenic environment. AC losses in the system will require ongoing reduction through advances in the conductor fabrication, (filamentation to handle hysteretic loss, transposition to handle coupling loss) but clear paths have been demonstrated to reach these goals. Long length fabrication (>400 m) of the clad conductor has been demonstrated including inspection, insulation and handling.

Functional transformer designs were developed and critical technology demonstrated for using HTS conductors in the windings of a FCL transformer. Winding approaches used in both the LV and HV windings have been demonstrated using conventional winding techniques as much as possible. The FCL transformer design has successfully incorporated the cryogenic cooling aspects required for system operation. Cooling channels have been successfully incorporated in the windings on a subscale HV test module. This module was used for the successful FCL demonstration tests and coil ac loss measurements. Siting issues with a utility were vetted and approaches developed that were satisfactory to all parties.

The conductor fabrication and FCL transformer winding processes have been developed sufficiently that a future FCL transformer project can be considered that can lead to commercial units. With conductor prices expected to continue to drop and more compact cryocooling options becoming available, the commercial viability of FCL transformers can become more attractive in the future.

5.0 Recommended next steps

For the next steps, it is recommended that further demonstration and development projects be undertaken to validate the technology and to incorporate advances in conductor and cryogenic cooling. In particular, we should evaluate the potential use of cables HTS conductors for the LV, high current windings. Advances in this area over the past 5 years make this a viable approach for this application.

We continue to discuss going forward with this technology with manufacturers of transformers and other substation equipment. The benefits of a FCL transformer are recognized, but the utility industry has been slow to adopt it without significant runtime data. Future demonstrations and ptrototypes will provide this data that will enable this technology to begin to enter the marketplace.

[end of report]

.

Appendix 1

SPX Final Report

SPX Transformer Solutions Inc.

PROJECT REPORT - Fault Current Limiting Superconducting Transformer

08/01/2014 Raj Ahuja

1. **OBJECTIVES**:

The project objective was to design, develop, manufacture and install 28 MVA 70.5/12.47 KV Three Phase superconducting transformer with fault current limiting (FCL) capability. Due to lack of assurance and prospect of near term commercially saleable product, SPX Transformer Solutions Inc. decided to discontinue working on the project and provided 60 day notice of termination of its participation on April 24, 2014.

2. Project activity completed by SPX Transformer Solutions Inc. from 2011 to April 24, 2014

- Conceptual design of HTS Transformer and development of key technologies
- Electrical Design, Mechanical design and test plan of a single phase "alpha" unit.
- Electrical Design and Mechanical Design of a three phase "beta" unit.

3. Conceptual Design and development of key technologies of HTS Transformer:

- The initial design procedure focuses on the electrical and mechanical specifications which the transformer must fulfil. At this stage, details such as tank geometry, bushing selection, and instrumentation are not considered. The transformer must function properly at the line voltages to which it is attached and must have a specified reactance in the circuit. It must also have sufficient cooling to limit temperatures within a specified range. The cooling is necessary to handle the electrical losses mainly due to eddy currents induced by the stray magnetic field. There are also small I^2R losses in the superconducting windings under normal operation.
- In addition to the steady-state normal operation requirements, the transformer must be designed to withstand possible lightning and switching surges appearing on the transmission lines without electrical breakdown. It must also be designed to withstand possible faults such as short circuits on the terminals or the attached transmission lines without mechanical breakdown. Because the fault currents can be quite high, they generate high forces and resulting mechanical stresses on the windings. There are various modes of mechanical breakdown which must be addressed in order that the windings suffer no permanent deformation.
- One of the first issues which it is necessary to address is the design of the winding conductor or wire. Since superconducting conductors are so thin, they lack adequate mechanical support to withstand the short circuit forces. Thus it was necessary to have

a sturdier conductor backing for the HTS film. This required some innovative research to get a thick enough backing material which could carry the current when the superconductor goes normal during a fault but one which has a high enough resistance that, when paralleled with the superconductor gone normal or partially normal, it limits the fault current sufficiently. A composite backing material was chosen of 1 mm thickness. The superconductor film itself is about 0.1 mm thick. Because of manufacturing constraints, the width of the HTS film was chosen to be 12 mm with the possibly of subdividing it in 4mm wide x 3, using a scribing procedure, to reduce the losses.

3.1 Optimization

The first step in the design is to run the optimization software which is subject to various constraints. This produces an initial starting design which is further refined when tested with additional more detailed design tools. Aside from the cable constraint mentioned above, additional constraints on the 3 phase design are:

Minimum MVA	28.0
Maximum MVA	40.6
Frequency (Hz)	60
HV Line-Line Voltage (kV)	70.5
LV Line-Line Voltage (kV)	12.47
HV Connection	Delta
LV Connection	Grounded Y
HV-LV Leakage Reactance (%)	13.0
Core Design	3 Phase Core-Form

2 Series Connected LV Windings were selected so that high current LV winding terminations are at the top of winding to facilitate reduction of Lead length and bushing connection.

There were also several inequality constraints such as upper limits on the flux density in the core and on the core radius.

As mentioned previously, the design was later tweaked. The evolution of the design can be seen in the comparison from the initial optimized design to the final adjusted design. The following shows the parameter comparison (units in mm):

Item	**Original**	**Final**
HV Voltage (kV)	70.5	68.8
Core electrical radius	265 (530 D)	280 (560D)
Window height	2100	2200
Winding height	1274	1320
Slack in window	826	880
Inner duct to core	71	98.5
Volts/turn	87.8	87.8
Flux Density	1.73	1.53
Leg center to center	1138	1220
Phase to Phase	134	155
LV conductors (#radial x #axial)	4 x 2	5 x 2

Inner LV inner radius (IR)	336	378.5
# Inner LV radial turns	1	1
# Inner LV cooling ducts	1	0
Inner LV paper thickness	0.5	0.8
Inner LV radial build	11	10
# Turns inner LV	41	41
Gap between inner and outer LV	15	19
Outer LV IR	362	407.5
# Outer LV radial turns	1	1
# Outer LV cooling ducts	1	0
Outer LV paper thickness	0.5	0.8
Outer LV radial build	11	10
# Turns outer LV	41	41
Gap between Outer LV and HV	97	90
HV IR	470	507.5
HV conductors (#radial x #axial)	1 x 1	1 x 1
# HV radial turns	12	11
# HV cooling ducts	2	0
HV paper thickness	0.8	1.0
HV radial build	32	25
# Turns HV	803	783
HV outer radius (OR)	502	532.5 (1065D)

Parameters not mentioned in the above comparison have remained the same. This includes the line-line voltage and the leakage reactance.

3.2 Leakage Reactance:

The leakage reactance at 28 MVA was calculated with our detailed flux mapping code. The winding currents were: LV Inner and outer winding -1296.4 Amps, HV 135.76 Amps. These are rms currents. These currents insured proper Amp-turn balance in the windings. The reactance obtained was 12.77 %. This can be converted to Ohms on the HV or LV side of the transformer by using the base impedance associated with either winding.

3.3 Fault Current Calculations:

Fault currents are applied suddenly on the transformer. From an analysis of the fault circuit, this sudden application results in a current overshoot, called the asymmetry factor. This factor depends on the ratio of reactance/resistance and is defined as the peak current at overshoot divided by the steady state rms current. Thus if there is no overshoot, this factor would be $\sqrt{2}$. For our purposes, we prefer to work with a modified asymmetry factor which is 1.0 for the case where there is no overshoot. During the short circuit, we expect the resistance to exceed the reactance. The smaller the reactance/resistance ratio, the closer the asymmetry factor is to 1.0. We have chosen to calculate the maximum fault

currents for an asymmetry factor of 1.25. For a single line to ground fault on the LV terminal, which is usually the most severe, the fault currents are: LV inner and outer winding: -12779.2 Amps, HV winding 1338.3 Amps. These are rms currents and achieve Amp-turn balance. Comparing with the normal currents, given for the leakage reactance calculation above, these currents are about a factor of 10 higher. Because of the imbalanced fault type, there is a ground current of 12952.6 Amps. The grounding cable needs to accommodate this current without overheating.

3.4 Force and Mechanical Stress Calculation:

Using the fault currents calculated above, we calculated the maximum forces and stresses on the windings and winding constraints. Since the maximum forces depend on the peak currents, the fault currents were multiplied by $\sqrt{2}$ or equivalently the forces were multiplied by 2 using the rms fault currents. This is because the forces depend on the square of the currents.

The Young's modulus of the backing material of 1.586×10^5 MPa was used in the stress calculations. This is much higher than the modulus for copper of 1.10×10^5 MPa. Also the proof stress of the backing material was 165 MPa compared with the proof stress of normal copper of 83 MPa. The proof stress as used here is the stress which would produce a 0.2 % permanent deformation in the material when the stress is relieved. Since such dimensional changes can accumulate over a series of faults, the calculated fault stresses should be below this value with some margin. The calculated maximum stresses, which must be within established limits, are listed below in MPa. The coils are numbered from the core outward with 1 = LV Inner, 2 = LV Outer, 3 = HV.

	Coil	Stress	Limit	
Hoop Stress	1	-18	157	
	2	-58	157	
	3	51	157	
Comment	A tensile stress is positive and a compressive stress is negative.			
Buckling Stress	1	83	Must be > Absolute Value of Hoop stress	
	2	72	Must be > Absolute Value of Hoop stress	
Comment	Buckling only occurs for windings under compressive stress. The value is determined by the wire dimensions, the winding radius, and the stress-strain curve of the wire material.			
Radial Bending Stress	1	33	Must be < Proof Stress = 165	
	2	110	Must be < Proof Stress = 165	

Comment This is an inward bending which only occurs for windings under compressive stress.

Axial Bending Stress	1	5	Must be < Proof Stress = 165
	2	6	Must be < Proof Stress = 165
	3	7	Must be < Proof Stress = 165

Comment This is a bending of the cable considered as a beam between the key spacers acting as supports and is due to an axial force.

	Coil	**Stress**	**Limit**
Compressive Stress on Spacers	1	11	80
	2	9	80
	3	11	80

Tilting Strength	1	2.43	Must be > 1
	2	2.87	Must be > 1
	3	1.42	Must be > 1

Comment The limit is not strictly a stress but a ratio of forces. It is determined by calculating the axial pressure acting on the wire strands which would lead to tilting and multiplying this by the area occupied by the wire strands for one turn of the winding. This resulting force is divided by the maximum axial compressive force acting at some position along the winding. The resulting ratio must be > 1 to avoid tilting.

In addition to the winding stresses and forces, there are also forces on the winding supporting structures such as the tie (flitch) bars and the compression rings. These were all well within the limits as were all the winding stresses.

3.5 Impulse Calculations:

The impulse calculation uses an applied voltage pulse on a transformer terminal with a shape characteristic of a lightning strike. This pulse has a steeply rising front followed by a gradually declining tail. The pulse rises to the BIL level (basic impulse level) of the terminal. This is called a full wave impulse. Another version chops the tail of the wave abruptly after a short time. This is called a chopped wave impulse. For the latter type of impulse, the initial pulse rises to 10 % above the BIL level so it is sometimes considered a more severe case. However, due to oscillations in the resulting voltages at various parts of the windings, either type could be more severe. The simulation program considers capacitances between various parts of each winding and between windings and windings to core or to tank. It also considers inductances and mutual inductances for various subdivisions of each winding and between subdivisions on different windings. Winding resistances are also included. In the following, we calculate the both types of impulse on the HV terminal. The BIL level of this terminal is 350 kV. Only the maximum electrical voltages and stresses are given.

	Voltage Across Gaps (kV)		Oil Stress in Gaps (kV/mm)	
Gap #	**Full Wave**	**Chopped Wave**	**Full Wave**	**Chopped**
Wave				
1	20.3	30.4	0.3	0.4
2	35.7	43.5	2.0	2.5
3	457.6	385.0	6.0	5.0
4	451.1	385.0	3.2	2.7

Comment: Gap 1 is between the innermost winding and the core and gap 4 is between the outermost winding and the tank. Since the stresses are what can lead to oil breakdown, there are only upper limits on the stresses. For the gaps the stress limit is 16 kV/mm.

	Voltages Between Disks (kV)		Stresses Between Disks (kV/mm)		
Coil #	**Full Wave**	**Chopped**	**Full Wave**	**Chopped**	**Limit**
1	4.4	7.4	1.8	3.1	31.6
2	4.0	6.8	1.7	2.8	31.6
3	55.9	63.8	12.4	14.1	24.6

Comment: These voltages and stresses are between adjacent disk pairs. The limit is only on the stresses since these can lead to breakdown of the oil.

	Inner Corner Stress(kV/mm)		Outer Corner Stress (kV/mm)		
Coil #	**Full Wave**	**Chopped**	**Full Wave**	**Chopped**	**Limit**
1	1.9	3.2	2.7	4.0	33
2	2.8	3.8	6.6	4.6	33
3	16.0	18.3	15.2	17.4	33

Comment: These stresses occur at the corners of the rectangular cross-section disks. Since the disks have a paper cover, the stresses occur in the oil outside the paper. This mitigates the sharpness of the corner.

From the above all the stresses are within the limits. It should be noted that 2 pairs of disks at either end of the HV winding were fitted with wound-in-shields in order to increase the disk to disk capacitance and reduce the voltage stresses at the coil ends.

3.6 Losses:

The losses investigated here were the eddy current losses in the backing material due to stray flux from the rated current in the superconducting layer. Since the backing material has no current during rated operation, there are no I^2R losses. The losses in the HTS superconductor are due to the current they carry as well as to the stray flux. These are obtained by other means and are reported elsewhere. We obtained the losses in the backing material with our flux mapping program. These losses also depend on the resistivity of the backing material at liquid nitrogen temperatures. We estimate this to be

$\rho_{backing} = 0.0426 \times 10^{-8}$. We obtained the LV winding losses for all 3 phases of 80 Watts. The HV winding loss for all 3 phases was also 80 Watts. Thus the total eddy current loss in the backing was 0.16 kW.
There were essentially no stray losses due to the fact that the coils are sitting in a fiberglass containment vessel filled with liquid nitrogen and with non-metallic supports. Including the superconductor losses, the total loss which must be dissipated through cooling is about 8 kW.

3.7 Cooling:

The preferred cooling option is to use cryo-coolers so this method was analyzed. In this method of cooling, the liquid nitrogen is pumped but it is not specifically directed into the windings. However, we assumed that about 10 % of the pumped flow volume would enter the windings. The rest of the winding flow would be thermo-siphon flow, which is buoyancy driven. Since the appropriate pumped flow rate was unknown, several different flow rates were tried in order to see which one gave acceptable temperature rises. A reasonable flow rate appeared to be 40 liters/min. This flow could be subdivided among more than one cooler. We assumed a base temperature of 70 °K = -203 °C. The top liquid nitrogen temperature rise above the base obtained was 7.2 °C and the average LN2 rise was 3.6 °C. The individual average winding rises were 4.3, 4.2, and 4.5 °C for coils 1, 2, 3 respectively. The maximum temperature rise for the 3 coils was 8.5, 8.4, and 8.7 °C. These rises should not be high enough to create bubbles in the LN2.

4. Study on Effect of Fault Current Caused by the Superconductor to Normal Transition:

Fault circuit model:

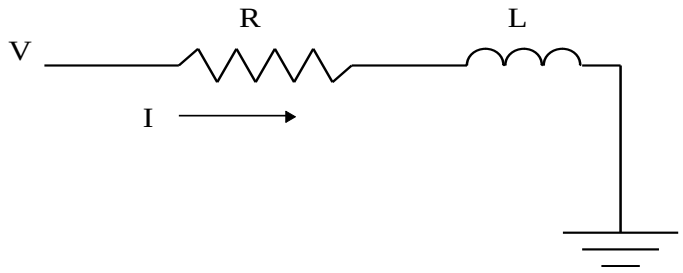

Circuit differential equation:

$$V_p \, sin(\omega t + \varphi) = RI + L\frac{dI}{dt}$$

V_p = peak voltage
I = current
$\omega = 2\pi f$, f = frequency

ϕ = phase angle
R = resistance
L = leakage inductance = X/ ω, X = leakage reactance

Normally L and R are constants but we want to allow R to vary as the superconductor goes normal. Also the superconductor is in parallel with a normal conductor for both the HV and LV windings.
We will view the transformer from the HV side of the circuit. Letting N_1 be the number of HV turns, N_2 the number of LV turns and R_1 the HV winding resistance, R_2 the LV winding resistance, the circuit resistance in the above equation is

$$R = R_1 + R_2\left(\frac{N_1}{N_2}\right)^2$$

We also have

$$R_1 = \frac{R_{c1}R_{s1}}{R_{c1}+R_{s1}} \quad , \quad R_2 = \frac{R_{c2}R_{s2}}{R_{c2}+R_{s2}}$$

where R_{c1} and R_{s1} are the resistances of the metallic conductor and the superconductor which are in parallel in the HV winding (winding 1) and similarly for the LV winding (winding 2).
We note that initially, before the fault occurs, the superconductor resistances are very low since the operating currents are designed to be below the critical current. Therefore R_{s1} is much less than R_{c1} and similarly for R_{s2} and R_{c2}. Thus the last equation implies that $R_1 = R_{s1}$ and $R_2 = R_{s2}$. However, after the fault occurs, if the fault currents in the HV and LV are sufficiently high, the superconductors will go normal and their resistances become very large compared with the metallic conductor resistances. In this case, the last equation shows that $R_1 = R_{c1}$ and $R_2 = R_{c2}$.
In the transition region between the superconductor's critical current and its quench current, a useful model of the superconductor's resistance is needed. This will probably require a complicated calculation or be based on test results. For the purposes of this study, we will use several models to assess how they affect the short circuit current. More realistic models may be used as future information becomes available. We assume the superconductor's resistance in the transition region varies according to:

$$R_s = A_0 \quad , \quad I_s \le I_{crit} \qquad \text{Models 1 and 2}$$

Model 1

$$R_s = A_0 + A_1\left(\frac{I_s - I_{crit}}{I_{crit}}\right)^n \quad , \quad I_s > I_{crit}$$

Model 2

$$R_s = A_0 + A_1 \tan\left[\frac{\pi}{2}\left(\frac{I_s - I_{crit}}{I_{quench} - I_{crit}}\right)\right] \quad , \quad I_{crit} < I_s < I_{quench}$$

Model 3

$$R_s = A_0 \qquad , \quad I \le I_{quench}$$
$$R_s = R_{quench} \qquad , \quad I > I_{quench}$$

Here A_0 is the initial superconductor resistance, assumed very low. A_1 and n should be chosen so that R_s becomes very large when the current, I_s, reaches the quench current. I_s is the current in the superconductor. R_{quench} is a high resistance for the superconductor when it becomes normal.

When $A_1 = 1$, the superconductor resistances given above are assumed to apply to a single strand and we will take them to mean resistances per unit length. Since the strands in both the HV and LV windings have the same cross-section, the actual resistance for an HV or LV strand will be given by choosing A_1 to be the length of the strand or some multiple of the strand length

We will use one of these forms for R_s, along with the other resistance equations, to solve the differential equation governing the fault current. We use a Runge-Kutta method to solve the differential equation. The variable resistance can be accommodated as the fault current changes in time.

At this point, we need to insert some numerical values in the above equations. Although the fault is assumed to occur on the LV side of the transformer, we are viewing it from the HV side. The HV rms voltage is 70,500 volts and the peak voltage V_p is $\sqrt{2}$ times the rms voltage. It turns out that the maximum offset current occurs when $\varphi = 0°$ so this is what will be used. From the optimization program, the HV and LV turns were obtained. Also the lengths of the HV and LV conductors were obtained. The HV conductor metallic part had a cross-sectional area of 12 mm × 1 mm and the LV conductor cross-sectional area was 8 × 12 mm × 1 mm since it had 8 strands in parallel. Assuming an effective resistivity of the metallic conductors of 1.95×10^{-7} at 70 °K, the metallic resistances can be calculated. Thus, we have

V_p = 99,702 volts, $\phi = 0°$, f = 60 Hz
L_1 = 2434 m, L_2 = 177 m, R_1 = 39.47 Ω, R_2 = 0.362 Ω

Assuming only the metallic resistances, we get

$$R = R_1 + R_2\left(\frac{N_1}{N_2}\right)^2 = 39.47 + 0.362\left(\frac{802}{82}\right)^2 = 74.0\,\Omega$$

where the HV and LV turns have been inserted.

We also need the leakage inductance. This can be obtained from the transformer's rated reactance at 28 MVA. This is 13.07 %. The base reactance on the HV side is 532.53 Ω. Thus X = 0.1307 × 532.53 = 69.6 Ω and therefore

$L = X/\omega = 0.1846$ Henrys

For the superconductor's transition resistance, we assume

$A_0 = 0.001$, $A_1 = 10L_1$, $10L_2$ for Model 1, $A_1 = L_1$, L_2 for Model 2
$n = 2$, $I_{crit} = 425$ Amps, $I_{quench} \sim 3.5 \times I_{crit}$, $R_{quench} = 20 \times R = 1480\ \Omega$

The quench resistance was chosen to be sufficiently high so that the bulk of the current would transition to the metallic resistance in parallel. We also note that the HV winding is made up of one conductor strand, whereas the LV winding has 8 strands in parallel. This means that the phase current entering the HV winding all goes into the single strand, but the phase current entering the LV winding is equally divided among the 8 strands, assuming they are transposed sufficiently. Also the superconductor resistance of the LV winding is the single strand resistance given in the formulas above, divided by 8 since the 8 strands are in parallel.

The HV voltage is the same for all the cases studied and varies in time as shown in Figure

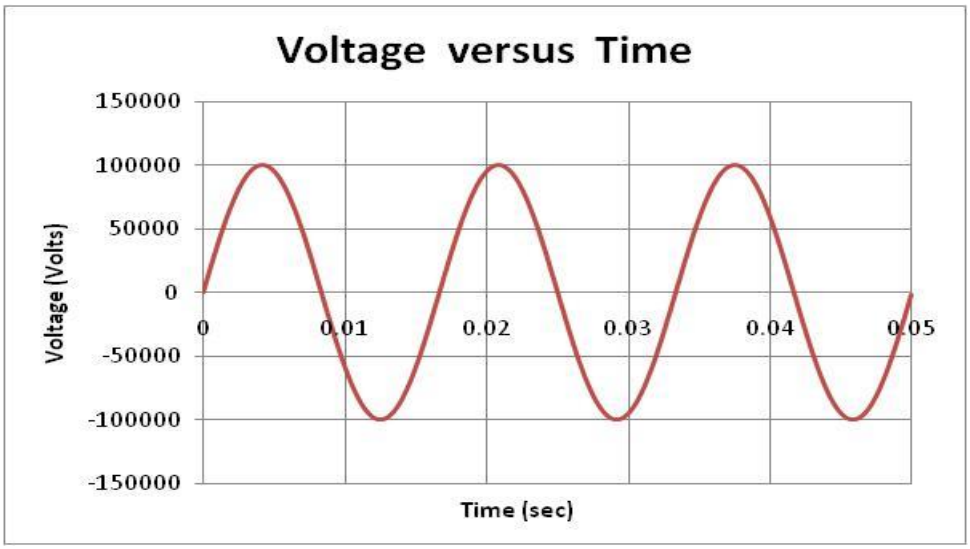

1.

Figure 1 Voltage driving the fault on the high voltage side versus time

The differential equation was solved for the case where $R = 0.1 \times X$, or $X/R = 10$. This is a typical case for large power transformers. The current wave form is shown in Figure 2.

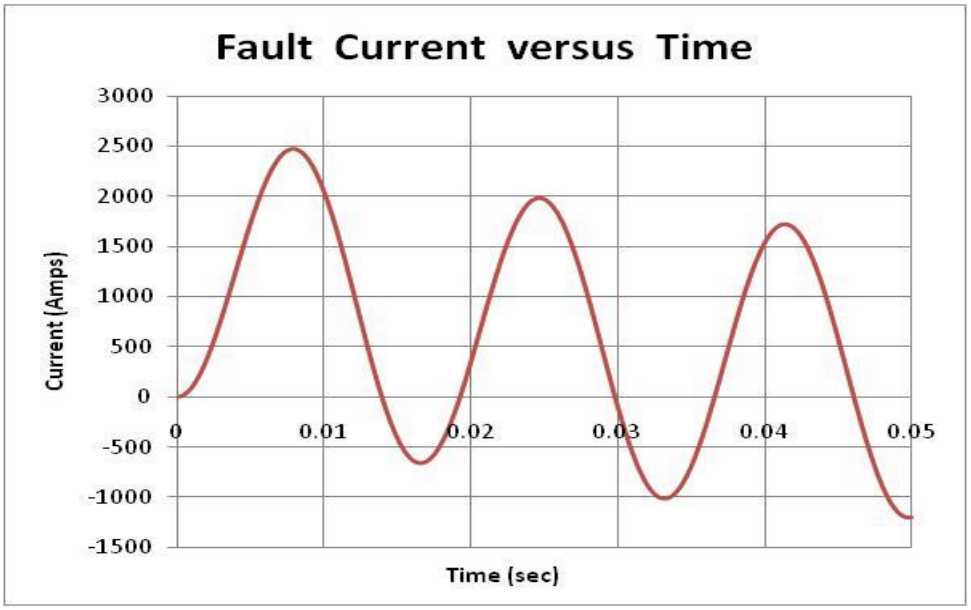

Figure 2 Fault current in the HV winding with X/R = 10

Note that the peak steady state current is given by

$$I_{p,ss} = \frac{V_{p,ss}}{\sqrt{X^2 + R^2}}$$

where p,ss labels peak steady state quantities, R and X are the steady state resistance and reactance respectively. The peak current divided by the peak steady state current is called the asymmetry factor. It is 1.737 for Figure 2.
Next the differential equation was solved for the case where $R = A_0 = 0.001\ \Omega$. This would be the case if the superconductor did not go normal. In this case X/R is very large. The HV short circuit current is shown in Figure 3.

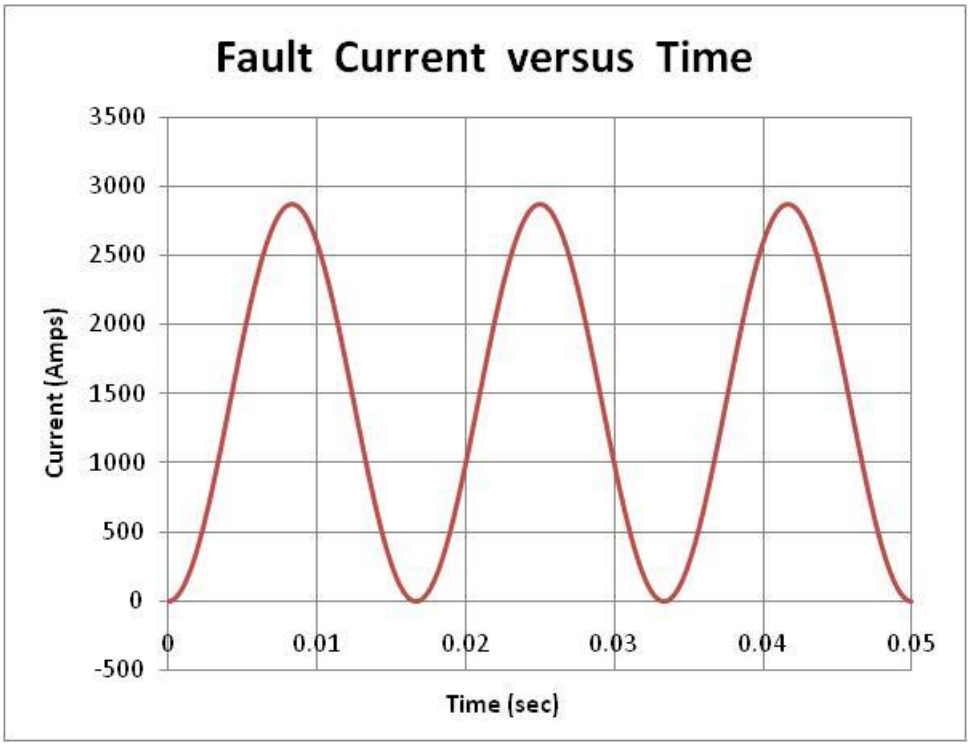

Figure 3 Fault current with circuit resistance = initial superconductor resistance (0.001 Ohms)

Figure 3 is the worst case situation where the steady state fault current is essentially only limited by the reactance in the circuit and the asymmetry factor is as large as possible, namely 2.0.
Next we examine the case where the resistances are due to the metallic component only so that R = 74.0 Ω. In this case X/R = 0.94.

The HV current is shown in Figure 4.

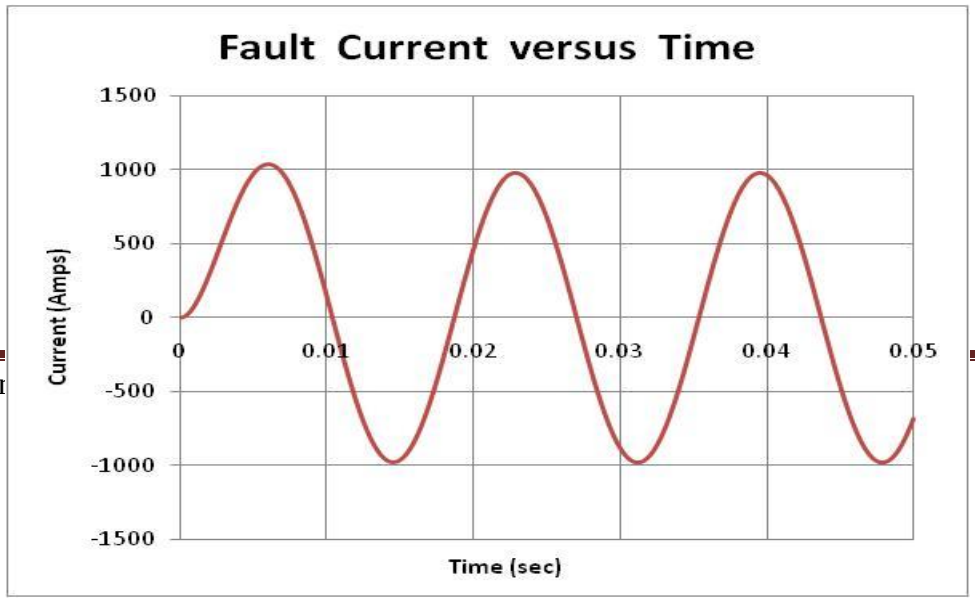

Figure 4 Fault current with the circuit resistance kept constant at its metallic conductor value (74 Ohms)

Figure 4 is the best possible case for the present transformer since the resistance is all due to the metallic conductor resistance and the asymmetry factor is therefore as low as it can get, namely 1.06.
We next examine the case where the superconductor's play a role in the transition region. We note that the LV current is given in terms of the HV current by

$$I_2 = I_1\left(\frac{N_1}{N_2}\right)$$

Since $N_1/N_2 = 9.78$, the LV current is almost a factor of 10 higher than the HV current. However, the current entering a single LV strand is $I_2/8$. We also note that these currents are shared between the superconducting and metallic resistances of their respective winding according to

$$I_{s1} = I_1\left(\frac{R_{c1}}{R_{c1}+R_{s1}}\right) \quad , \quad I_{c1} = I_1\left(\frac{R_{s1}}{R_{c1}+R_{s1}}\right)$$
$$I_{s2} = I_2\left(\frac{R_{c2}}{R_{c2}+R_{s2}}\right) \quad , \quad I_{c2} = I_2\left(\frac{R_{s2}}{R_{c2}+R_{s2}}\right)$$

Because the LV winding (winding 2) has 8 strands in parallel, the strand current is $I_{s2}/8$. Also R_{s2} in the above formula should be the single strand resistance divided by 8. The currents in the superconducting parts should be used in the transition region formula. The superconductor resistances are allowed to increase until they reach a maximum or until they increase to the quench resistance. After this, they remain at their maximum value. The superconductor resistances, as a ratio to the metallic resistance, and the overall circuit resistance are shown in Figures 5 and 6 for Model 1.

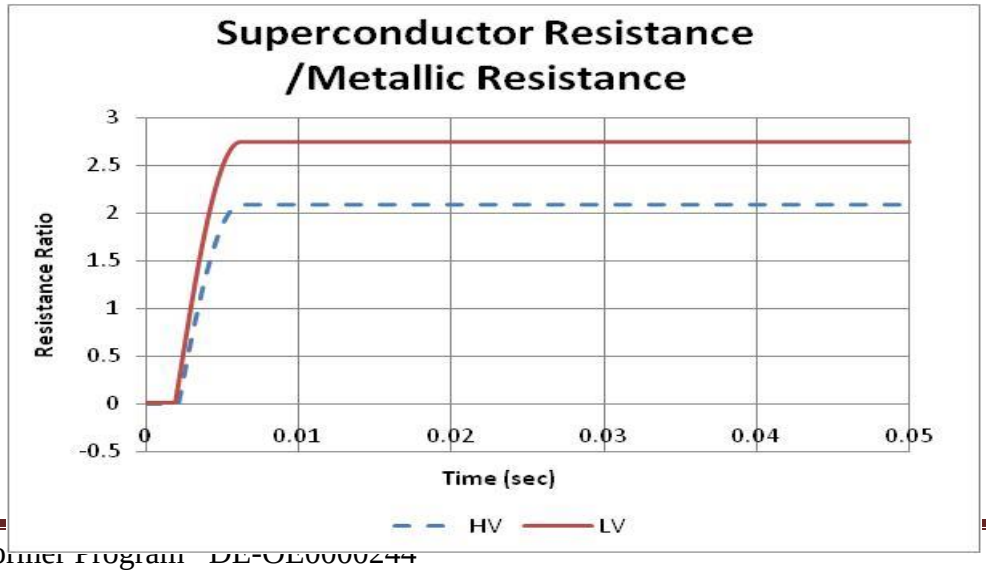

Figure 5 Resistance ratios of the HV and LV superconductors as they go through the

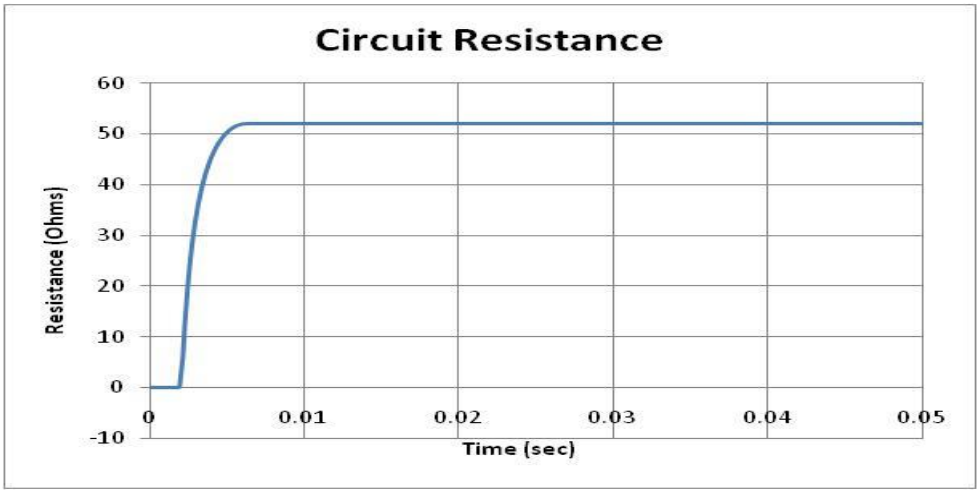

superconducting to normal transition during the fault using Model 1.

Figure 6 Circuit resistance as it varies during the fault due to the variable superconductor resistances using Model 1.

The short circuit current in the HV winding is shown in Figure 7.

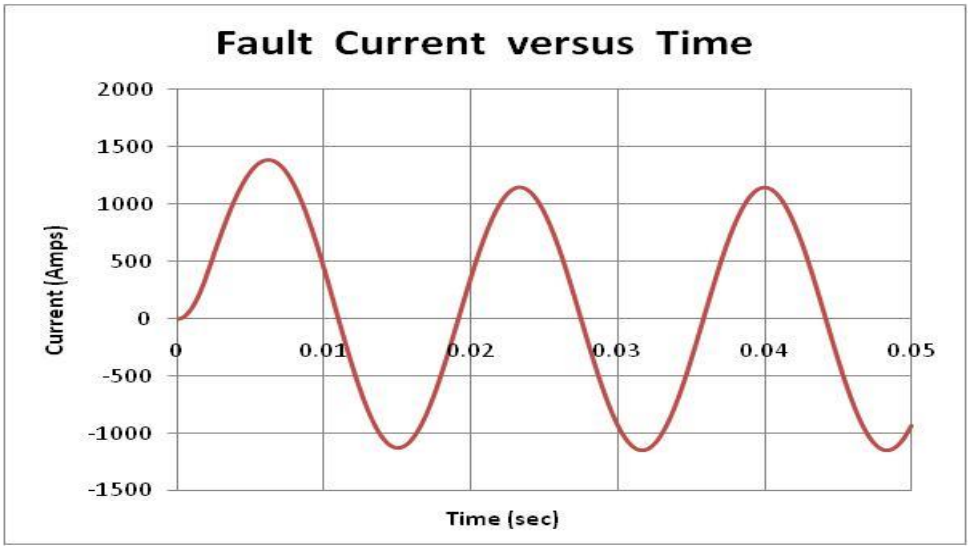

Figure 7 Fault current with variable resistances due to the superconductor to normal transition during the fault using Model 1.

We see that in Figure 5, the resistances do not go completely normal. This is because the fault currents subdivide between the superconductor and metallic resistances. Therefore, as the fault current in the superconductor increases, its resistance increases and this drives more current into the metallic resistance in parallel. This then limits the increase in the

fraction of the current going into the superconductor which prevents its resistance from rising. This results in a negative feedback on the rise in the superconductor resistance. It may be that, once triggered, the superconductor may inevitably go normal possibly due to thermal effects, in which case, the circuit resistance may achieve a higher value than shown in Figure 6. The circuit resistance is always limited to the metallic resistance of 74 Ω at 70 °K.

We also performed the analysis for the Model 2 case. The output is shown in the following figures 8 - 13.

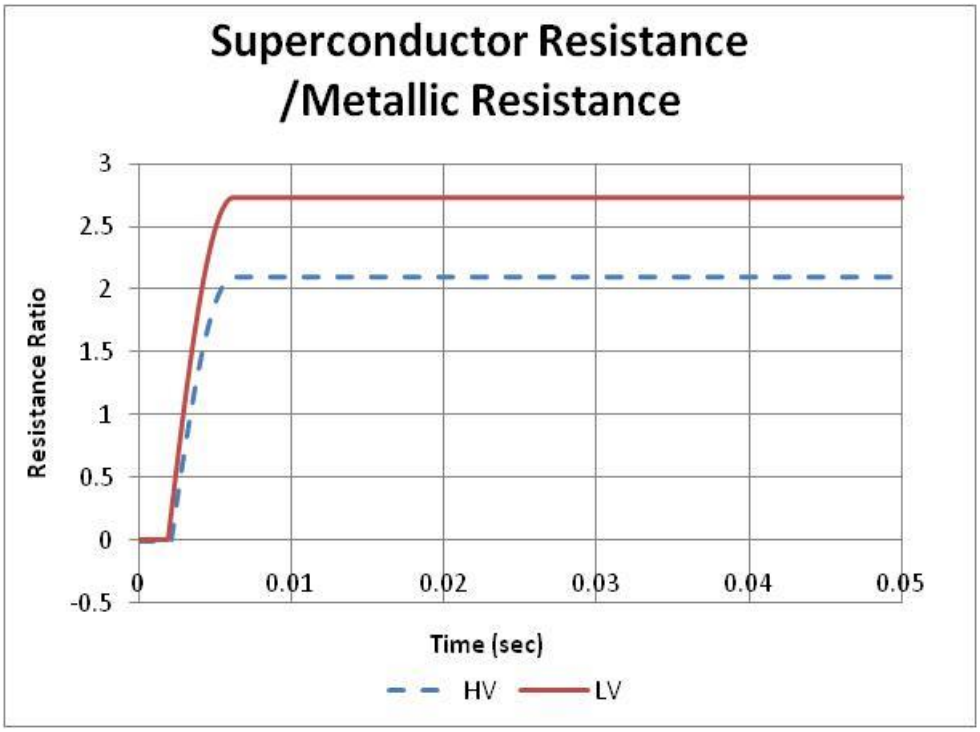

Figure 8 Resistance ratios of the HV and LV superconductors as they go through the superconducting to normal transition during the fault using Model 2.

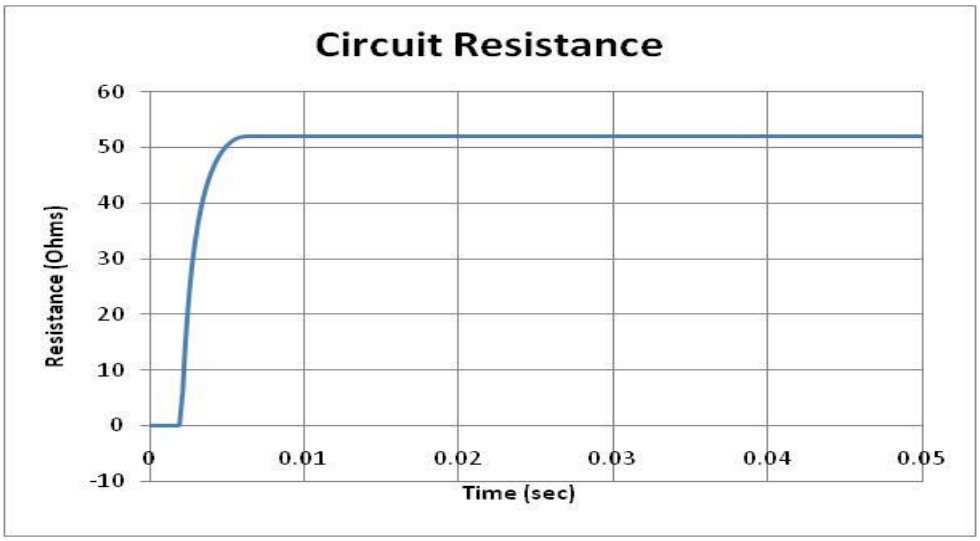

Figure 9 Circuit resistance as it varies during the fault due to the variable superconductor resistances using Model 2

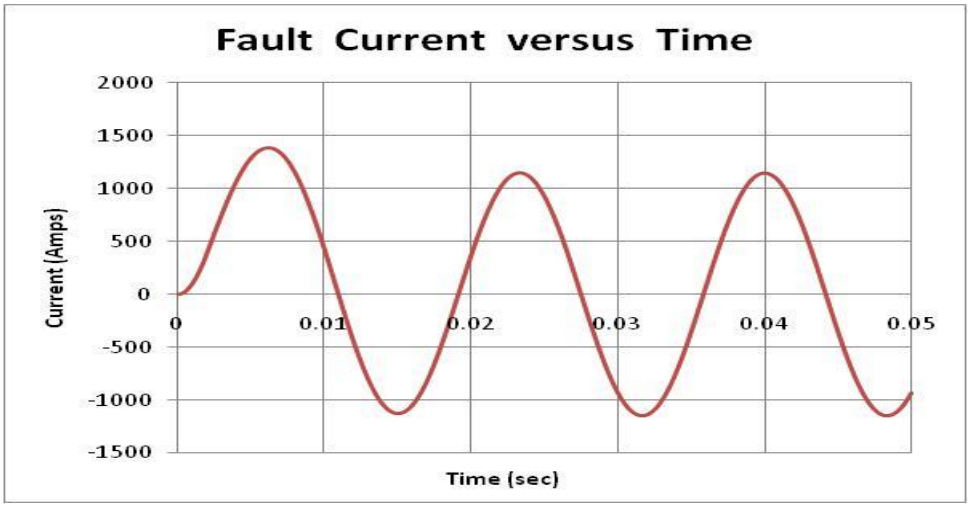

Figure 10 Fault current with variable resistances due to the superconductor to normal transition during the fault using Model 2.

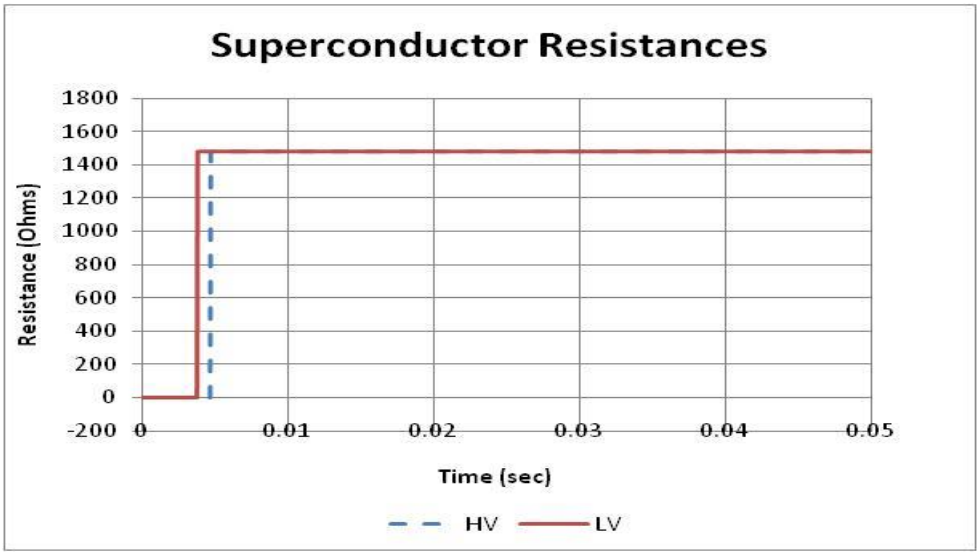

Figure 11 Resistances of the HV and LV superconductors as they go through the superconducting to normal transition during the fault using Model 3.

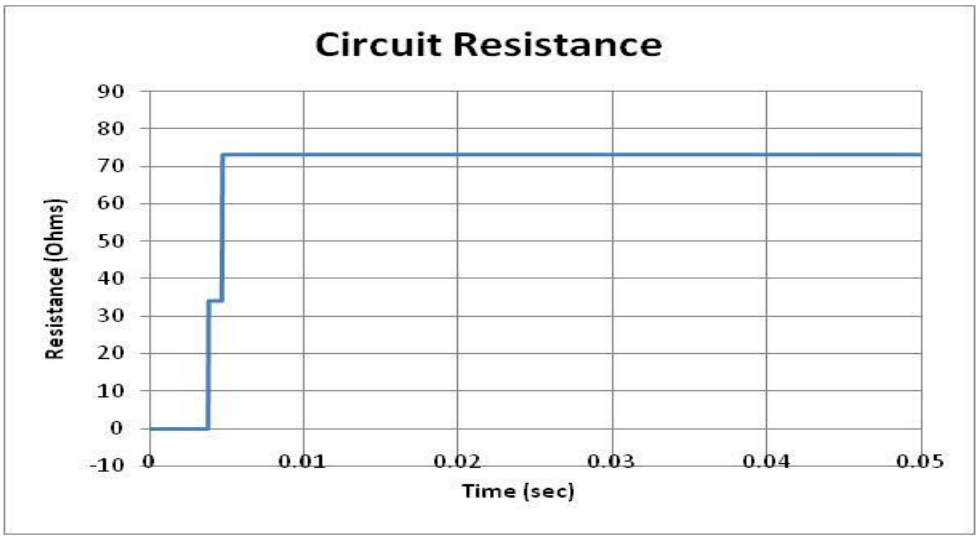

Figure 12 Circuit resistance as it varies during the fault due to the variable superconductor resistances using Model 3.

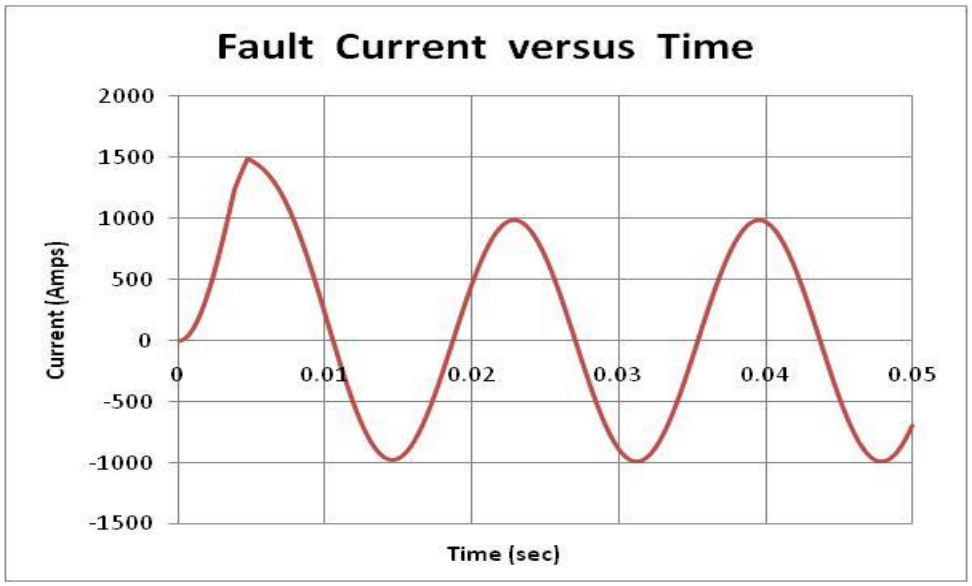

Figure 13 Fault current with variable resistances due to the superconductor to normal transition during the fault using Model 3.

The results of the above analysis can best be summarized in the following table. We have included a calculation of an effective circuit resistance and asymmetry factor which would be needed to achieve the maximum peak current if the resistance had a constant value throughout the fault duration.

Case	R Circuit steady state (Ω)	Steady state peak current (A)	Max peak current (A)	Asymm Factor	R Circuit Effective (Ω)	Asymm Factor Effective
X/R = 10	6.96	1425.4	2475.5	1.737		
All Supercond	0.001	1432.5	2864.9	2.000		
All Metallic	74.0	981.0	1039.6	1.060		
Model 1	52.0	1147.4	1338.0	1.210	45.5	1.157
Model 2	52.0	1147.5	1386.2	1.208	45.5	1.156
Model 3	73.3	988.3	1487.6	1.505	39.6	1.195

5. COMPARISON OF FCL TRANSFORMER COOLING OPTIONS

Option 1—Six Cryomech coolers with natural convection circulation

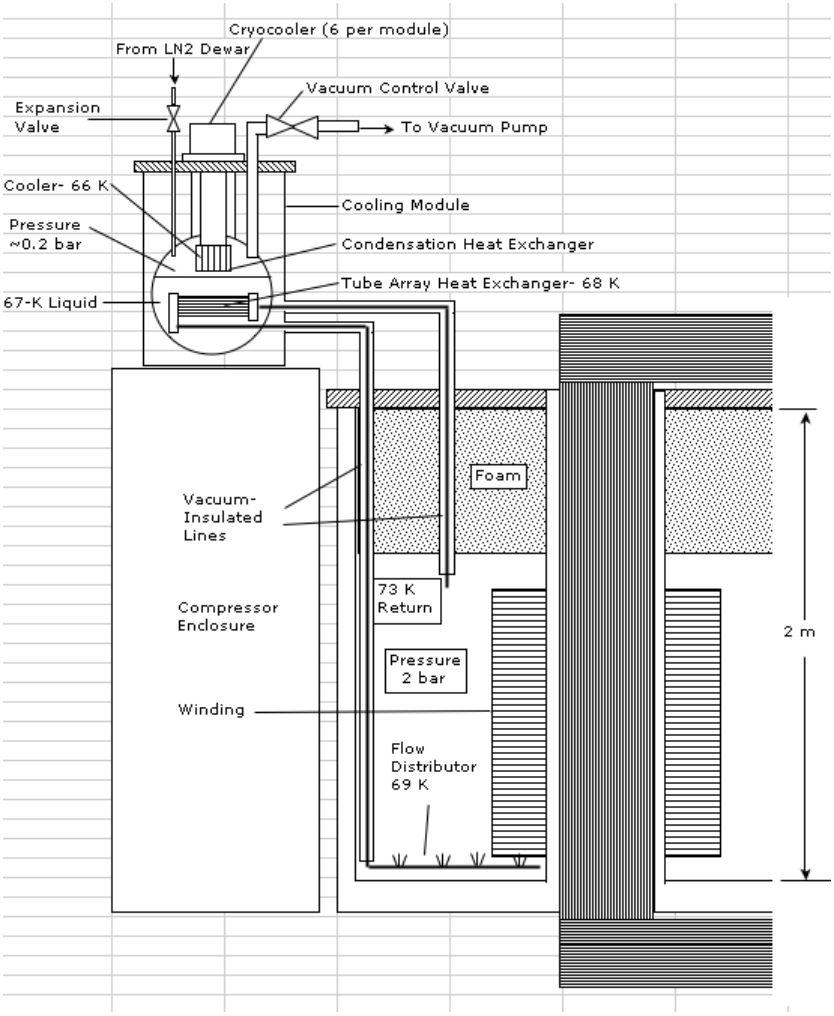

Fig. 1. Schematic of cooling module Option 1 connected to transformer.

Fig. 1 shows a schematic of the cooling module connected to the transformer. The transformer windings are cooled to 70 K by subcooled 2-bar nitrogen which circulates by natural convection through a heat exchanger mounted in the cooling module. This exchanger sits in a bath of boiling nitrogen at approximately 68 K. Boiloff from the bath is re-condensed in a closed cycle by an array of coolers mounted in the top plate of the cooling module. Vacuum-insulated lines from the cooling module penetrate the top plate of the transformer to supply the cold nitrogen to the windings. The module is mounted high on the frame and enclosure surrounding the six compressors. The difference in density between the 68-K supply and 72-K return nitrogen provides a differential pressure head that drives the circulation. The coldbox has a vacuum-insulated external fill line from a supply dewar and a vent line leading to a vacuum pump or atmospheric vent. Both of these lines have control valves with positioners that allow them to be operated by the control system. These lines will be used for initial fill and cooldown, and also to

supply liquid nitrogen from an external storage dewar if the transformer heat load should exceed the cryocooler capacity.

Auxiliary Power–

6 x 15 kW = 90 kW for 6 compressors and associated air cooling fans.

4 kW for 5-hp liquid ring vacuum pump, for 3 kW from extra liquid nitrogen supply.

1 kW for turbo and backing pump, TOTAL– 95 kW

Advantages:

1) No circulation pump required; flow self-regulated by supply/rtn temp difference.
2) Vertical stacking gives small footprint.
3) System is its own subcooler; no extra one needed.
4) Simple system; fewest components, probably lowest cost.

Disadvantages:

1) Difficult to get a very high flow rate with natural convection.
2) Large passages and large exchangers needed to keep pressure drops down.
3) Several interfaces between coolers and 2-bar nitrogen-- leads to increased temperature differentials.
4) High-mounted module is difficult to service.
5) US vendors are uncomfortable with natural convection concept.

Option 2—Six Cryomech coolers with nitrogen pump and subcooler

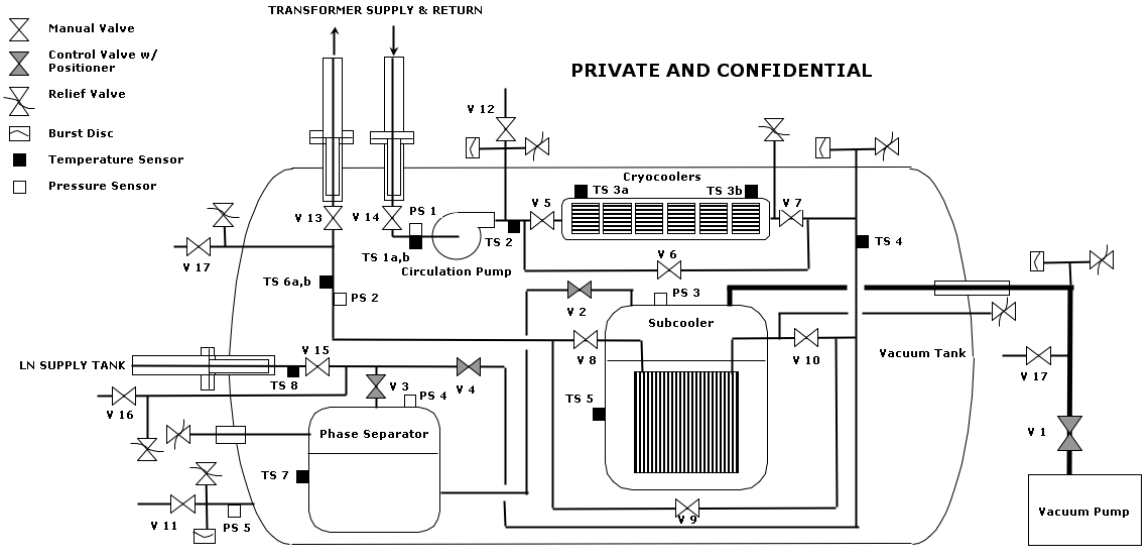

Fig. 2. Schematic of Cooling Module Option 2.

Fig. 2 shows a schematic of cooling module option 2. All equipment is in a vacuum tank. The transformer windings are cooled to 70 K by subcooled 2-bar nitrogen which circulates through heat exchangers.
The first set of exchangers consists of multiple channels in an aluminum or copper block coupled to an array of six cryocoolers mounted in the top of the cooling module. These are followed by a bath-type subcooler heat exchanger cooled by a flow of liquid nitrogen from an external tank. The flow would be pumped at the exit end to produce subcooling below 68 K.
A nitrogen pump would be provided at the inlet of the 2-bar return from the transformer to drive the circulation. A phase separator at the inlet to the subcooler would be vented to atmosphere to pre-cool liquid nitrogen from the storage tank to 77 K, reducing the required capacity of the subcooler pump.
Vacuum-insulated lines from the cooling module penetrate the top plate of the transformer to supply the cold nitrogen to the windings. Another set of ducts carries the helium lines from the compressors to the cryocooler coldheads.

Auxiliary Power–

Option 1 + 2 kW for LN circulator & drive electronics.

TOTAL– 97 kW

Advantages:

1) Higher pressure and more flow available from nitrogen pump.
2) Flow passages and heat exchangers can be smaller.
3) 2-bar flow is linked directly to coolers; lower temp differentials.
4) Six separate exchangers can be mounted on the coolers, allowing the upstream ones to operate at higher temperature with greater capacity.
5) All equipment is at ground level; easy to service.
6) Well-known concept to US vendors.

Disadvantages:

1) Equipment is spread out--larger footprint.
2) Nitrogen pump introduces extra heat.
3) Nitrogen pump adds ~$50K extra cost and additional maintenance.
4) Greater complexity; more difficult to operate.

Option 3—Bulk open-cycle liquid nitrogen supply

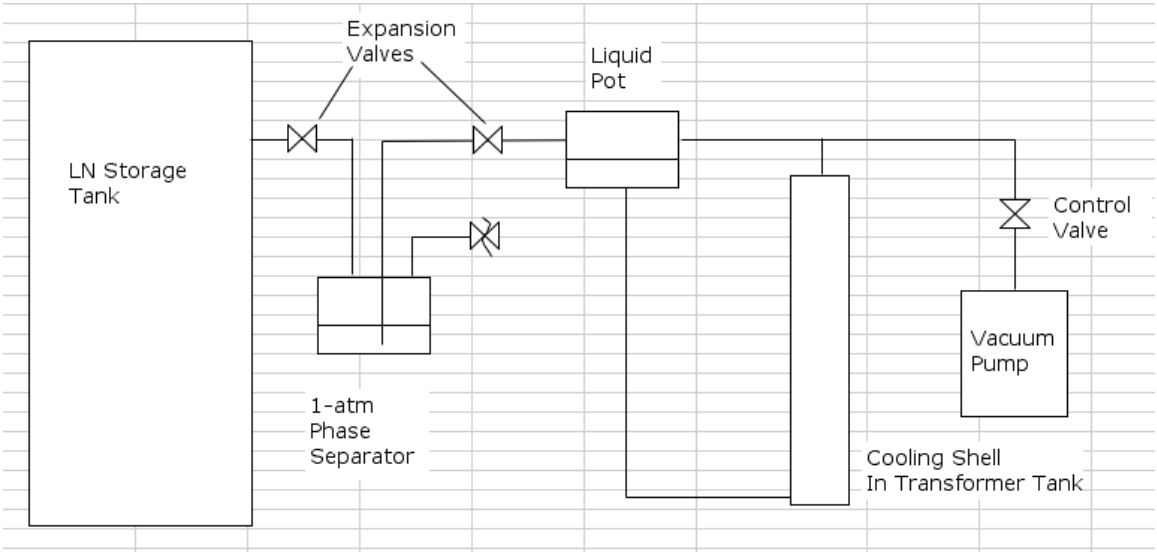

A bulk liquid nitrogen tank near the transformer stores liquid at about 35 psia and 86 K. Liquid is expanded through a control valve into a phase separator that is vented to atmosphere through a check valve. The resulting 77-K liquid is expanded into another liquid pot that is pumped to about 4 psia and 68 K by a large vacuum pump with a vacuum control valve. The liquid pot feeds a cooling shell in the transformer tank by natural convection. Alternatively, a heat exchanger containing 30-psia subcooled nitrogen could be immersed in the bath in the liquid pot. This could feed directly to the transformer tank by natural convection or with a nitrogen pump.

Auxiliary Power–
Assuming the cryocoolers are replaced by another 3 kW of subcooling, 8 kW for two 5-hp liquid ring pumps, plus 1 kW for turbo & backing pump.

TOTAL– 9 kW

Advantages:

1) Simple system, lowest capital cost, no cryocoolers to buy or maintain.
2) Liquid easily available to replenish after a quench.
3) Cooling capacity is limited only by the capacity of the vacuum pump (but heat exchangers must also be sized for maximum desired load to avoid higher temperature differentials at high loads).
4) Very low auxiliary power requirement.
5) No worries about water or air cooling for cryocoolers.

6) Vendors will be comfortable with this design.

Disadvantages:

1) Logistics of locating and supplying bulk storage tank.
2) Operating cost of supplying liquid full-time (may still be less than cooler cost over test duration).
3) Probably not relevant as a demo system for commercial units.
4) If natural convection is chosen, liquid pot must be above transformer.

Here is a Table that summarizes all these numbers:

HEAT LOAD (kW):	14 MVA	28 MVA	40 MVA
Estimated AC Loss (kW) (B-I eqtn)	1.4	7.1	17.5
Current Leads (kW)	200	250	440
Interconnects (kW) (If all copper)	8	30	60
Dewar-- Radiation & Conduction (kW)	400	400	400
TOTALS (kW)	2.0	7.8	18.4
Cryocooler Capacity (kW)	3.0	3.0	3.0
Required Subcooler Capacity (kW)	0.0	4.8	15.4
Subcooler LN Consumption (L/day)	N/A	2700	8600
LN Storage Tank Capacity (L)	N/A	20,000	20,000
Min. Time Between Refills (days)	N/A	7.4	2.3
AUXILIARY POWER (kW):			
Option 1	Option 2	Option 3	Option 4
95	97	120	9

The time between refills would really be longer than noted above depending on daily variation of the transformer load.

6. Mechanical Design of Three Phase HTS FCL Transformer:

Mechanical Design using 3D PRO_E Modeling Software for various internal subassemblies of HTS FCL Transformer were done, Design Steps followed were as given below –

- Finalize Core Step details
- Design of Core clamps, Tie Plates, Crossbars for bottom and top core assembly
- Design of Winding Insulation assembly
- Clamping arrangement for windings
- Crossover Design and Lead connections for each winding
- Turn distribution with spacers for balanced field distribution in windings
- Design of Winding End Insulation assembly
- Design of Winding to Core, LV1 to LV2 Winding, LV2 to HV winding and Phase to Phase insulation.

- Design of top and bottom Coil Clamping Rings
- Conductor to Lead jointing, Lead to the Bushing connections
- Assembly of windings on the Core
- Core & Coil Internal assembly with LV and HV connections
- Design of Cover and tank
- Finalize design data for Cryostat and Final assembly
- Analysis of Cooling flow of LN2, Design of open ventilation system for LN2
- Complete assembly of HTS Transformer with Controls
- Top yoke/Core encapsulation and ventilation design for Forced air

Some of the views of subassemblies of HTS FCL Transformer are shown here –

- **3 Phase Core Assembly with top cross-bar and bottom yoke clamping**
- **3 Phase Core Assembly with bottom cross-bar and top yoke clamping**
- **3 Phase Core & Winding Assembly with LV connections**
- **3 Phase Core & Winding Assembly with HV connections**
- **Cryostat and Core & Coil assembly**
- **Final Assembly with Conservator and top cover**

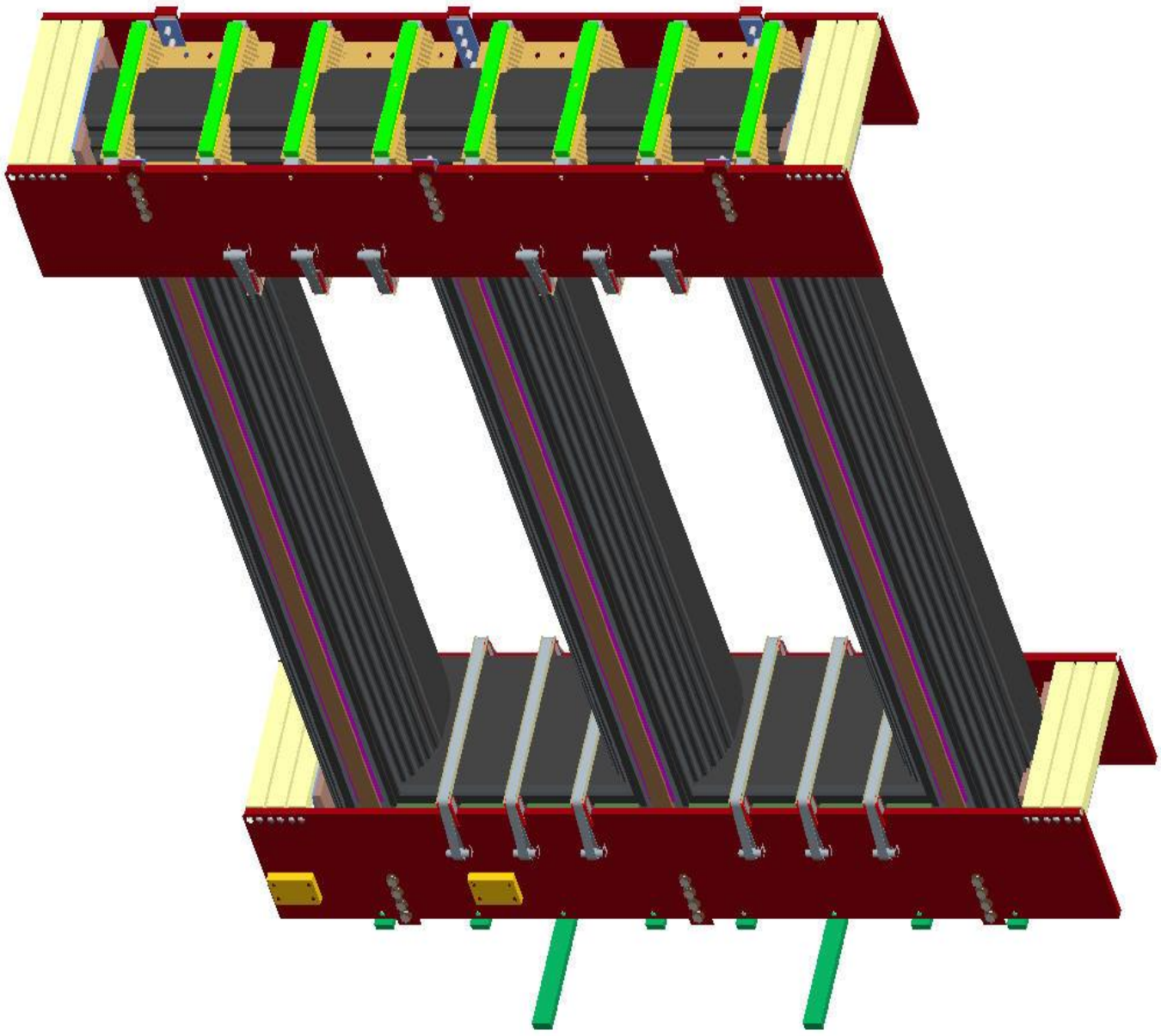

3 Phase Core Assembly with Top cross bars and bottom yoke clamping

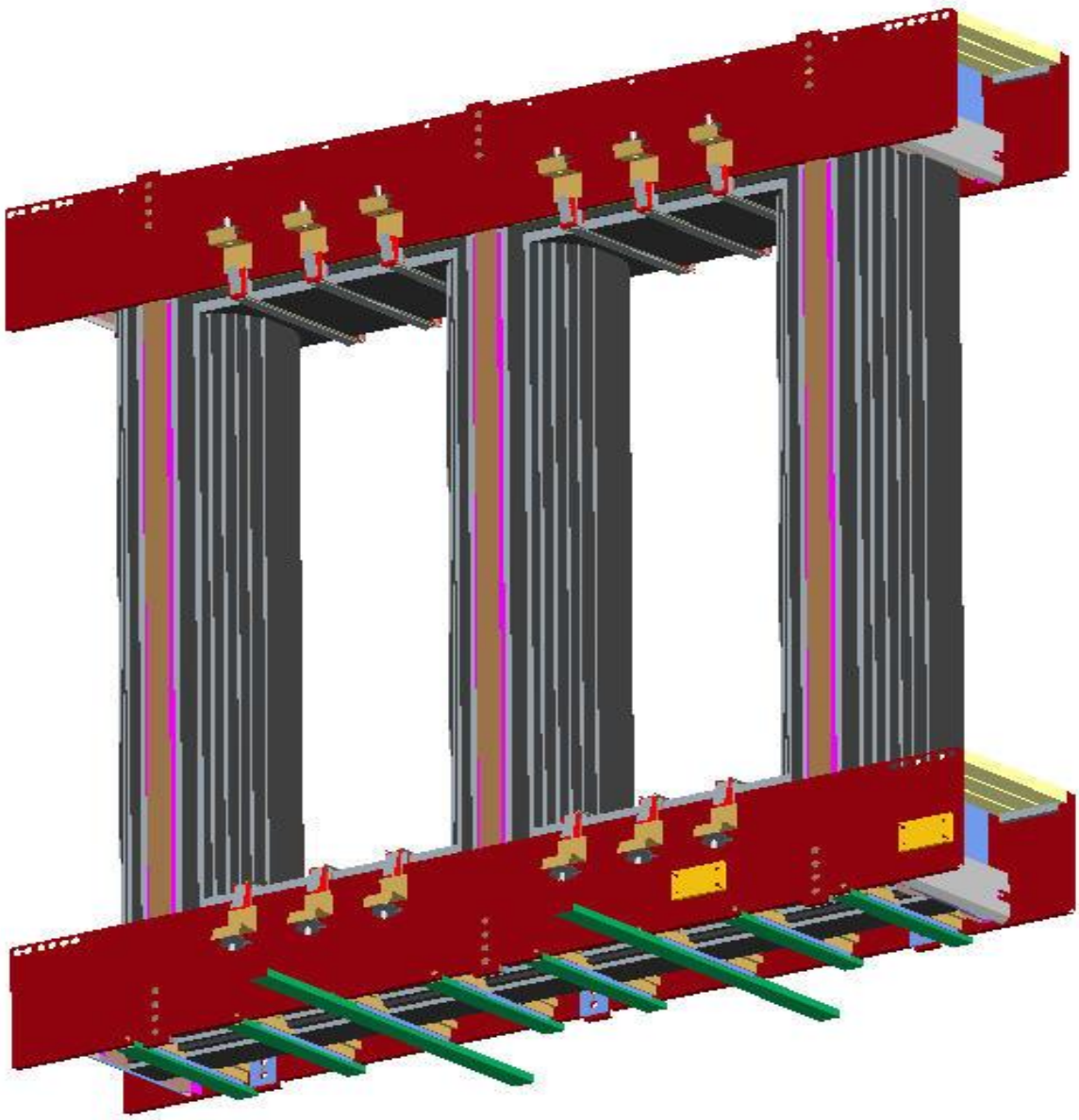

3 Phase Core Assembly, with bottom Cross bar and top yoke clamping details

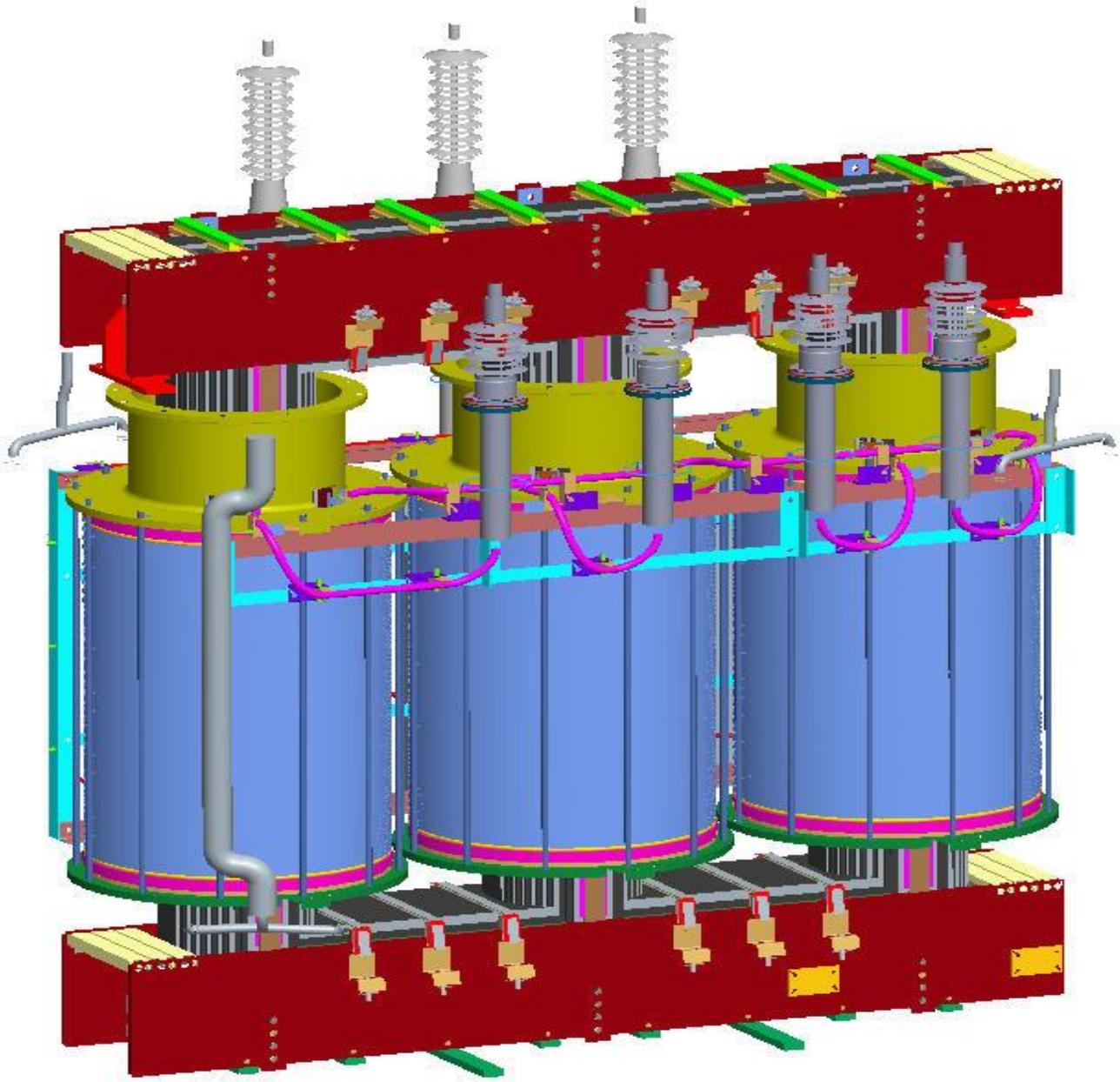

3 Phase Core and Winding Assembly with LV Connections

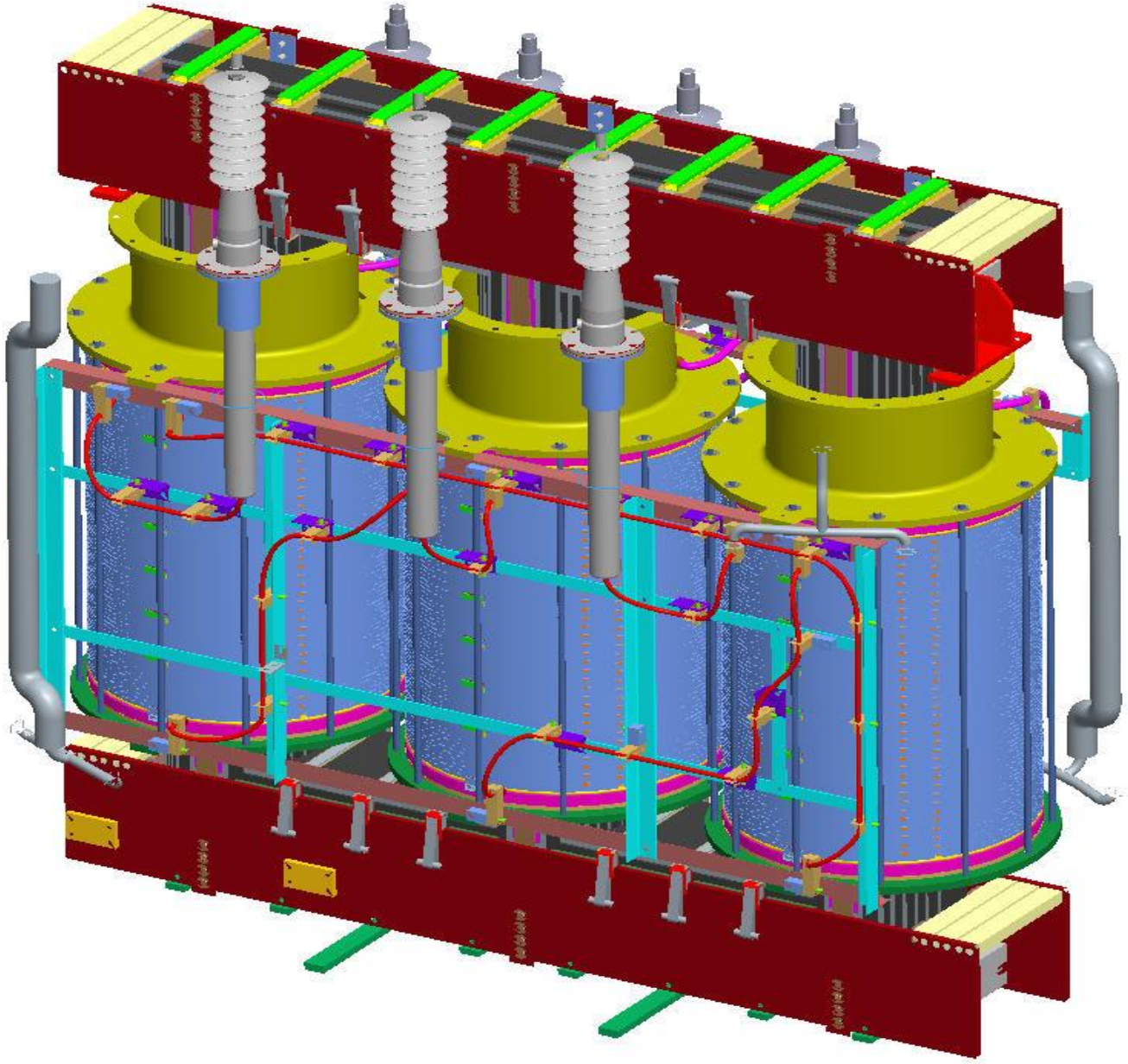

3 Phase Core & Winding Assembly with HV Connections

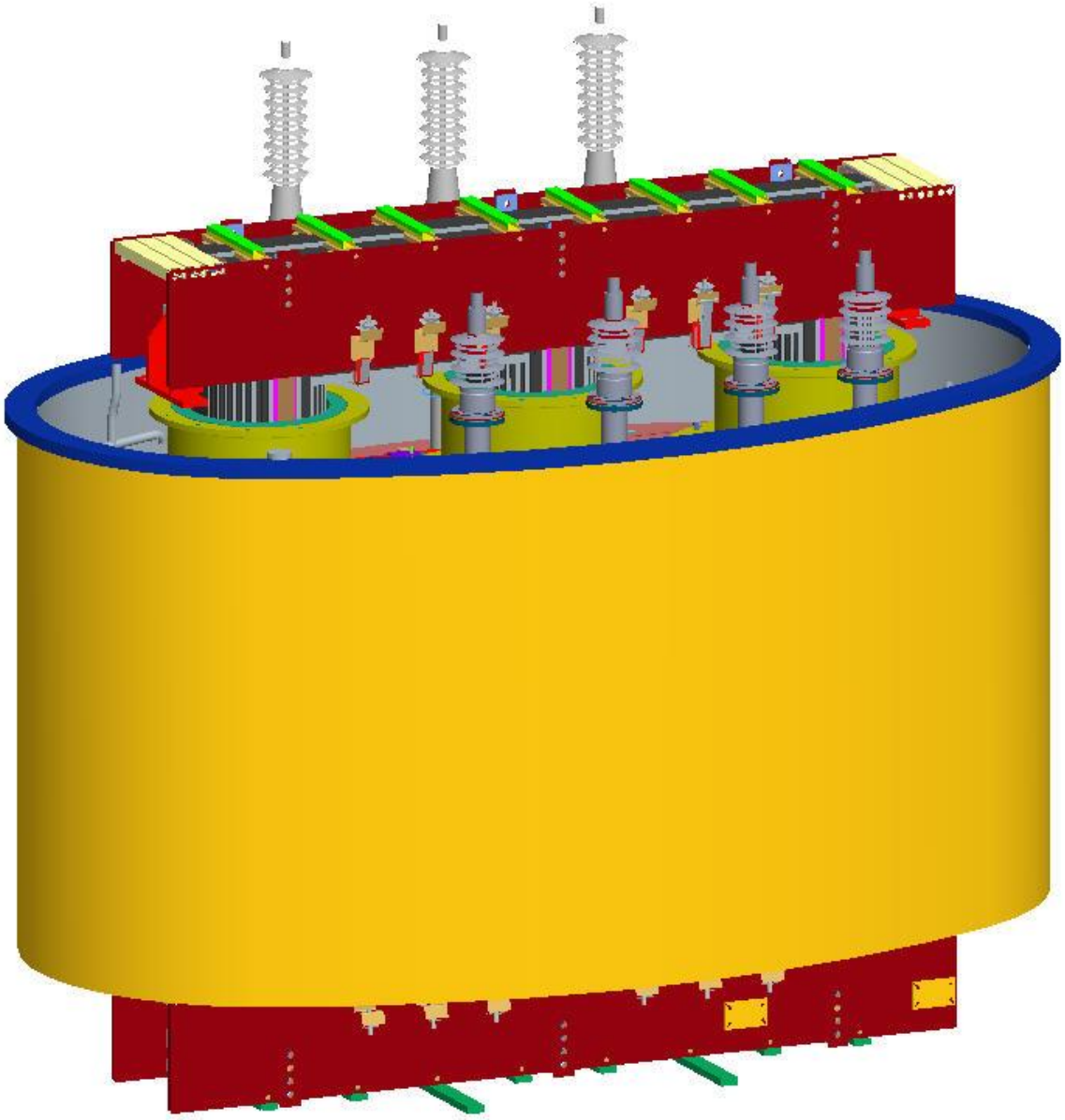

Cryostat and Core & Coil Assembly

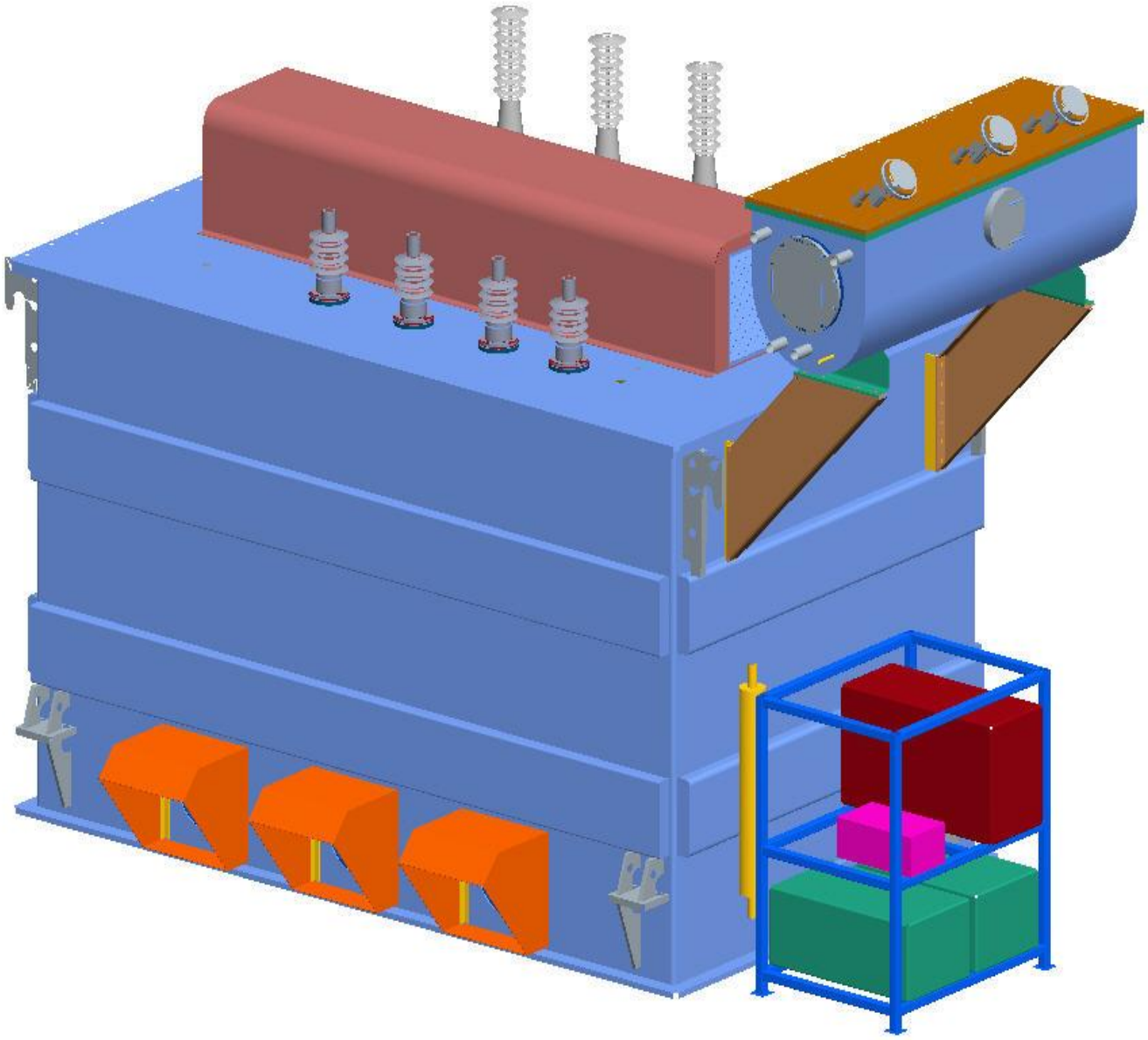

Final Assembly with Conservator and top cover

Attachments:

1. All attachments provided by SPX Transformer Solutions were marked as either Proprietary & Confidential or as Protected Data and are, therefore, not included in the public version of this report.

Appendix 2

University of Houston Final Report

Final Report

Award Number	G099895 / G107365
Title of Research	FCL Transformer - 2G HTS Conductor Development
Principal Investigator	Dr. Venkat Selvamanickam
Organization	University of Houston

Objectives

This subcontract effort at the University of Houston in the Fault Current Limiter (FCL) transformer program was geared towards the development of low AC loss RE-Ba-Cu-O (REBCO, RE=rare earth) coated conductors. AC loss is a critical issue that was identified in the use of superconducting transformers. The main objective of this work at the University of Houston is to scale up multifilamentary REBCO coated conductor technology to long lengths and achieve uniform performance. A second objective is to develop a high resistive Cu-Ni stabilizer on REBCO coated conductors by electroplating.

Introduction

Now that superconductors tapes are manufactured with good critical current levels [1],[2], reducing their AC losses is an important goal to deploy these conductors in AC applications. Filamentization has been proven to be a viable way to reduce magnetization AC losses to acceptable levels. Many striation techniques have been evaluated including striation via laser [3],[4], mechanical [5], inkjet printing [6, 7] as well as the recently-developed selective electroplating technique [8]. However, striation can lead to another magnetization AC loss mechanism called coupling and this component has been found to be significant enough to sometimes reduce or eliminate the effectiveness of the filamentization on AC loss reduction [9]. Striation can also result in a drastic reduction in I_c and the final product after filamentization may not be useful for any application. An effective method to fabricate multifilamentary 2G HTS tapes without significant loss of I_c is therefore very important.

Multifilamentary Tape Fabrication

The tape without stabilizer used in this study manufactured by SuperPower Inc. The conductor architecture consists of buffer layers of Al_2O_3, Y_2O_3, MgO and $LaMnO_3$, deposited on non-magnetic electro-polished Hastelloy substrate followed by deposition of ~1.4 μm thick RE-Ba-Cu-O (REBCO, RE=rare-earth) by metal organic chemical vapor deposition (MOCVD). The superconducting film was covered by a 2 μm sputtered silver protective layer. Striation was performed by a diode-pumped femtosecond laser with a pulse duration of 350 fs, repetition frequency of 100 kHz, wavelength of 1033 nm and power varying from 2.6 to 1 W. 12-filament tapes with 1 mm wide filaments were prepared. After striation, the tapes were oxygenated to form

an oxide layer on the grooves to avoid copper electroplating on the grooves. The tapes were then selectively electroplated with the copper being deposited only on the top and sides of the filaments.

Fig. 1 is a micrograph of typical laser cut groove that reveals ~10 µm of quite uniform depth and a ~30 µm width after electroplating of Cu. The electroplated Cu grows both above the filaments and laterally across the grooves and reduces the width of the groove from ~60 µm to ~30 µm. A translational stage was used during the striation and 5 sequential cuttings were performed for each one of the groove to obtain desired groove width and depth.

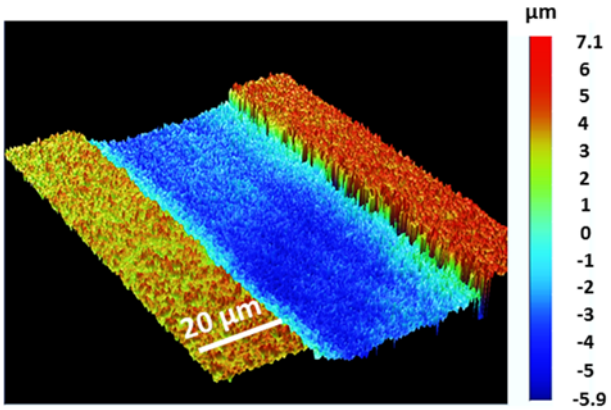

Figure 1: Optical microscope image of a groove from L2 revealing ~10 µm groove depth and ~30 µm groove width.

Optimization of oxygenation process to minimize for I_c degradation

Since the diffusion barrier layer (Al_2O_3) in the 2G HTS tape stack is removed by striation, the elements in Hastelloy alloy can migrate to the REBCO film and poison it during the high temperature oxygenation process. The oxygenation process is necessary to reduce electrical coupling loss and selectively electroplate Cu only on the filaments [8]. Energy Dispersive X-ray Spectroscopy (EDS) analysis across a groove and filament on striated samples post-oxygenated at 700 and 750 °C has shown evidence of such diffusion. EDS analysis of the sample oxygenated at 700 °C indicated the presence of Cr and Ni diffusion from the Hastelloy to the REBCO filaments and this diffusion was found to be more pronounced in the sample oxygenated at 750 °C. The measured I_c of the striated samples oxygenated at 700 °C has been found to be very low and samples oxygenated at 750 °C were tested to be non-superconductive. The diffusion of aforementioned elements is probably responsible for the I_c degradation in those samples exposed to post-oxygenation. This inference was further ascertained by T_c measurements that showed no superconductive transition in the striated region but a sharp transition in the non-striated region of

the sample. Given these results, further investigation was focused on oxygenating the samples at temperatures below 700 °C to investigate AC coupling loss, I_c behavior of the selectively electroplated samples.

Four 12-filamentized samples along with an untreated sample were prepared to investigate the oxygenation temperature effect on I_c reduction and degree of electrical coupling loss. These were labeled L1 through L4 and oxygenated at different temperatures to allow selectively electroplating of Cu stabilizer. Sample property details are provided in Table I.

TABLE I
SAMPLE DETAILS

Sample	Groove width (μm)	Oxygenation Temperature (°C)	I_c (A)/12 mm	Plating thickness (μm)
L1	~ 65	500	~ 345	~ 19
L2	~ 65	550	~ 310	~ 20
L3	~ 70	650	~ 245	~ 30
L4	~ 60	Not oxygenated	~ 316	—
Ref.	—	Not oxygenated	~ 338	~ 30

Sample L4 was not oxygenated to eliminate the oxygenation effect on I_c and to examine the effect of striation alone on I_c degradation. Samples were electroplated in a beaker and in contrast to commercial acidic Cu electroplating solution, an acid free $Cu(NO_3)_2$ solution was used. The benefit of using acid free solution is that it eliminates the contingency of the acid destroying REBCO superconducting layer, especially in the case of striated tape where the protective Ag and Cu stabilizer layers are removed. To obtain uniform thickness across the width, a shield was used in order to reduce ion concentration at the edges of the tape. This reduces the deposition on the edges and provides a more uniform thickness of the plated copper. Only samples L1 through L3 were electroplated Cu along with a reference sample. The plating thickness is about 20 μm and slightly higher in L3 (30 μm).

The sample oxygenated at 500 °C exhibited significant Cu island depositions on the grooves after Cu electroplating (Fig. 2a). The depositions decreased in samples oxygenated at higher oxygenation temperature (Fig. 2b) and eventually no deposition was seen (Fig. 2c). This suggests that the groove resistance changed by post-oxygenation temperature and allowed nucleation of Cu deposits on the groove at relatively low temperatures.

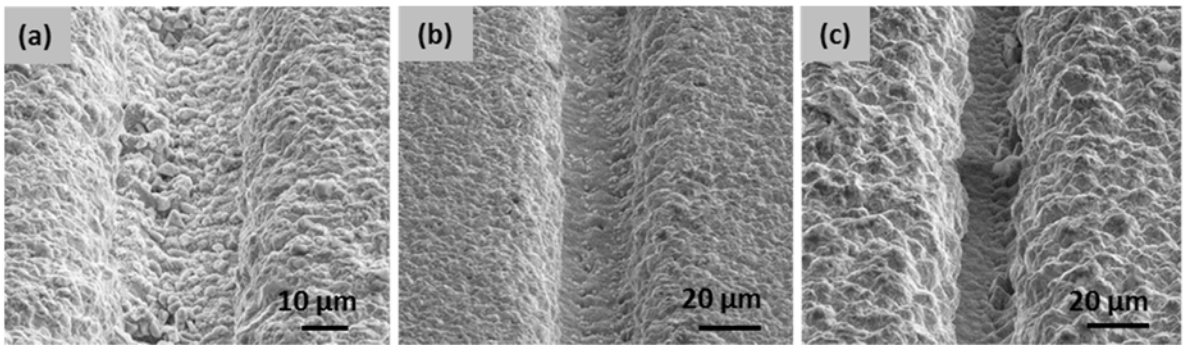

Figure 2: SEM images of the striated samples oxygenated at different temperatures followed by copper electroplating. The figures provided in (a), (b) and (c) are taken from L1, L2 and L3 respectively.

A standard four-probe method was used for I_c measurements with 1 µV/cm criterion. Magnetization AC loss measurements were performed using a pickup coil method at frequencies between 40 and 500 Hz at 77 K. The lengths of the samples measured were 44 mm. Microstructures were investigated by Scanning Electron Microscope (SEM) coupled with Focused Ion Beam (FIB) and optical microscopes.

The I_c values of the samples are provided in Table I. One important finding is that at higher temperatures, I_c degrades drastically since the diffusion of Hastelloy elements is more at higher temperatures as explained earlier. The degradation is ~27% and ~8% in L3 and L2 respectively. Surprisingly the I_c of L1 is higher than that of the untreated reference sample. This indicates that the parent-tape has some nonuniformity in terms of I_c along the length. The degradation without oxygenation was found to be about 6.5% on comparison of the I_c values of L4 and the reference. The calculated reduction of I_c from material removal by striation in L4 is ~5.5%. Therefore, only a ~1% increase in I_c reduction came from the laser ablation process. The implication of this result is that the heating zone in samples treated with femtosecond lasers is very localized and the ablation does not contribute significantly to I_c degradation while oxygenation temperature has strong effect on degradation of I_c.

Electrical Coupling Loss

Calculations of eddy current losses have been conducted and it was found that the eddy current component of the total loss can be ignored since it depends on filament width to the third power and is reduced drastically by filamentization [10]. A theoretical model has been proposed to

describe electrical coupling loss [11];

$$P_{\mathrm{mc}} = ((fB_0L_p)^2/2\rho)d_nW, \qquad (1)$$

where W is the width of the tape or filament, L_p is the length of the sample, B_0 is the peak value of AC applied field, ρ is the effective transverse resistivity, d_n is the thickness of the coupling material and f is the frequency. The hysteresis loss per length per cycle can be written with the sheet critical current density, J_c, and $B_c = \mu_0 J_c / \pi$ [10, 12];

$$P_{\mathrm{mh}} \approx W^2 J_c B_o = W I_c B_o, \qquad B_0 >> B_c \qquad (2)$$

The relative contribution of the electrical coupling loss component can be extracted from the frequency-dependent AC losses. The losses per cycle should be independent of frequency according to Eqn. (2). The total magnetization AC losses can be found as the sum of the individual contributions, $P_t = P_{mh} + P_{mc}$ where $P_{mc} = C_1(fB_o)^2/\rho$ and $P_{mh} = C_2 B_o f$. The constants (C_1 and C_2) can be found from Eqns. (1) and (2) respectively. P_t can be normalized by frequency $P_t/f \approx C_1 f B_o^2/\rho + C_2 B_o$. Since B_o is constant for a specific field, the equation can be reduced to $P_t/f \approx C_3 f\rho^{-1} + C_4$, where C_3 and C_4 are new constants. This equation indicates that the slopes obtained from the frequency-dependent AC loss per cycle plots represent the electrical coupling loss if the eddy current contribution is neglected and depend only on the effective groove resistance, ρ. Shown in Fig. 3 are the plots for frequency-dependent AC losses normalized by respective frequencies at four different field amplitudes, 30, 40, 70, and 90 mT. All samples showed frequency-dependent slopes indicating the presence of electrical coupling losses. The smallest slope was seen in L3 (annealed at 650 ºC) while the largest was seen in L1 (annealed at 500 ºC). There is no clear trend for the frequency-dependent slope ratios or the electrical coupling loss ratios with respect to the applied field. The values are more or less the same. The averaged electrical coupling loss ratios were found to be L1/L2=2, L1/L3=3.29, and L2/L3=1.62.

The frequency-dependent analysis was performed on seven different field values; however, for clarity only four are presented in Fig. 3. The slopes obtained from Fig. 3 are seen to increase with the applied field and this increase is not linear. It is obvious from the Eqn. (1) the applied field has a second order contribution to the electrical coupling loss. This has been confirmed by the nearly second order slope increase in Fig. 4.

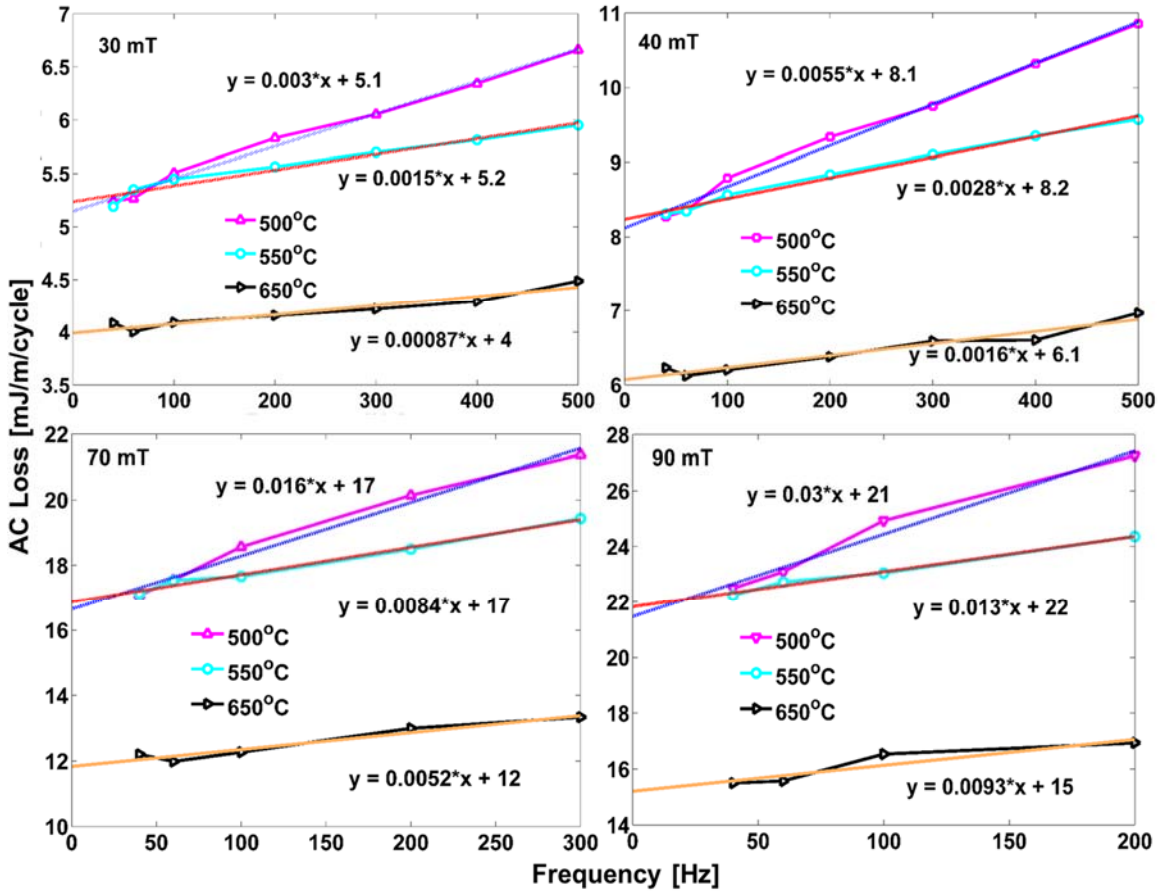

Figure 3: Frequency-dependent normalized losses to analyze coupling contribution at 30, 40, 70 and 90 mT.

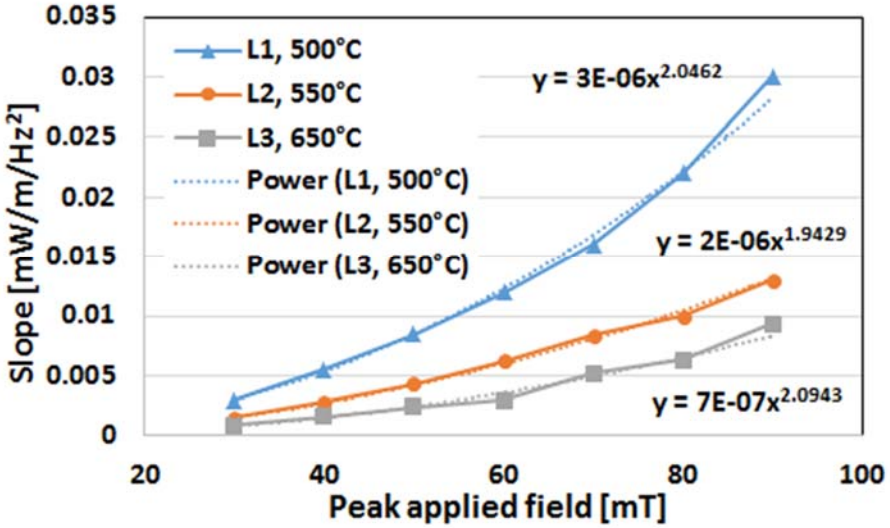

Figure 4: Field dependence plot of the slopes extracted from Fig. 3.

Scaling-up multifilamentary tapes to longer lengths

We have implemented our newly-developed selective electroplating techniques to produce long fully filamentized tapes. For the first time a 12 mm wide, 10 m long tape with 12 filaments and thick Cu stabilizer (~20 μm, see Fig. 8a) layer has been fabricated by R2R laser ablation and selective electroplating [13]. The same laser which was used to fabricate the short samples was employed for the long tape striation. In total, eleven filaments were made consecutively with ~2 cm overlaps. The speed of the tape was adjusted to synchronize the laser head motion to prevent any discontinuity on the ablation. Then the tape was electroplated in a R2R continuous electroplating system after oxygenation at 550 °C. The benefit of this technique is that any desired length can be fabricated in a continuous manner since both ablation and electroplating processes are done in a R2R method. Photographs of 10 m multifilamentary tape before electroplating (left) and after electroplating of Cu (right) are shown in Fig. 5. The striations are clearly visible before and after the electroplating of Cu stabilizer layer.

Figure 5: Reel to reel striated 10 m tape before copper electroplating (left) and after copper electroplating (right).

After fabrication of the fully-filamentized long tape, sections of unstriated and R2R striated tapes were cut for characterization (about 7 cm). I_c and magnetization AC loss of both tapes were measured. The I_cs of the striated and reference sample were measured to be 271 and 290 A respectively and current-voltage (I-V) curves are provided in Fig. 6 with a criterion of 1 μV/cm. The degradation of I_c is about ~6.5% which is very close to the value calculated from the material

removal considering an average ~60 µm groove width before electroplating. This result is also consistent with the short sample (L2) data discussed in Table I.

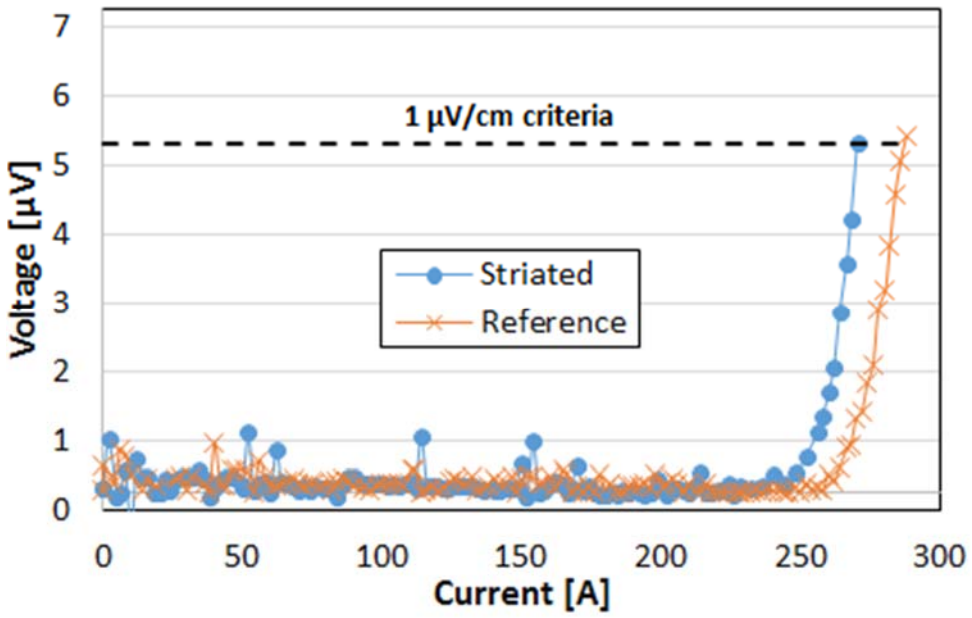

Figure 6: Critical current measurement results for R2R striated and reference samples with 1 µV/cm criterion.

Magnetization AC loss per cycle per length versus peak applied field is shown in Fig. 7 for the R2R striated, short striated (L3) and reference samples. The results showed ~5 times reduction in high field regime while at relatively low field, the effectiveness of striation was lost and the losses of the R2R striated tape became equal to the losses of the reference tape. This typical behavior was frequently reported in other studies and attributed to magnetic coupling in between two neighboring filaments [5],[14],[15],[16]; however, this is not the case in field values well above the full penetration field. Ideally in an isolated striated tape, the hysteretic loss is proportional to the width of the tape and it can be reduced proportionally by making the width of the tape narrower according to Eqn. (2). If the reduction is calculated by eliminating the I_c effect on the hysteretic loss, a value of 12-fold reduction would be expected since the width of the tape is reduced to ~1 mm from 12 mm. This calculated reduction of the AC loss is almost two times higher than the value obtained experimentally. For comparison purpose, AC losses of one of the short samples (L3) are also plotted in the same figure. This sample is almost ideally decoupled (shows ideal reduction) and the R2R striated tape follows a behavior in between L3 and the reference unstriated sample. As it can be seen from the Fig. 7, the loss in L3 is almost half of the R2R striated tape at high fields.

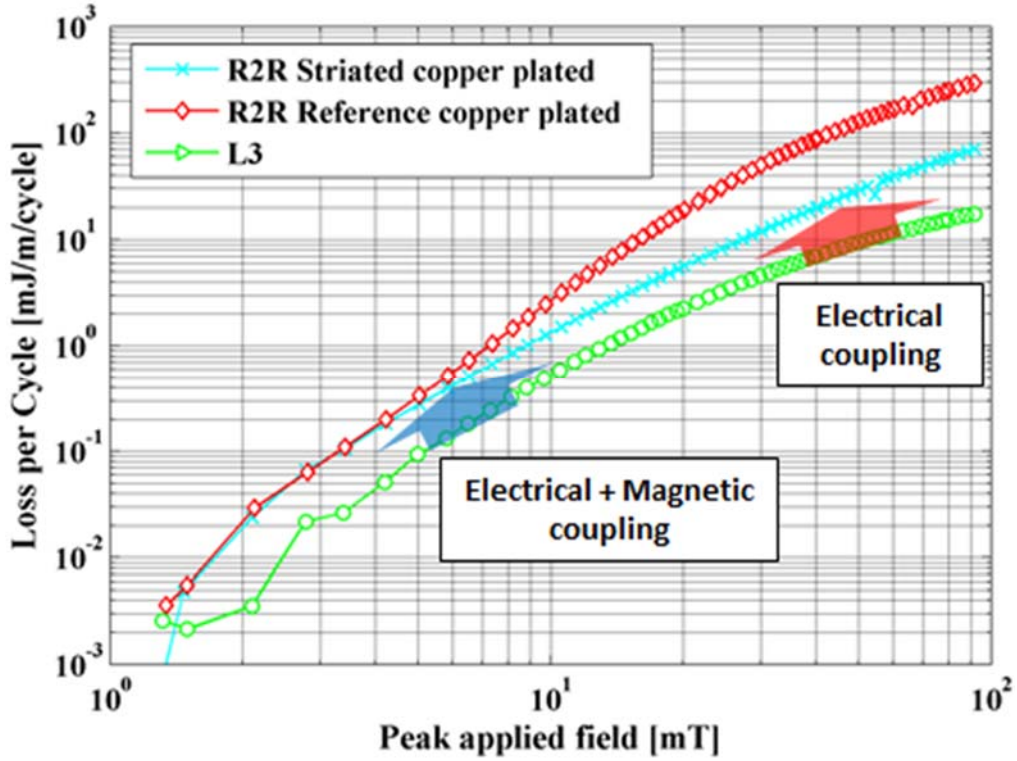

Figure 7: Magnetization AC loss (per cycle per length) versus peak applied field for R2R striated and unstriated reference samples.

This low reduction of AC loss was probed further by examining at the microstructures of the grooves. R2R electroplating is quite different than the beaker electroplating and the shield design is not straightforward. The shield was designed such that to obtain the best thickness uniformity along the width. After implementing the shield, quite uniform thickness were obtained. One problem is that even after obtaining quite uniform Cu thickness distribution along the width, the grooves located close to edge of the tape exhibit extensive lateral sideway Cu growth as shown in Fig. 8b. The grooves close to middle of the tape are free of any deposit (see Fig. 8a). This extensive sideway growth of the Cu deposit was probably a result of shape of the shield and of the electroplating cell and might be the reason for increase in the electrical coupling loss. At low field, both electrical and magnetic coupling contribute to the total loss and reduce the striation effect on AC losses (see Fig. 7).

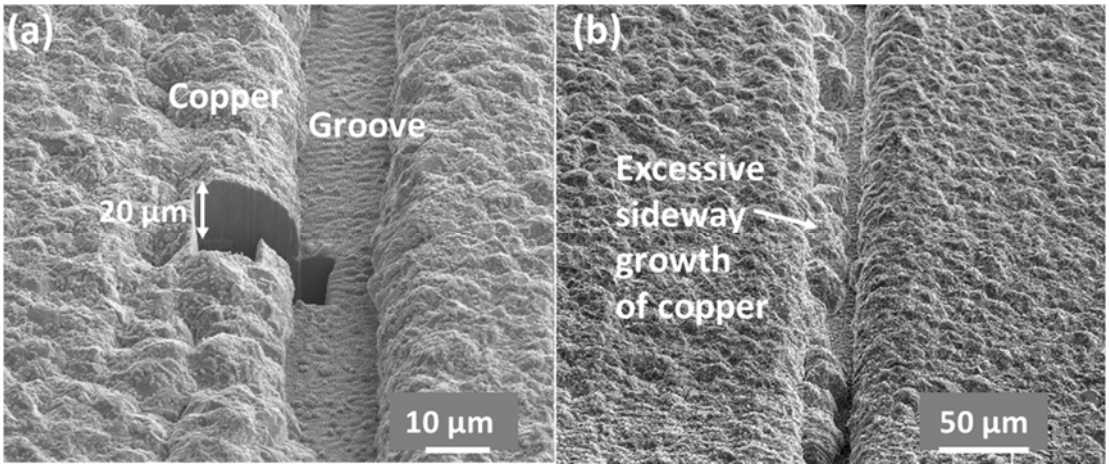

Figure 8: SEM images of R2R striated sample. Cross-section and a groove free from copper deposit (a), sideway growth of copper through (b).

Scanning Hall Probe System

A major challenge in manufacturing of long multifilamentary tapes is the homogeneity and uniformity current flow over all narrow filaments over long lengths. It would be important to assurance the integrity of every filament in order to prevent deterioration in critical current due to local filament damage. In this program, we built a second reel-to-reel system based on Scanning Hall Probe Microscopy (SHPM) to directly image current flow through every filament. A photograph of the reel-to-reel SHPM system is shown in Fig. 9.

During the measurement, the tape is continuously driven by the reel-to-reel motion system from the left to the right. The tape is first cooled at zero field and then magnetized by the magnetic loop with a permanent magnet. The magnetic circuit is to focus the field and to greatly reduce the effect of reversing field at tape exit of the magnetizing zone. The peak flux density in the magnetic loop is around 1 T, which is well above twice the penetration field of the samples, which ensures the measured field profile is the maximum trapped field and the persistent current density is J_c. Due to thermally-activated flux creep, the trapped flux will decay with time. A typical time for the tape to move from the magnetization zone to the measurement spot is longer than 20 second. In the measurement zone, the Hall sensor is moving fast in the direction perpendicular to tape motion, driven by the scanner shown in Fig. 9 as 5).

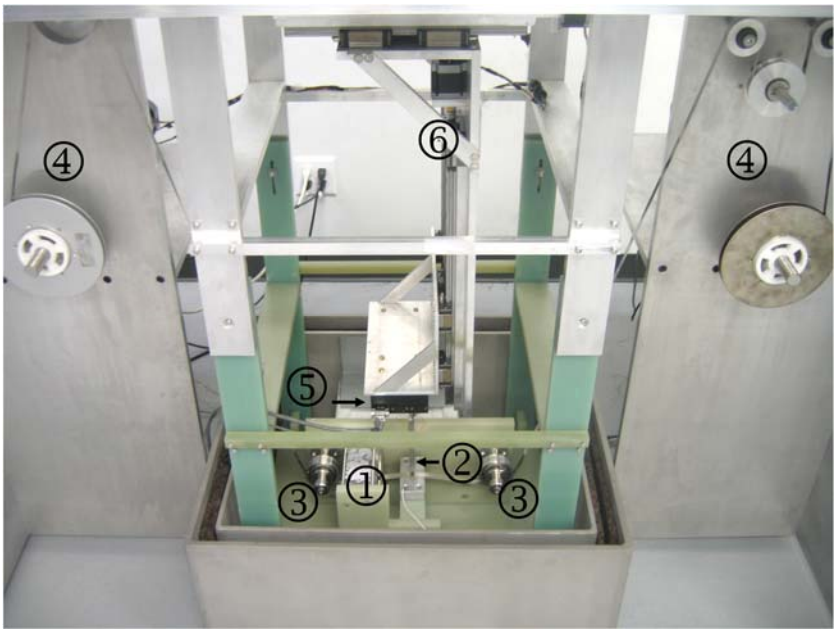

Figure 9: A photo of the SHPM system. 1). the magnetic loop, 2). holder for the Hall probe, 3). roller bearings, 4). reel-to-reel tape motion system, 5). fast scanning stage, 6). 3-D locating system of the scanner.

The Hall sensor is excited by an AC current of 10~40 kHz, 10 mA rms. One point worth mentioning is that due to the unknown electromagnetic interference which varies from day to day, we have to re-select a proper frequency for each individual measurement, otherwise the noise effect might be significant. The Hall voltage is analyzed by a signal-recovery 7265 lock-in amplifier. The position of the Hall probe and the Hall voltage is collected by a high-frequency data acquisition unit. Data frequency is 10^5 Hz and the data is averaged afterwards by computer. The nominal setting of time constant on the lock-in amplifier is 640 μs, to activate the fast analog output. However the effective time constant is depends on the averaging rate. For example, if the averaging is on 500 data points, the effective time constant will be no less than $500/10^5 = 5\times10^{-3}$ (s). The measurement speed can vary, depending on the scan range along the width, the resolution requirement along the tape length and the SNR (higher noise require higher effective time constant which means slower measurement). A typical measurement speed on a 12 mm coated conductor will be 14 m/h with a resolution of 1 mm along the length; the maximum speed tested was 21 m/h. Considering the wider scan range, the scanning speed is comparable with the value reported [17]. The reel-to-reel SHPM system is now routinely used for qualification of long multifilamentary tapes.

Electroplating of Copper-Nickel Alloy Stabilizer Layer

Quench might occur in 2G-HTS tapes during application due to factors such as local defects in the conductors, over-load operation, a failure in power supply and cooling system, etc. Quench produces excessive heat in a winding coil and the overheating may cause the conductors to meltdown [18]. The Ni or Hastelloy substrate can become highly resistive when quench happens. Therefore the stabilizing conducting layer, a Cu or/and Ag layer, is coated around the tape to protect the 2G-HTS from the damage due to the quenches. The stabilizer layer is generally dense and thermally and electrically conductive. Large-scale, reel-to-reel electroplating processes of both Cu and Ag layers for 2G-HTS has been successfully demonstrated [9,19,20]

However, in a fault current limiter (FCL), a highly conductive stabilizer is not preferable. The high electrical and thermal conductivity of Ag and Cu will affect the overcurrent limiting action of a FCL. So a highly resistive metallic alloy stabilizer layer is needed. The nearly temperature independent electric resistance of CuNi (Table II) makes it a preferable choice as a stabilizer for FCL applications.

Table II: Comparison of the specific electrical resistance of Cu alloys and YBCO at different temperatures.

	ρ (77K) [μΩcm]	ρ (100K) [μΩcm]	ρ (293K) [μΩcm]
$YBa_2Cu_3O_{7-x}$		800	1200
Cu, metallic	0.2	0.4	1.6
CuZn 70/30, brass	4.6	4.9	6.8
CuNi 70/30, Monel	36.5	37	38

The objective of this task is to develop an electroplating process to deposit a CuNi alloy stabilizer layer without damaging the superconducting properties of the 2G-HTS tapes.

Challenges in electroplating CuNi alloys

Electroplating of a CuNi alloy coating is a common surface treatment for steel. This CuNi alloy coating serves as an anti-corrosive layer for marine applications. The standard reduction

potentials of copper and nickel are +3.4V and −2.5V respectively against standard hydrogen electrode (SHE) [21]. Because of the large disparity of the reduction potentials between the two metals, a complexing agent, *e.g.*, citrates [22], cyanides [23] or sulfamates [24], is needed to decrease the gap.

Unfortunately, due to the chemical sensitivity of YBCO, the general electroplating processes for Cu-Ni are not directly applicable to the superconductor tapes. The superconducting film has an intrinsic chemical instability due to the existence of the non-equilibrium Cu^{3+} ions. YBCO will disintegrate in water (equation 3) [24] and will seriously degrade in acidic environment (equation 4). Though the dense sputtered Ag layer shields the YBCO layer from an external environment, the water and protons might be able to penetrate through the Ag layer resulting in the degradation of critical current. Moreover, the low standard potential of nickel might cause the reduction of the metal ions in YBCO during the electroplating of CuNi alloy.

$$2YBa_2Cu_3O_7 + 3H_2O \rightarrow Y_2BaCuO_5 + 5CuO + 3Ba(OH)_2 + \frac{1}{2}O_2 \quad (3)$$

$$YBa_2Cu_3O_7 + 14H^+ + \frac{1}{2}H_2O \rightarrow Y^{3+} + 2Ba^{2+} + 3Cu^{2+} + H^+ + 7H_2O + \frac{1}{4}O_2 \quad (4)$$

The electroplating recipes involving cyanides have been excluded in our study because of the high toxicities of cyanides. Citrate bath is the most common recipe for electroplating CuNi [22]. With the complexation effects, citrate ions act as the leveling, buffering and brightening agents at the same time, which eliminates the need for addition of other additives. However, since citrate acid is a common etchant for YBCO, even though the plating bath has a pH of 8, as hydrogen ions gather at the cathode surface, the YBCO in the sample is etched away after only 5 min of plating. Sulfamate bath is also one of the common recipes for the process, but acidic sulfamate is often used as a sliver polisher [24]. Etching away of the thin Ag over layer on 2G-HTS tapes happens before the electroplating starts.

Consequently, an appropriate or novel electroplating recipe of CuNi electroplating had to be developed in this program.

Potential window for YBCO

All CuNi electroplating experiments were conducted in an electrochemical cell with three-electrode configuration as shown in Figure 10, *i.e.*, using a 2G-HTS tape, Pt wire, and Ag/AgCl (saturated KCl) as the working electrode, counter electrode, and reference electrode, respectively.

Figure 10: Electrochemical cell for CuNi electroplating on 2G-HTS tapes.

A CuNi electroplating experiment was first conducted at constant current of 50 mA. The electrolyte consisted of 200 ml water, 20.70 g Na_2SO_4, 14.71 g Na_3Cit, 1.25 g $CuSO_4 \cdot 5H_2O$, and 8.67 g $NiSO_4 \cdot 6H_2O$. During electroplating, the potential on the 2G-HTS tape was monitored. It was quite constant at about −1.53 V vs. Ag/AgCl. It is a very low potential which brings about detrimental effects to the 2G-HTS tape. As shown in Figure 11, the electroplating coating and the Ag layer peeled off and the YBCO layer is damaged. The most possible reason is that the YBCO layer was reduced at such a low potential and oxygen gas is released. The lower limit potential of the CuNi electroplating on a 2G-HTS tape has to be determined to avoid the occurrence of such damage of the YBCO film.

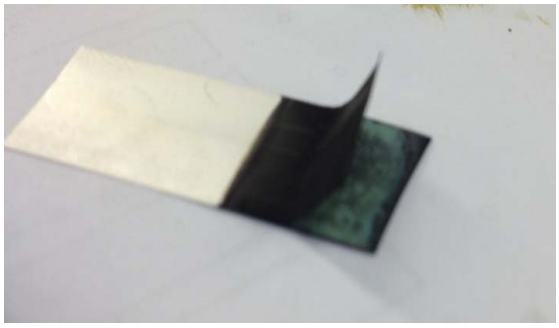

Figure 11: 2G-HTS tape after the CuNi electroplating in citrate bath. Cu and Ni are properly deposited on the Ag surface, but the YBCO beneath the Ag overlayer is etched away, resulted in severe delamination.

In order to find out the workable potential window for the 2G-HTS tapes, a single-potential amperometry technique was employed. The electrolyte consisted of 200 ml water, 20.70 g Na_2SO_4, and 14.71 g Na_3Cit without $CuSO_4 \cdot 5H_2O$ and $NiSO_4 \cdot 6H_2O$. 2G-HTS tapes without the sputtered Ag protection layer were used as the working electrode. The potential from −0.2V to −0.5V was imposed on the tape against the Ag/AgCl reference electrode and the current change was monitored. After the amperometric experiments, the samples were characterized by General Area Detector Diffractometer (GADDS) X-ray Diffraction (XRD) to examine for any damage to the YBCO film.

Figure 12 shows the current-time curves obtained at four different potentials. The curves from −0.5 V and −0.4 V vs. Ag/AgCl in Figures 12a and b show an obvious increase in current after the

initial decrease, indicating there are some electrochemical reactions taking place. At −0.3 V in Figure 12c, the current does not increase drastically as at lower potentials, but the current still increases during the 10 min long run. As the potential goes higher to −0.2 V, the current decreases as if there is no reduction reaction, as shown in Figure 12d. This means that YBCO will be safe if the potential is higher than −0.2 V.

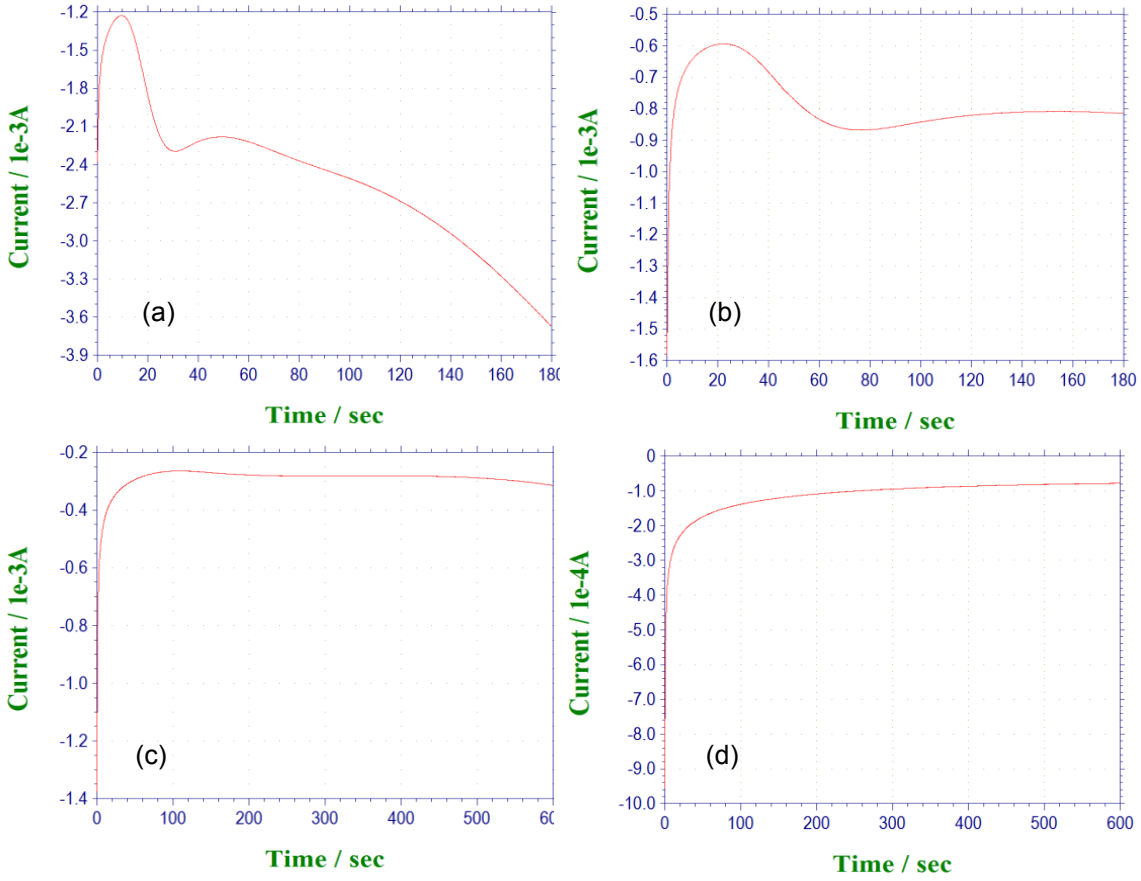

Figure 12: The time-current relation shown in the amperometric curves at different potentials of (a) −0.5 V, 3 min; (b) −0.4 V, 3 min; (c) −0.3 V, 10 min; and (d) −0.2 V, 10 min.

The GADDS XRD patterns of the samples after amperometric experiments are shown in Figure 13. There is no visible change in the epitaxial structure of the YBCO as shown in the inset of Figure 13. But 2θ XRD spectra of YBCO (005) obtained by integrating the χ angle show a drastic change of the peak intensity. The higher the potential and the longer the etching, the lower is the peak intensity of YBCO (005), which exactly matches the amperometry results in Figure 12. It is worth mentioning that even the −0.2V sample shows slightly lowered peak, indicating there might be detrimental effects without electrochemical reduction reaction involved. It is likely due to the reactions of YBCO with water and hydrogen ions as shown in equations 3 and 4.

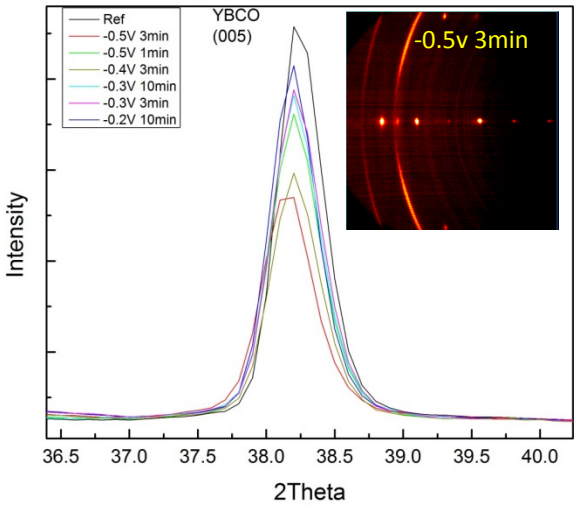

Figure 13: 2θ XRD spectra of YBCO (005) peaks obtained by integrating the χ angle in GADDS measurement. The inset is χ-2θ XRD pattern.

As a result, it becomes obvious that imposing a low potential on the 2G-HTS tape cathode during electroplating can be very harmful to the YBCO layer. An intensive low potential imposed on the cathode, which is very common in Ni electroplating due to the low standard potential of Ni, can badly accelerate the degradation of YBCO. Meanwhile, the −0.2V sample which showed noticeable electrochemistry reaction in amperometry, also showed some deterioration of the YBCO crystalline quality. It is confirmed that a proper protection of the YBCO during CuNi alloy electroplating is mandatory.

Protection by the silver over layer

While electroplating of CuNi alloy involves a much lower electrochemical potential on the cathode, it needs to be determined if the Ag over layer can still protect YBCO from degradation.

Figure 14 compares the current–time curves at a potential of −0.5 V vs. Ag/AgCl of a tape with Ag coating but without YBCO and an YBCO tape with Ag coating. The difference can be easily observed. The current of the tape without YBCO in Figure 14a decreases to a minimum and then is constant, while the current of the tape with YBCO in Figure 14b starts to increase about 40 s later after reaching the minimum. It needs to be mentioned that the negative sign here only

means an electro-reduction current. This increase means some new electro-reduction reactions occur. It is very possible that the electrolyte permeates through the Ag over layer and contacts the YBCO, by which the electro-reduction of YBCO can start and continue.

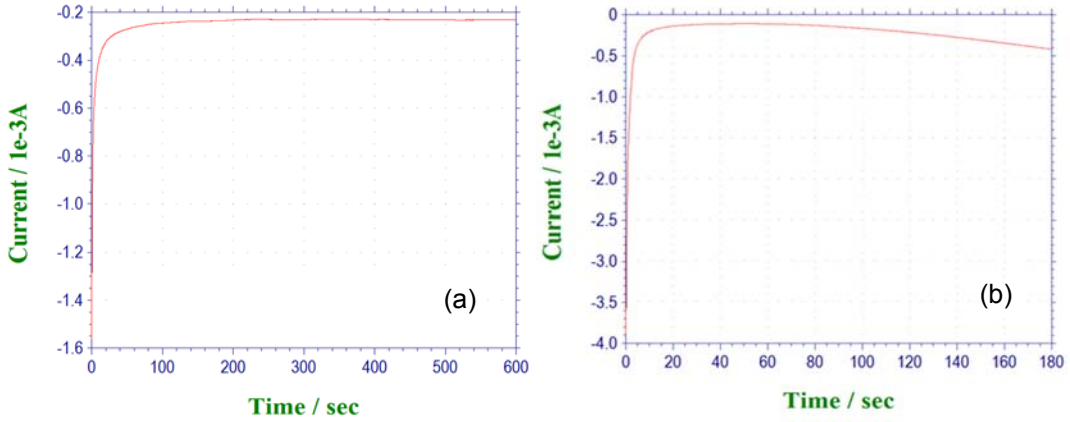

Figure 14: The current–time curves at potential of −0.5 V vs. Ag/AgCl of (a) tape with Ag coating but without YBCO (4 cm tape in the electrolyte) and (b) YBCO tape with Ag coating (2 cm of tape in the electrolyte).

Compared with the current–time curve in Figure 12a for a 2G-HTS tape without an Ag over layer, this increase is delayed and smaller, which suggests that the Ag layer can protect YBCO from reaction to some degree.

Cu and Ni plating ratio and concentration control

In order to study the synergy between the two elements during the electroplating process, aqueous electrolytes of 150 mL water, 45.0 g $NiSO_4•6H_2O$, 1.5 g HBO_3, and varied amount of $CuSO_4•5H_2O$ were used. The amount of $CuSO_4•5H_2O$ copper was adjusted to make the Ni:Cu ratio in the solution vary from 100:0.1 to 100:10, as shown in Table III. All the samples were obtained by electroplating in the corresponding electrolytes at −0.75 V vs. Ag/AgCl at 66.5 °C for 180 s. The photos of the samples are shown in Figure 15. It can be easily observed that sample 1 and 2 are in grey color, which suggests the coating is Ni. As the concentration of $CuSO_4•5H_2O$ increases, the coating color of the samples turns from bright grey to dark red, indicating the increase of Cu in the coating layer. EDS results in Table III show a consistent trend of Cu content.

Table III: Comparison of samples prepared in different electrolytes.

Sample	Ni:Cu in Solution	Ni deposited	Cu deposited	Ag
EDCN13-1	100:0.1	89.67	4.58	5.75
EDCN13-2	100:0.5	85.72	9.76	4.52
EDCN13-3	100:1	70.53	24.76	4.71
EDCN13-4	100:2	60	34.34	5.66
EDCN13-5	100:3	49.11	41.93	8.96
EDCN13-6	100:4	52.66	43.19	4.15

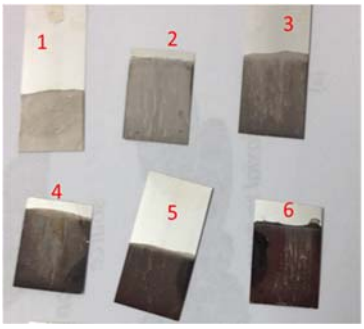

Figure 15: Photos of the samples.

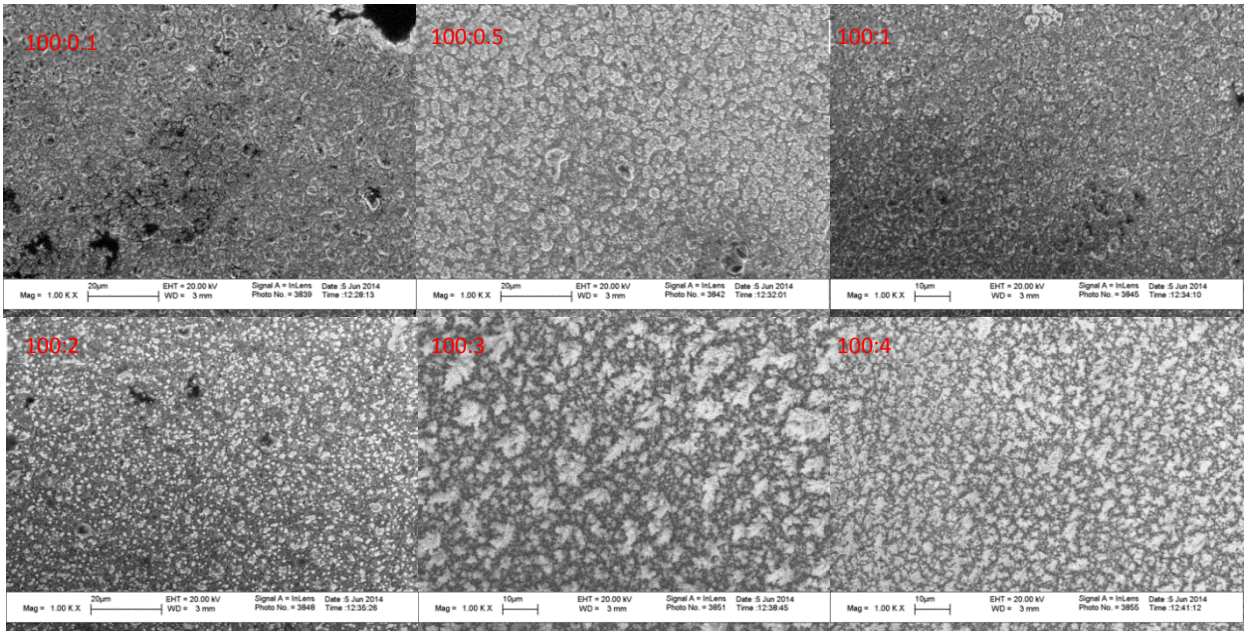

Figure 16: SEM image of the electroplated surface morphology. The number on the top right of the image indicating the Ni:cu ratio inside the solution.

The morphologies of the plated coatings on the samples were characterized by SEM, as shown in Figure 16. It can be easily observed from that the surfaces are not smooth. It is interesting that the EDS characterization indicated that the small clustered islands are Cu rich while the uniform background is Ni rich. This might be due to the reduction of Cu by hydrogen gas or hydrogen atoms produced on the tape during CuNi electroplating. Besides, the copper islands are closer to the bulk solution where the Cu concentration is higher than the local region on the surface. Therefore, the tips of the Cu islands grow faster than the bases, leading to the formation of

dendrites. To solve this issue, a vigorous stirring has been applied. The samples obtained after stirring show a shiny, smooth coating (Figure 17). Dendrites are not observed in the microstructure. However, some cavities or defects on the surface were found, which might be attributed to the large amount of hydrogen gas produced during the electroplating. Compared to the tape with only Cu coating, the XRD scan of the tape with CuNi coating shows a shift of Cu peak, indicating the alloy of Cu and Ni.

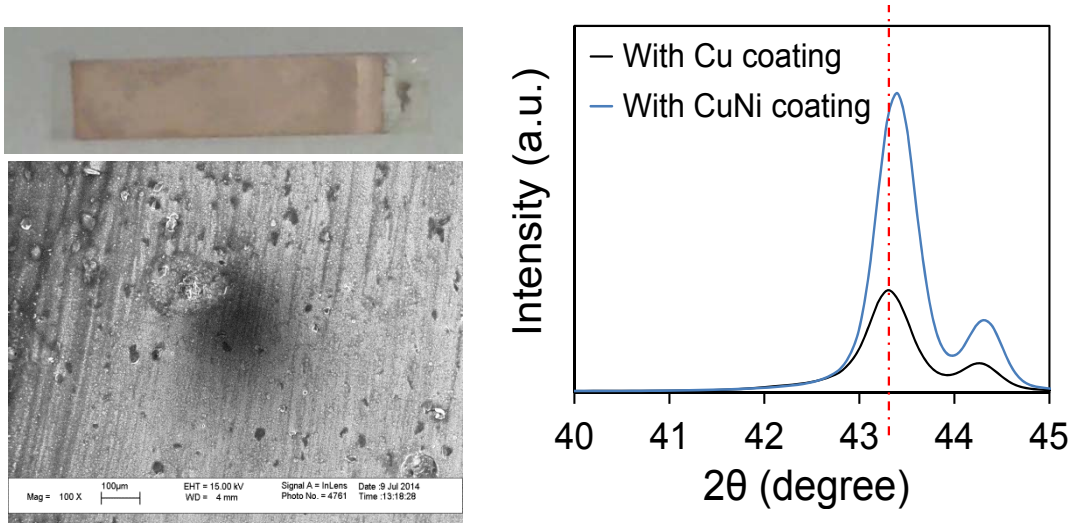

Figure 17: Photo, SEM image and XRD patterns of the samples prepared with a vigorous stirring during electroplating of Cu-Ni

Figure 18 shows the relationship between the Cu concentration in the electrolyte and the coated layer. A linear relation can be obtained by fitting the data. The Cu and Ni are found not to distribute uniformly in the coated layer. The major reason is that the produced hydrogen gas can reduce the Cu ions into metallic Cu. To obtain a uniform distribution, this effect has to be ruled out in future study.

Figure 19 shows the XRD peaks of Cu(111) and Ni(111) planes. Unlike EDS using an electron beam, X-ray can penetrate deeply into the 2G-HTS tape and thus the Ni signal of XRD comes also from the substrate of the tape. It can be found that the positions of Cu(111) peaks shift to higher 2θ degree, confirming the alloy of CuNi.

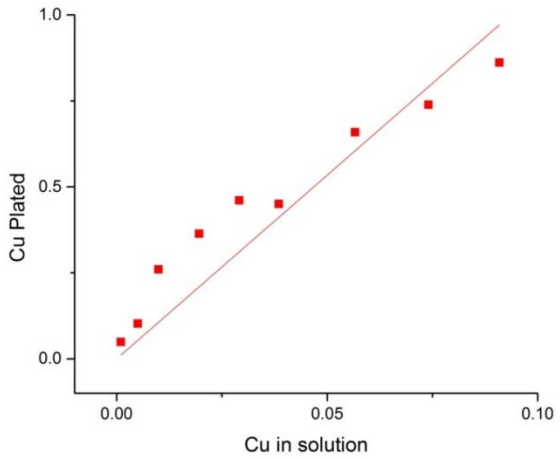

Figure 18: Relationship between Cu percentages in the electrolyte and in the coated layer.

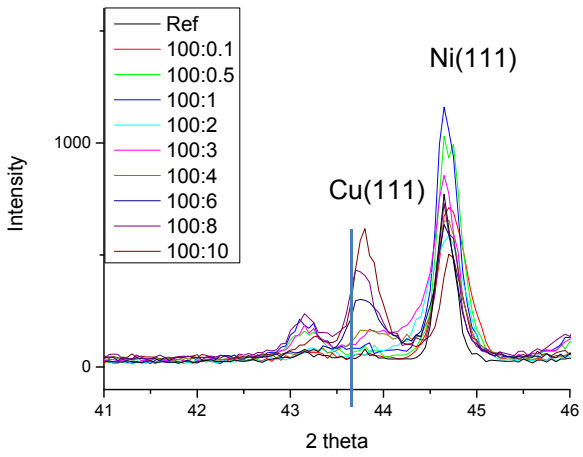

Figure 19: XRD patterns of the samples listed in Table III.

Summary

Post-oxygenation temperature has been found to have a strong effect on electrical coupling loss contribution and I_c degradation in laser striated coated conductors. The highest electrical coupling contribution was seen in striated tape oxygenated at 500 °C and the lowest in the tape oxygenated at 650 °C. This probably resulted from the differences in resistivity of the groove due to the changing oxide structure at different oxygenation temperatures. The highest I_c degradation was found to be in the striated tape oxygenated at high temperatures while least degradation was in the tape oxygenated at low temperatures due to the higher diffusion rate of Hastelloy elements at higher temperatures. In addition, the experiments were conducted to scale-up this newly developed technique. For the first time, a 10 m long fully-filamentized thick Cu stabilized 2G-HTS tape was fabricated. In total 12 filaments were created by laser ablation. I_c measurements showed only 6.5% degradation in I_c which is very close to the value calculated based on material removal. Magnetization AC loss measurements were performed at 77 K and at least 5-fold reduction was measured in relatively high field regime. Since both striation and electroplating were conducted in a R2R mode, scalability to even longer lengths is feasible. Furthermore, the number of filaments could be increased without compromising the magnetization AC losses as proven in short sample. A reel-to-reel scanning hall microscope system has been successfully built and commissioned for rapid non-destructive quality assurance of long multifilamentary tapes.

Also in this program, an approach towards electroplating CuNi stabilizer layer has been demonstrated. Our work has proved that the commercial citrate or sulfamate based CuNi electroplating recipe is not applicable to 2G-HTS tapes. The workable potential window of YBCO was also determined, which shows that YBCO will not undergo electrochemical reduction in aqueous electrolyte above −0.2 V vs. Ag/AgCl. A lower potential might still be applicable if the penetration of electrolyte through the Ag layer and the YBCO reduction reaction rate are rather low. Though proper control of the composition, a CuNi coating has been achieved. Further investigation needs to be performed to understand and suppress the detrimental effects of hydrogen gas and water on the quality of CuNi coating layer.

References:

[1] V. Selvamanickam, A. Guevara, Y. Zhang, I. Kesgin, Y. Xie, G. Carota*, et al.*, "Enhanced and uniform in-field performance in long (Gd, Y)-Ba-Cu-O tapes with zirconium doping fabricated by metal-organic chemical vapor deposition," *Supercond. Sci. & Technol.,* vol. 23, Jan. 2010.

[2] V. Selvamanickam, Y. Chen, J. Xie, Y. Zhang, A. Guevara, I. Kesgin*, et al.*, "Influence of Zr and Ce doping on electromagnetic properties of (Gd,Y)-Ba-Cu-O superconducting tapes fabricated by metal organic chemical vapor deposition," *Phys. C, Supercond.,* vol. 469, pp. 2037-2043, Dec. 2009.

[3] G. A. Levin, P. N. Barnes, J. W. Kell, N. Amemiya, Z. Jiang, K. Yoda*, et al.*, "Multifilament YBa2Cu3O6+x-coated conductors with minimized coupling losses," *Appl. Phys. Lett.,* vol. 89, Jul 2006.

[4] H. Okamoto, H. Hayashi, A. Tomioka, M. Konno, M. Owa, A. Kawagoe*, et al.*, "AC loss properties in YBCO model coils for loss reduction," *Phys. C, Supercond.,* vol. 468, pp. 1731-1733, Sep. 2008.

[5] G. Majkic, I. Kesgin, Y. Zhang, Y. F. Qiao, R. Schmidt, and V. Selvamanickam, "AC Loss Filamentization of 2G HTS Tapes by Buffer Stack Removal," *IEEE Trans. on Appl. Supercond,* vol. 21, pp. 3297-3300, Jun. 2011.

[6] X. Cai, I. Kesgin, R. Schmidt, Y. Chen, and V. Selvamanickam, "Completely Etch-Free Fabrication of Multifilamentary Coated Conductor Using Inkjet Printing and Electrodeposition," *IEEE Trans. on Appl. Supercond,* vol. 23, pp. 6603005-6603010, Jun. 2013.

[7] R. C. Duckworth, M. P. Paranthaman, M. S. Bhuiyan, F. A. List, and M. J. Gouge, "AC losses in YBCO coated conductor with inkjet filaments," *I IEEE Trans. on Appl. Supercond,* vol. 17, pp. 3159-3162, Jun. 2007.

[8] I. Kesgin, G. Majkic, and V. Selvamanickam, "Fully filamentized HTS coated conductor via striation and selective electroplating," *Phys. C, Supercond.,* vol. 486, pp. 43-50, Mar. 2013.

[9] I. Kesgin, G. Majkic, and V. Selvamanickam, "Effect of Selectively Electrodeposited Stabilizer Thickness on AC Loss Behavior of Fully-Filamentized HTS Wire," *IEEE Trans. on Appl. Supercond,* vol. 23, pp. 5900505-5900510, Jun.2013.

[10] W. J. Carr, "Loss in a striated coated conductor," *Superconductor Science & Technology,* vol. 20, pp. 168-175, Mar. 2007.

[11] W. J. Carr and C. E. Oberly, "Filamentary YBCO conductors for AC applications," *IEEE Trans. on Appl. Supercond,* vol. 9, pp. 1475-1478, Jun. 1999.

[12] E. H. Brandt and M. Indenbom, "Type-II-superconductor strip with current in a perpendicular magnetic field," *Phys. Rev. B,* vol. 48, pp. 12893-12906, Dec. 1993.

[13] X. Cai, I. Kesgin, V. Selvamanickam, "Reel-to-reel selective electroplated Cu-stabilization layer on multifilamnetary coated conductors " *IEEE Trans. Appl. Supercond.* vol. 25, 6954395 (2015).

[14] Y. Mawatari, "Critical state of periodically arranged superconducting-strip lines in perpendicular fields," *Phys. Rev. B,* vol. 54, pp. 13215-13221, Dec. 1996.

[15] I. Kesgin, G. A. Levin, T. J. Haugan, and V. Selvamanickam, "Multifilament, copper-stabilized superconductor tapes with low alternating current loss," *Appl. Phys. Lett.,* vol. 103, pp. 252603, Dec. 2013.

[16] M. Marchevsky, E. Zhang, Y. Y. Xie, V. Selvamanickam, and P. G. Ganesan, "AC Losses and Magnetic Coupling in Multifilamentary 2G HTS Conductors and Tape Arrays," *IEEE Trans. on Appl. Supercond.,* vol. 19, pp. 3094-3097, Jun. 2009.

[17] K. Higashikawa, et. al., "High-speed scanning Hall-probe microscopy for two-dimensional characterization of local critical current density in long-length coated conductor," *Physics Procedia*, vol. 27, pp. 228-231, 2012.

[18] X. Wang, U. P. Trociewitz, and J. Schwartz, "Self-field quench behaviour of YBa 2 Cu 3 O 7−δ coated conductors with different stabilizers," *Supercond. Sci. Technol.*, vol. 22, no. 8, p. 085005, Aug. 2009.

[19] R. N. Bhattacharya, J. Mann, Y. Qiao, Y. Zhang, and V. Selvamanickam, "Electrodeposited Ag-stabilization layer for high temperature superconducting coated conductors", *Ceram. Trans.* **226,** 137-143 (2011).

[20] X. Cai, I. Kesgin, R. Schmidt, Y. Chen, and V. Selvamanickam, "Completely Etch-Free Fabrication of Multifilamentary Coated Conductor Using Inkjet Printing and Electrodeposition," *IEEE Trans. Appl. Supercond.*, vol. 23, no. 3, pp. 6603005–6603005, Jun. 2013.

[21] A. Panda, "Electrodeposition of nickel – copper alloys and nickel-copper-alumina nanocomposites into deep recesses for MEMS," Ph.D. Dissertation, Anna University 2003.

[22] S. Rode, C. Henninot, and M. Matlosz, "Complexation Chemistry in Nickel and Copper-Nickel Alloy Plating from Citrate Baths," *J. Electrochem. Soc.*, vol. 152, no. 4, p. C248, 2005.

[23] C. Faust and G. Montillon, “The Electrodeposition of Copper, Nickel and Zinc Alloys from Cyanide Solutions Part I,” *Trans. Electrochem. Soc.*, no. 1911, 1934.

[24] P. Bradley, S. Roy, and D. Landolt, “Pulse-plating of copper-nickel alloys from a sulfamate solution,” *J. Chem. Soc. Faraday Trans.*, vol. 92, no. 20, p. 4015, 1996.

[25] J. Zhou and J. T. Mcdevitt, “Reaction of the oxygen-deficient YBa2Cu3O6 phase with water,” *Solid State Commun.*, vol. 86, no. 1, pp. 0–3, 1993.

Appendix 3

SuperPower Conference Presentations

SuperPower Inc.
A Furukawa Company

4LPo2K-06

superior performance. powerful technology.

Development of 2G HTS conductor for a FCL Transformer

Drew W. Hazelton; Aarthi Sundaram; Joe Tanski; Yifei Zhang; Adam Weiner; Randall Kelley; Dana Swartout; Bill Magee; John Dackow
SuperPower Inc.

ASC 2016 Denver, USA ■ 08 September 2016

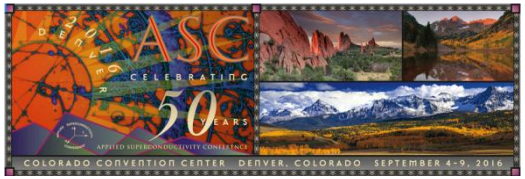

FURUKAWA ELECTRIC GROUP

SuperPower Inc. is a subsidiary of Furukawa Electric Co. Ltd.

Acknowledgements

- The authors would like to acknowledge the support of the management and our colleagues at SuperPower for their encouragement and assistance in the efforts carried out in this project.
- We would also like to acknowledge the cooperation and interaction of our partners in the broader FCL Transformer program.
  - SPX (Waukesha)
  - Southern California Edison
  - Oak Ridge National Laboratory
  - University of Houston
- Project supported in part by the US Department of Energy under award DE-OE0000244,006

Baseline conductor design

- Conductor design driven by program goals of:
  - Reduce utility total ownership costs by demonstrating integrated FCL capability
    - Less frequent replacement of downstream equipment and breakers
    - Enabled thru conductor bonding to Cu/Ni substrate
  - Greatly reduce steady state transformer losses and oil usage
    - Show how HTS technology can replace copper in Xfmr windings
  - Work to close cost gap with conventional transformers
    - AC loss reduction to reduce per unit refrigeration investments
    - Effort to increase conductor production piece lengths to enable fewer splices (“one length” windings) and lower conductor costs

Conductor requirements

- Conductor based on the requirements for a fault current limiting transformer with base performance of:
  - 28 MVA, 69 / 12.47 kV class
  - FCL function of 30-50% reduction in prospective fault current
- Single baseline conductor to be wound in parallel to target operating conditions depending on phase
- Piece lengths of up to 600 m required for HV modules
- Three basic conditions driving specification resulting in a bonded conductor
  - Ability to carry current under operating conditions
  - Target normal state resistance needed to be met for fault current limiting functionality (~ 25 mohm/m). Necessitates replacement of Ag with Ag alloy and limits selection of reinforcing substrate material.
  - Mechanically strong enough to handle forces due to:
    - fault current transient forces (hoop stress, axial buckling)
    - forces on the conductor during application of high voltage insulation

Conductor configuration

1 mm x 14 mm C715 CuNi substrate

6 layers of
“PPLP” insulation

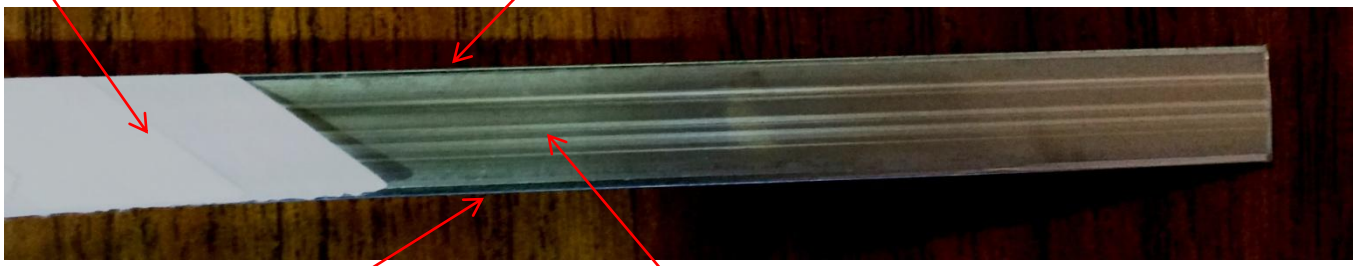

Solder interface layer

Modified SF12050 conductor
.. Ag alloy vs. Ag
.. Bonding interface layer on back of conductor

Bonding Line

Feed Reel Stand-Superconductor	Feed Reel-Laminate	Main controller Tension and heater	Pre-Clean	Pre-heat, Bond, edge & cool	Hot wire deburr	Post clean	Quality: X-ray for voids Laser check for burrs voids, dimensions	Drive system	Take up reel stand

Each component of the line has been developed, tested, validated and run production quantities of product

Pre-clean system

- Multiple trials run with various chemicals and agitation schemes
- Have current set up using KOH(Potassium Hydroxide) with ultrasonic cleaning enabled
  - Removes naturally occurring oxides and smut from solder
  - HTS tape does not require this step

HTS feed station

- Relocated to top of bonding station
- Allows more precise tension control of HTS, especially when delivering smaller tapes for striated samples such as 2, 3 or 4mm tapes

Bonding station

- Developed automatic flux application system to:
  - precisely administer correct amount of flux
  - Adds mechanical final clean to laminate to remove any residual
- Developed optical pyrometer feedback system for preheat wheel of laminate, controlling temperature +/-5 degrees
- Fine tuned heating profile of system and added active cooling to further enhance ability to solidify solder at desired time
- Enhanced top tensioning and excess solder control/removal
- Mechanical deburr to control excess solder at warm exit
- Hot wire deburr to reduce/remove/reconfigure any remaining excess solder(smoothes out solder burrs so as not to create high voltage peaks)
- Ability to be under N_2 environment if required

Laser Inspection - height and width

Purpose: To insure no burrs for insulating

Measures both width and height simultaneously

Specifically looking for sharp points(prevent tears in insulation)

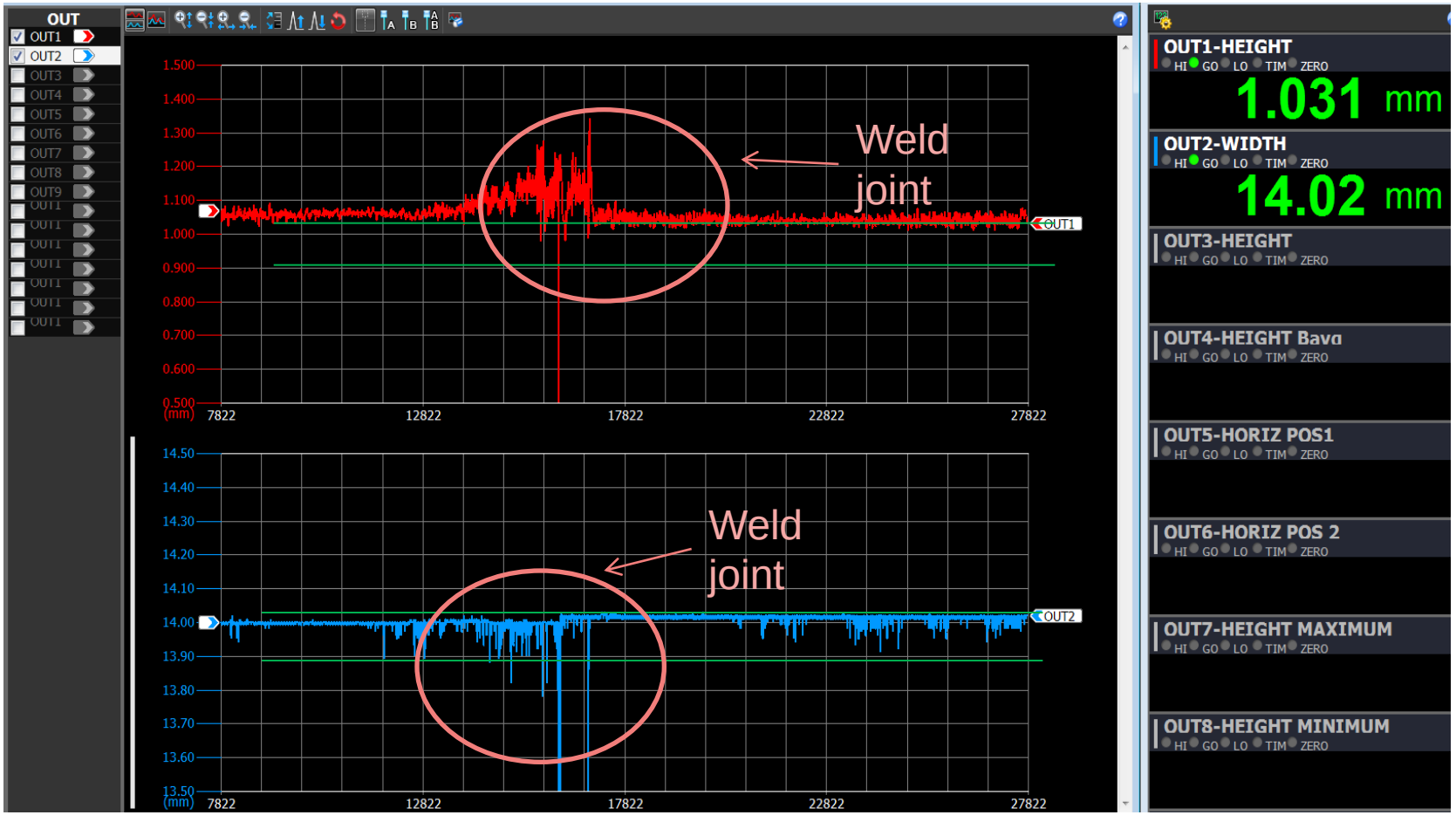

X-ray quality assurance system

- Based on initial parameters we set, algorithm checks
  - # of spots
  - Size of spots
  - Combinations and density of spots within given ar
- System is iterative and learns as it goes
- Final output for machine use is Go/NoGo
- System is designed and programmed as a production system.

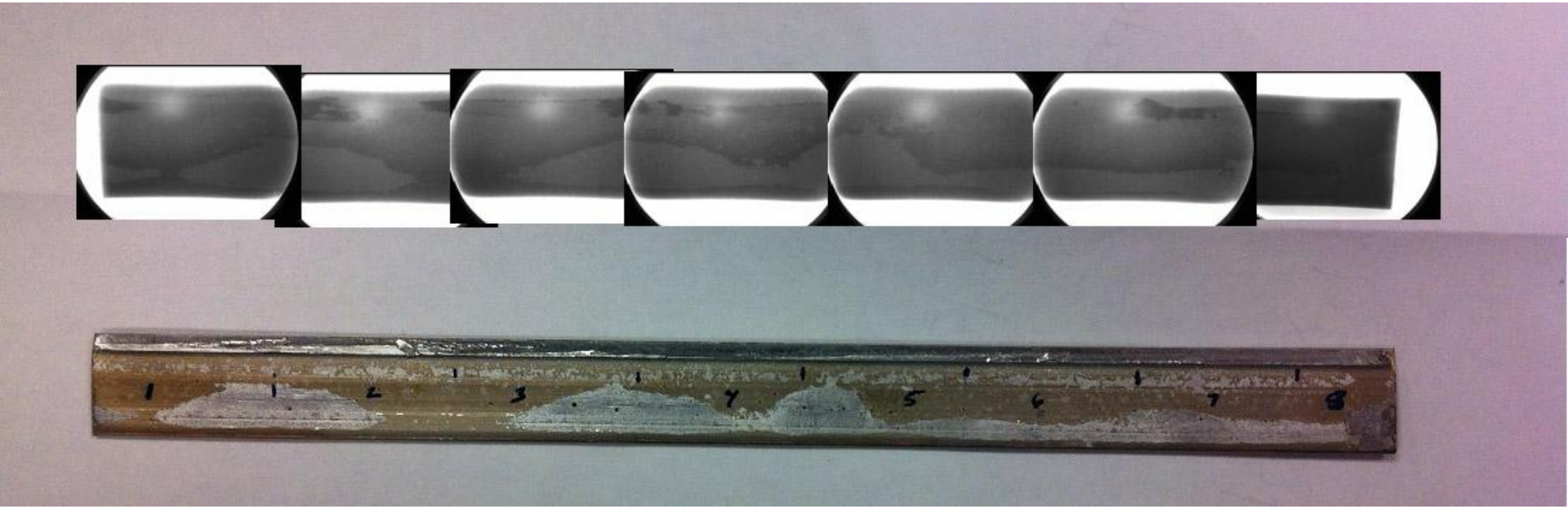

Post clean

- Ultrasonic cleaning system for removal of flux after soldering
- Trials complete, production runs successful

Tractor drive and take up reels

- Tractor drive insures constant speed of system, and provides smooth motion of bonded tape
- Micro adjustable speed controls for varying application needs
- Take up reels have separate tension controls to regulate wind tension

Insulation application

- Upgraded insulating equipment typically used to insulate transformer windings
- Uses 6 layers of “PPLP” type insulation applied in 2 x 3 layer overwrap
- Fully functional and has completed multiple production runs up to 600 m

Insulating equipment at SP

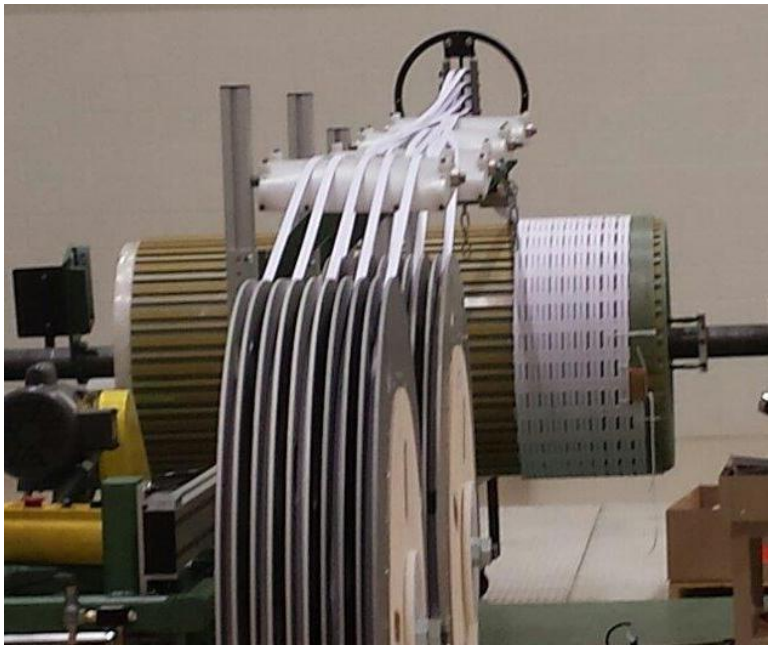

Test winding LV1 single phase insulated Cu being wound at SPX

insulating.MOV

Prototype HV windings fabricated

- Winding AC loss / FCL test coil
- Scaled version of HV coil module-using transformer winding technique

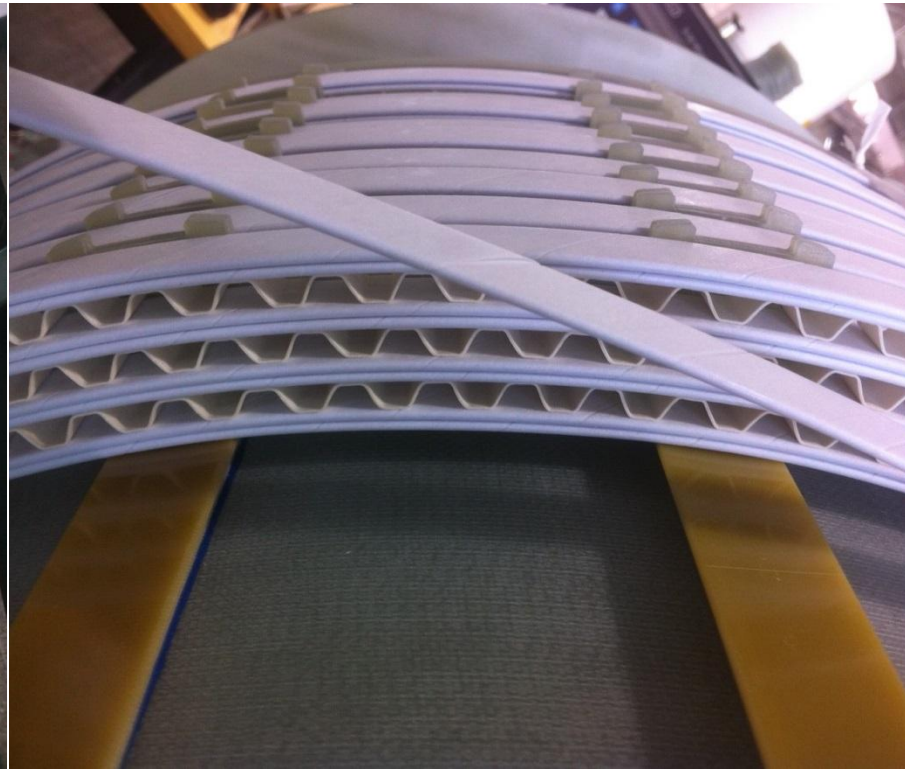

FCL functionality confirmed

FCL testing at CAPS(FSU)

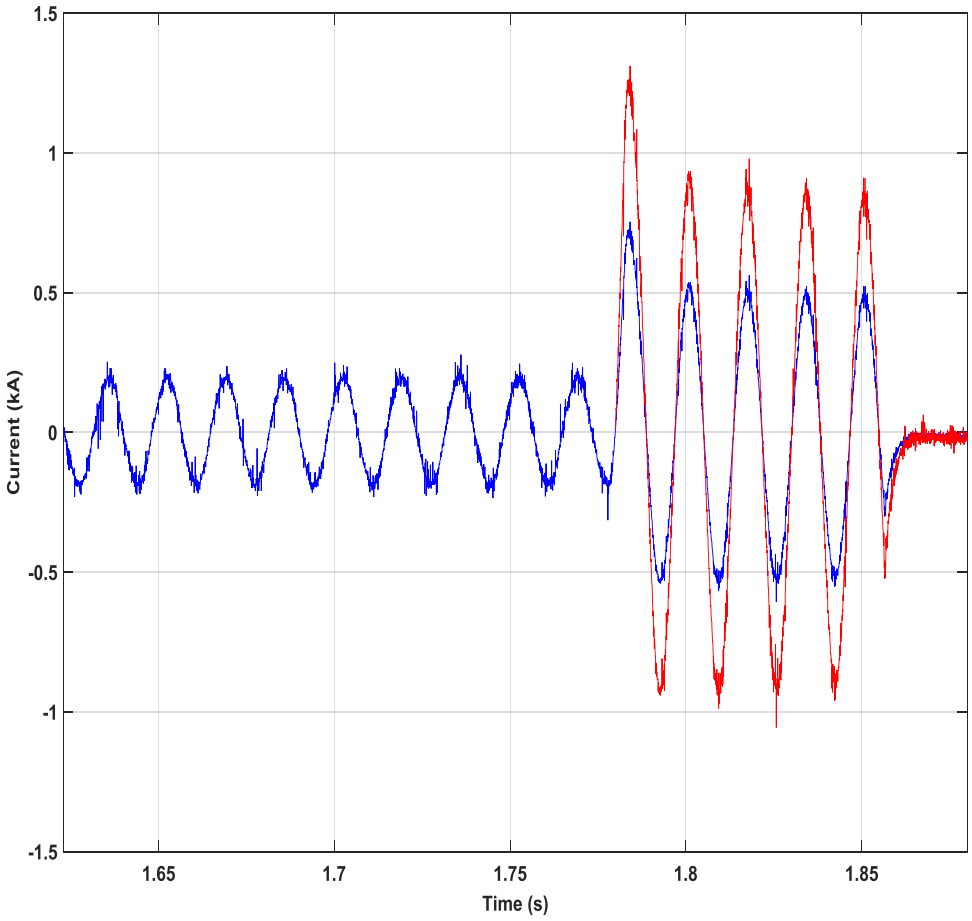

Red trace is calculated prospective current, based on empirical device impedance before current limiting effect

Prototype HV windings used in AC loss and FCL testing

- Developed calorimetric ac loss test system
- Baseline data of system taken and calibrated
- Multiple rounds of AC loss testing completed
- Data confirmed using 3 independent methods
  - Calorimetric
  - Search coil
  - Copley amplifier feedback
- AC loss modeling completed to calibrate to actuals

Gas warming before mass flow meter

AC loss data-actual

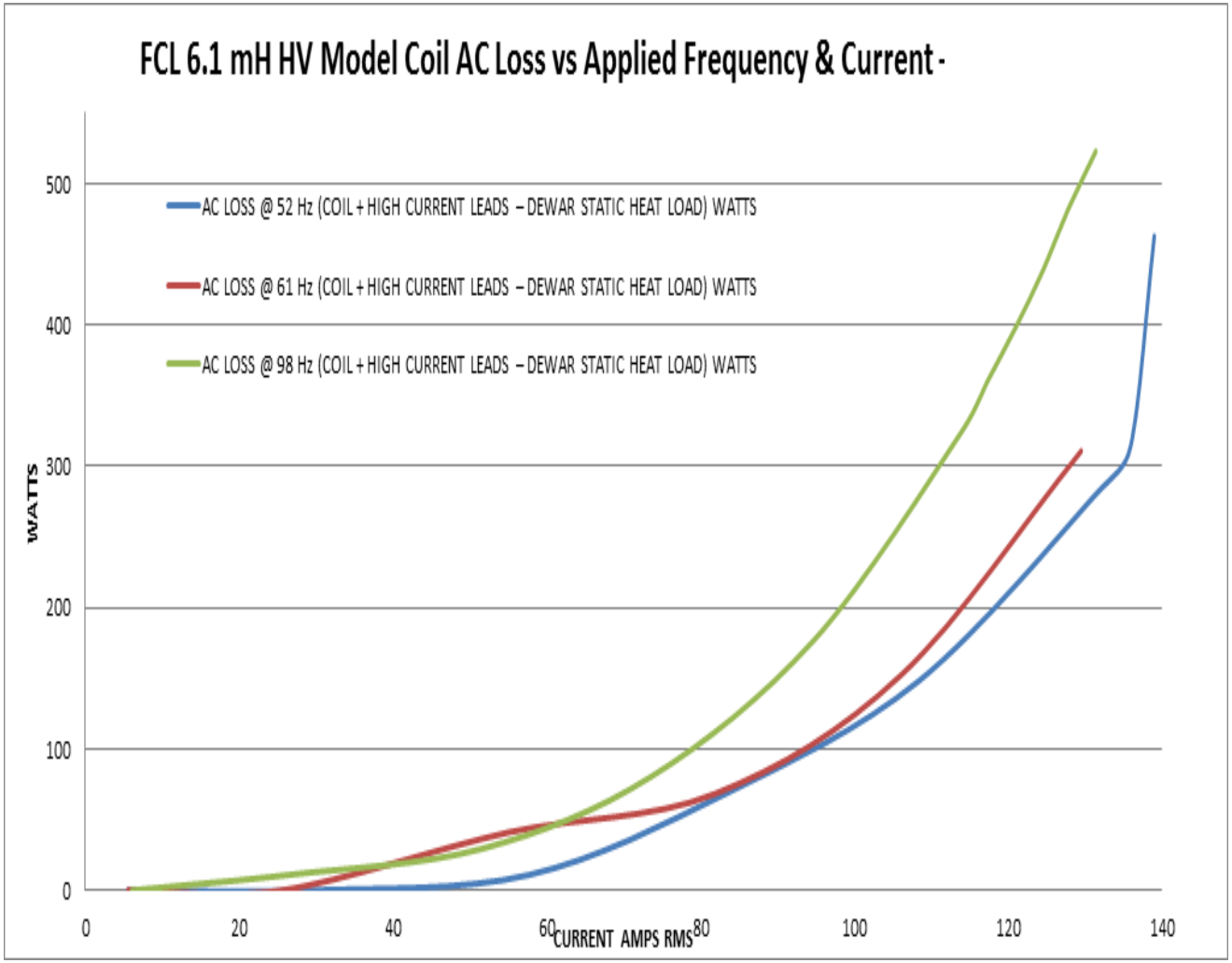

Modeling vs. actual comparison

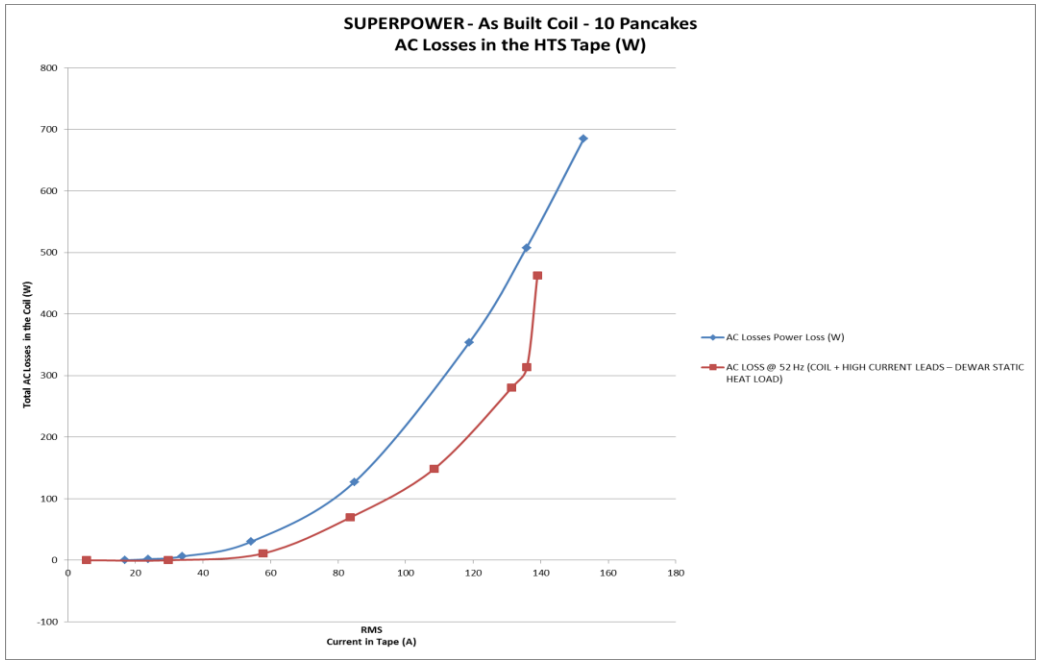

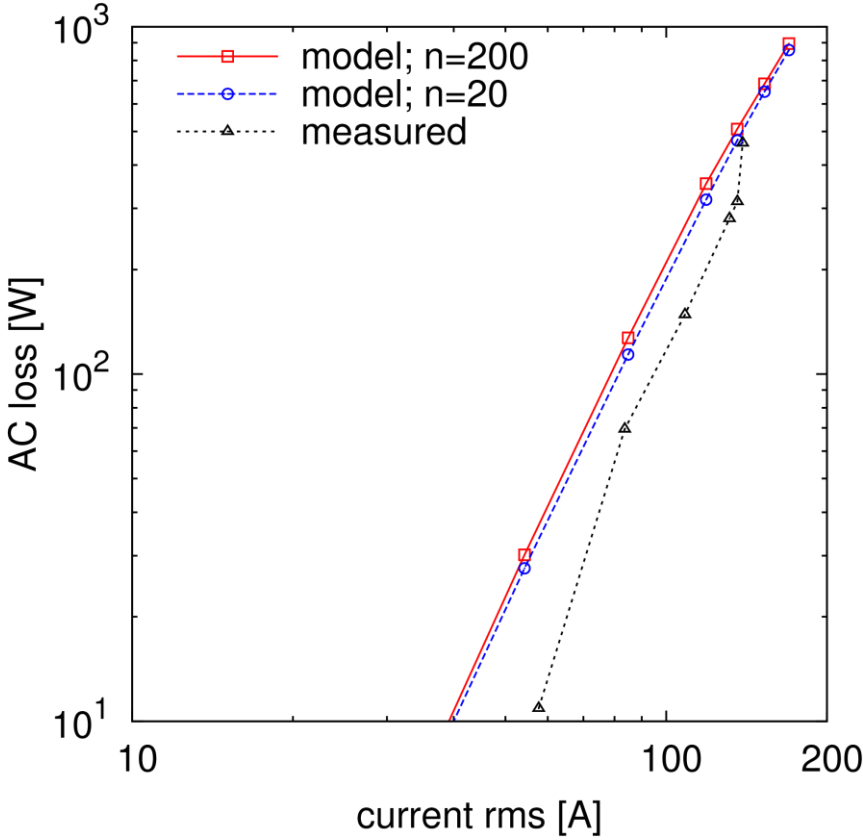

Summary

- Production capable system for producing clad 2G HTS conductor for FCL transformer application in place
- System can be readily adapted to other configurations
- Production quantity lengths of FCL transformer 2G HTS conductor have been successfully produced
- Functionality of the conductor has been demonstrated
  - Conductor successfully insulated without damage
  - Prototype windings using “industry standard” transformer winding configurations completed
  - FCL function demonstrated
- Calorimetric ac loss measurement system in place for measuring total losses in a large winding
  - Work on ac loss reduction ongoing

SuperPower Inc.
A Furukawa Company

superior performance. powerful technology.

CCA 2016 – Aspen, CO

2G HTS Wire Development at SuperPower

Drew W. Hazelton
Director of Research and Development / Applications (USA)

September 13, 2016

Work supported in part by the US Department of Energy under award DE-OE0000244,006

FURUKAWA ELECTRIC GROUP

SuperPower Inc. is a subsidiary of Furukawa Electric Co. Ltd.

2G HTS wire production at SuperPower

IBAD-MOCVD based REBCO wire on Hastelloy substrate

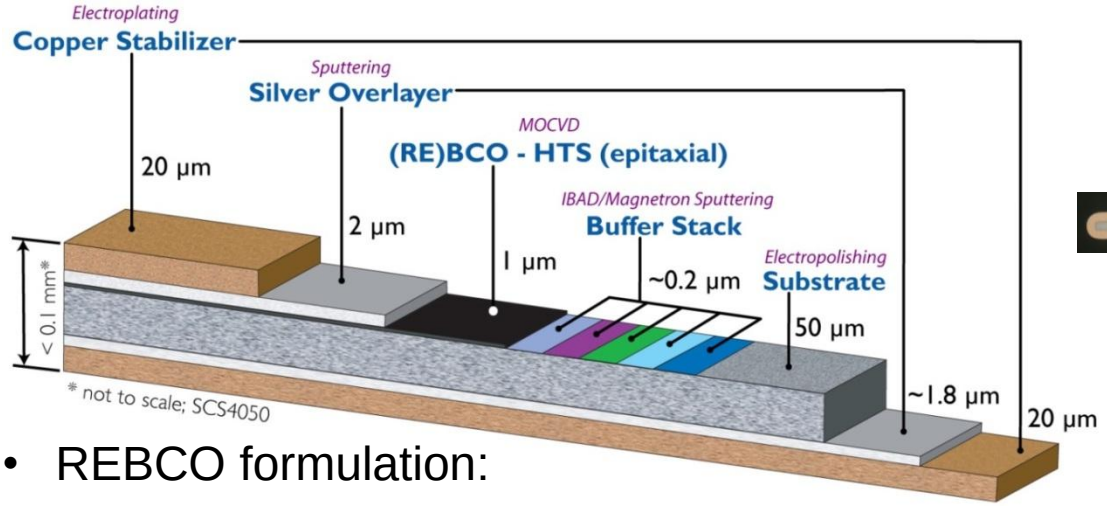

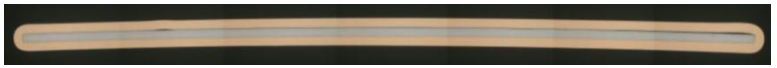

Cross-sectional image of a Cu-plated wire

- REBCO formulation:
  - **AP** (Advanced Pinning) – with enhanced in-field performance for B//c, targeting at coil applications such as high-field magnets, SMES, motors/generators
  - **CF** (Cable Formulation) – for cables, transformers, FCL
- I_c(77K, s.f.)/12mm = 400-600A, piece length = up to 500m.
- Variations in width (2-12mm), substrate thickness (30, 50 or 100µm)
  Ag thickness (1-5µm), Cu thickness (10-115µm), and insulation
- Bonding conductors : 2x2mm, 2x4mm, 2x12mm (face to face / back to back)
- Product lineup is expanding

Demanding applications and conductor requirements

- Our wires are being utilized for device/equipment development for many applications, including high-field magnets, accelerator magnets, fusion magnets, SMES, motors/generators, Maglev, medical applications, SFCL, etc.

- Conductor requirements
  - High Ic(B,T,θ) performance
  - Uniformity along length/across width
  - Robustness
  - Long piece length
  - Thinner substrate, Thicker substrate
  - Lower ac losses

- Continuous development and improvement driven by customers
  - Innovative conductor design
  - Processing optimization and control
  - In-line inspections
  - Property and quality measurements

- Higher performance + higher yield $\rightarrow$ lower cost/price

Conductor development areas

- Manufacturing improvements are a current focus area
  - Longer uniform piece lengths
  - Run-to-run repeatability
  - Tightening process windows
  - Improving process hardware

- Enhancing understanding of pinning optimization for operating conditions (4K/high field, 20-50K/2-5 T, 65K, lower fields)
  - Artificial pinning centers (BZO, others)
  - Process control

- Maximizing Je
  - Thinner substrates
  - Thicker films

Ic performance of Enhanced A.P wire at 77K/s.f

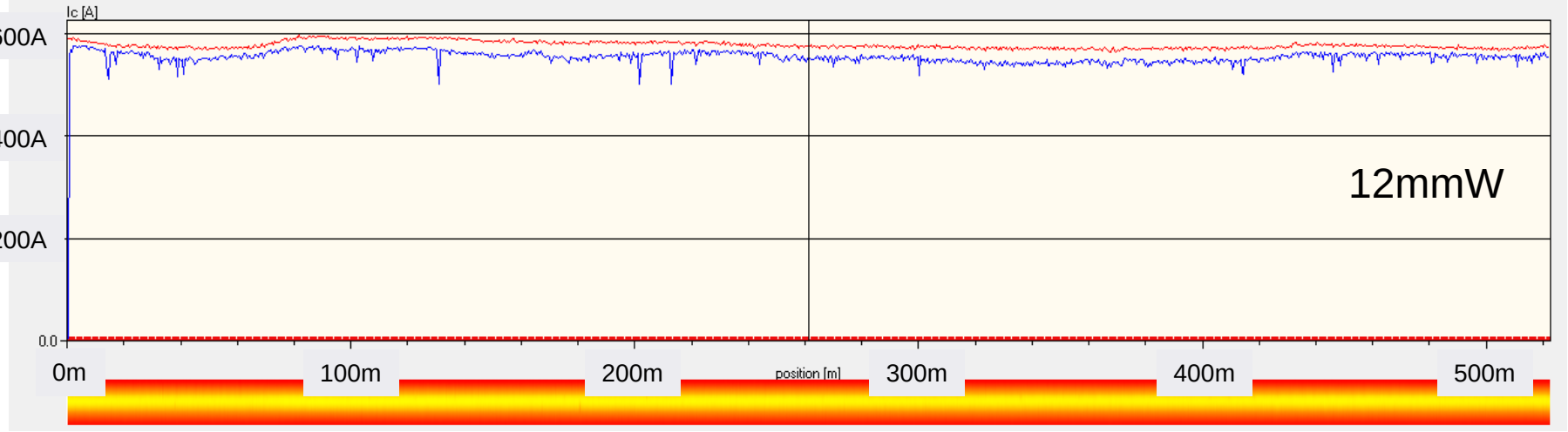

- Magnetic, non-contact measurement
- High special resolution, high speed, reel-to-reel
- Monitoring I_c at multiple production points after MOCVD
- Capable of quantitative 2D uniformity inspection

Ic performance of Enhanced A.P wire at 77K/s.f

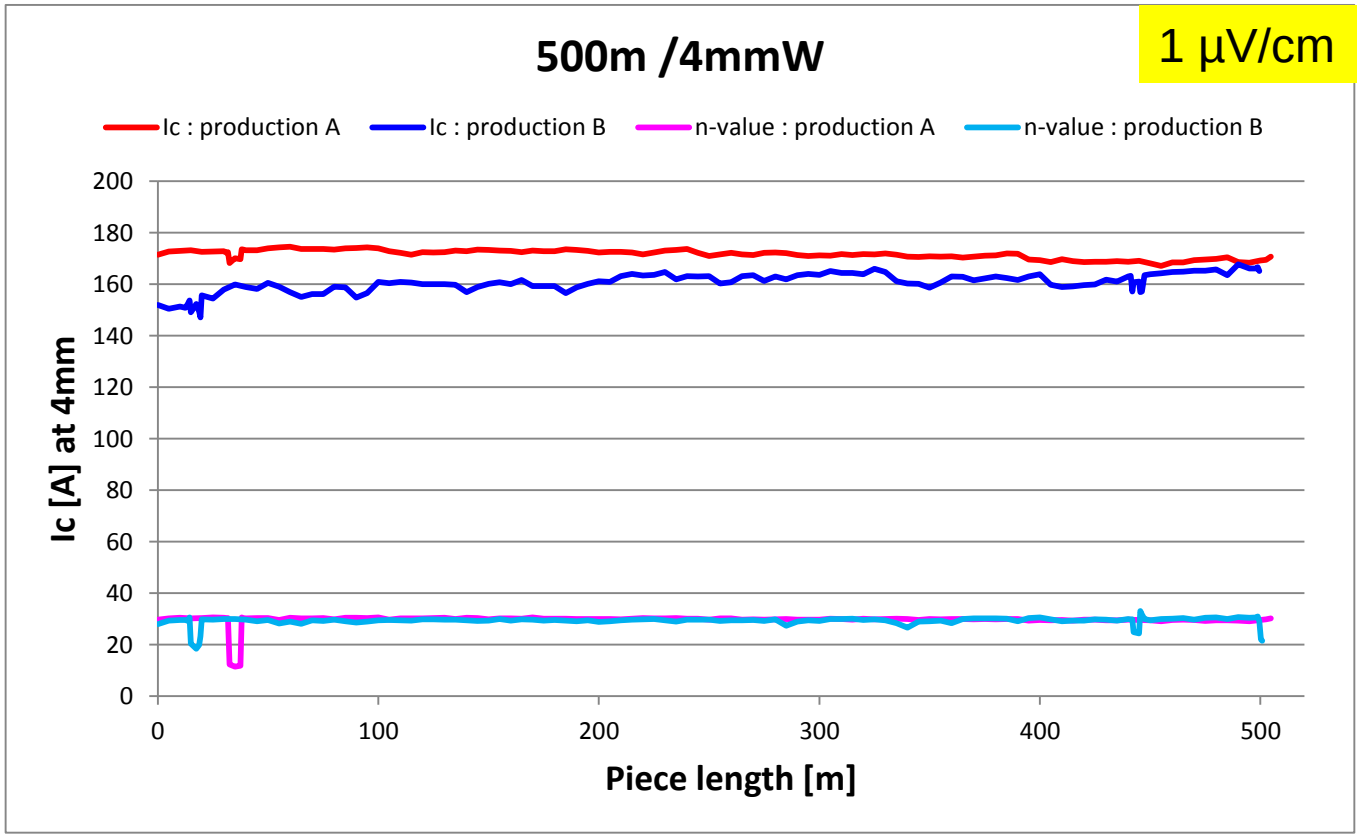

- Transport measurement by every 5m, with 40µm copper.
- Extend the piece length up to 500m

Performance of Enhanced A.P wire (7.5% Zr)

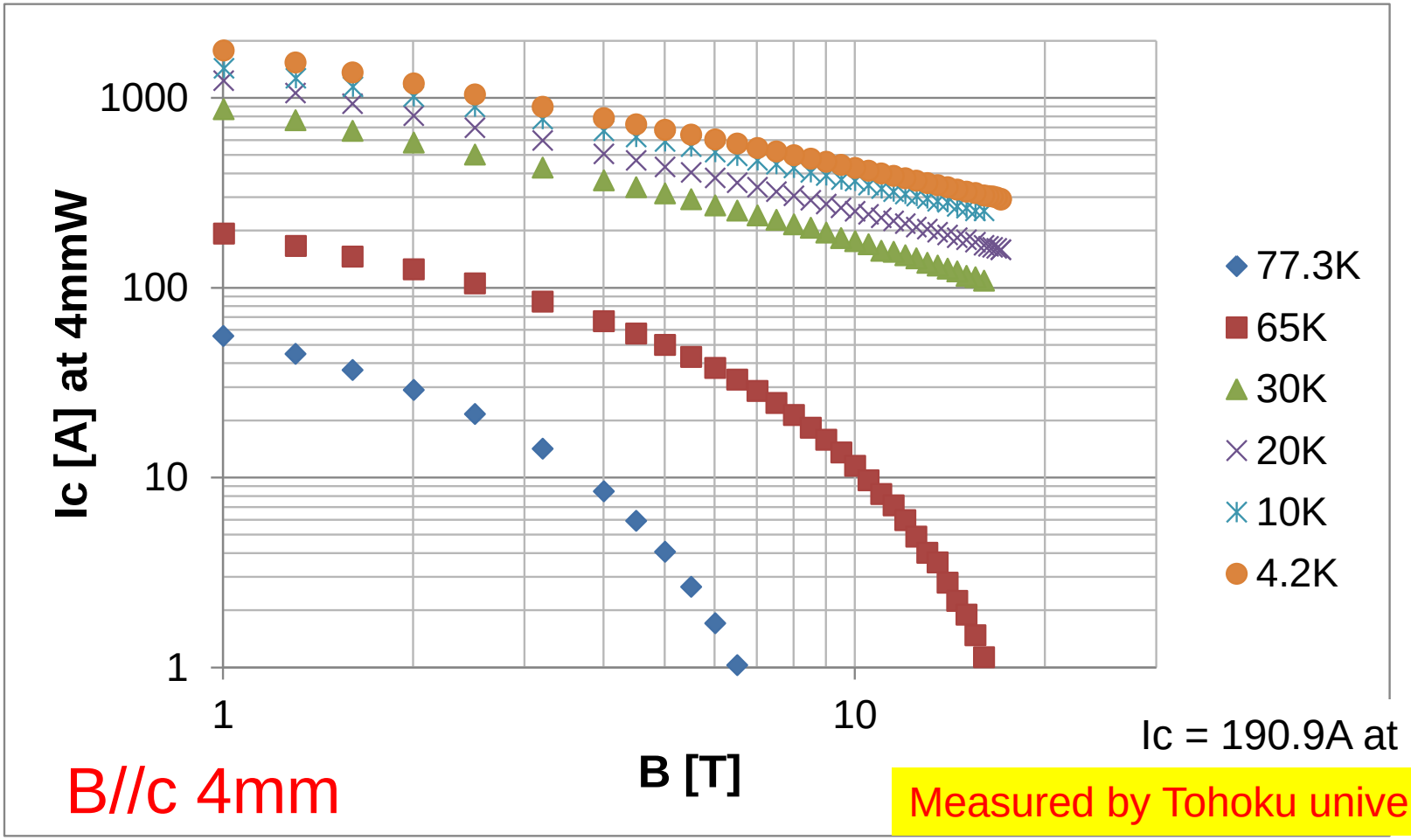

- Enhanced A.P wire shows high in-field performance

IcBT typical data – enhanced AP

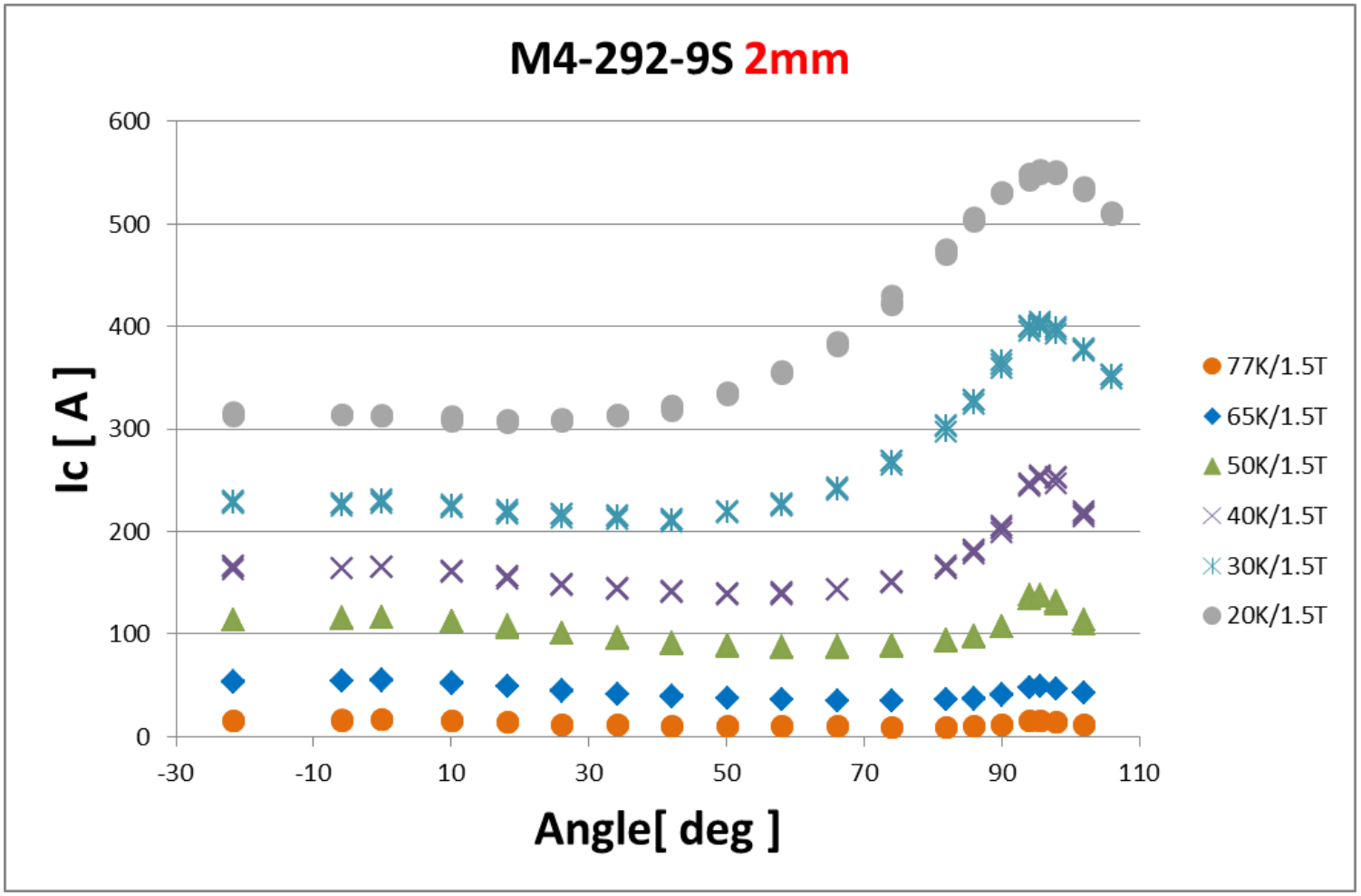

Electromechanical property - Ic under tension at 77K

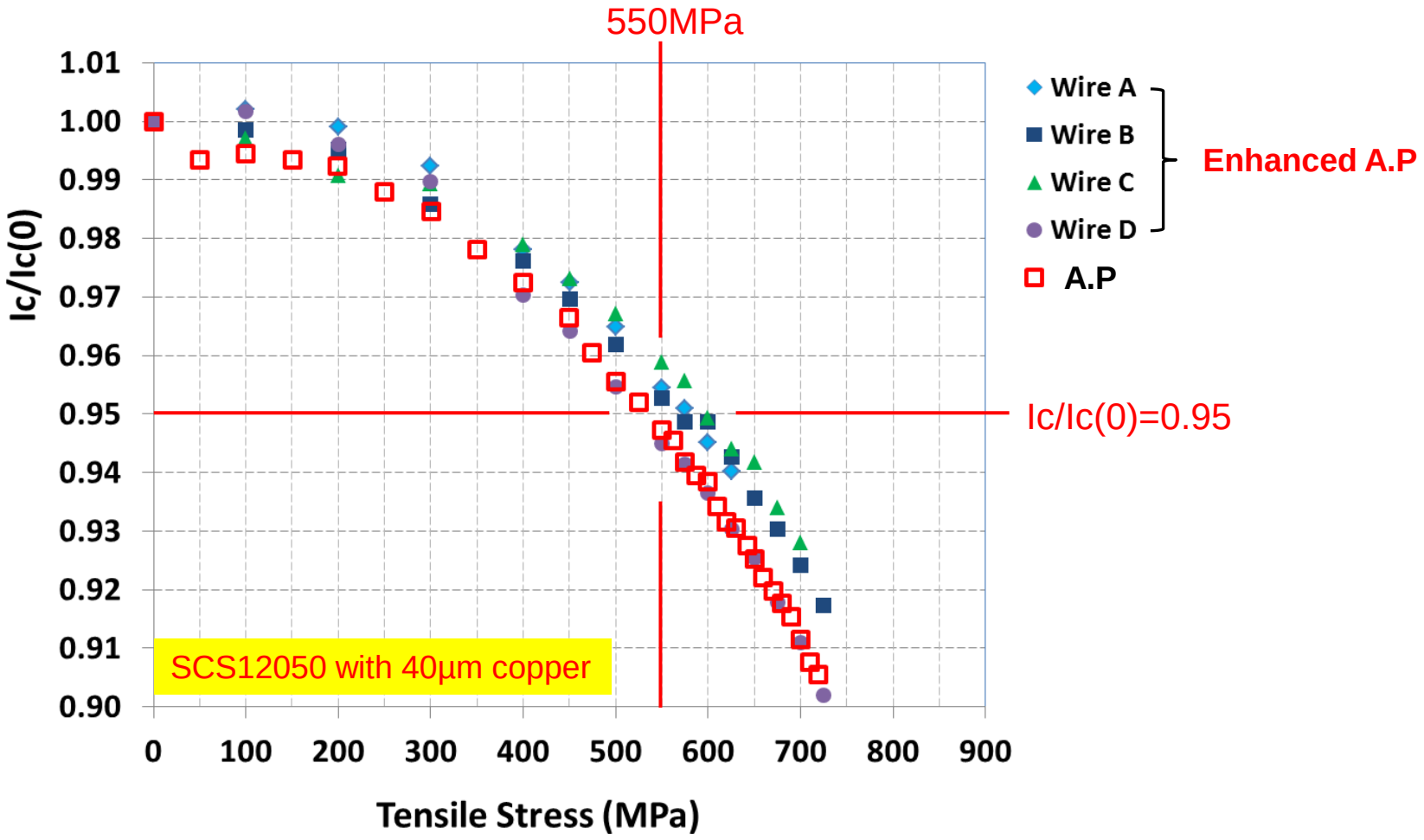

Development progress of 30µm substrate

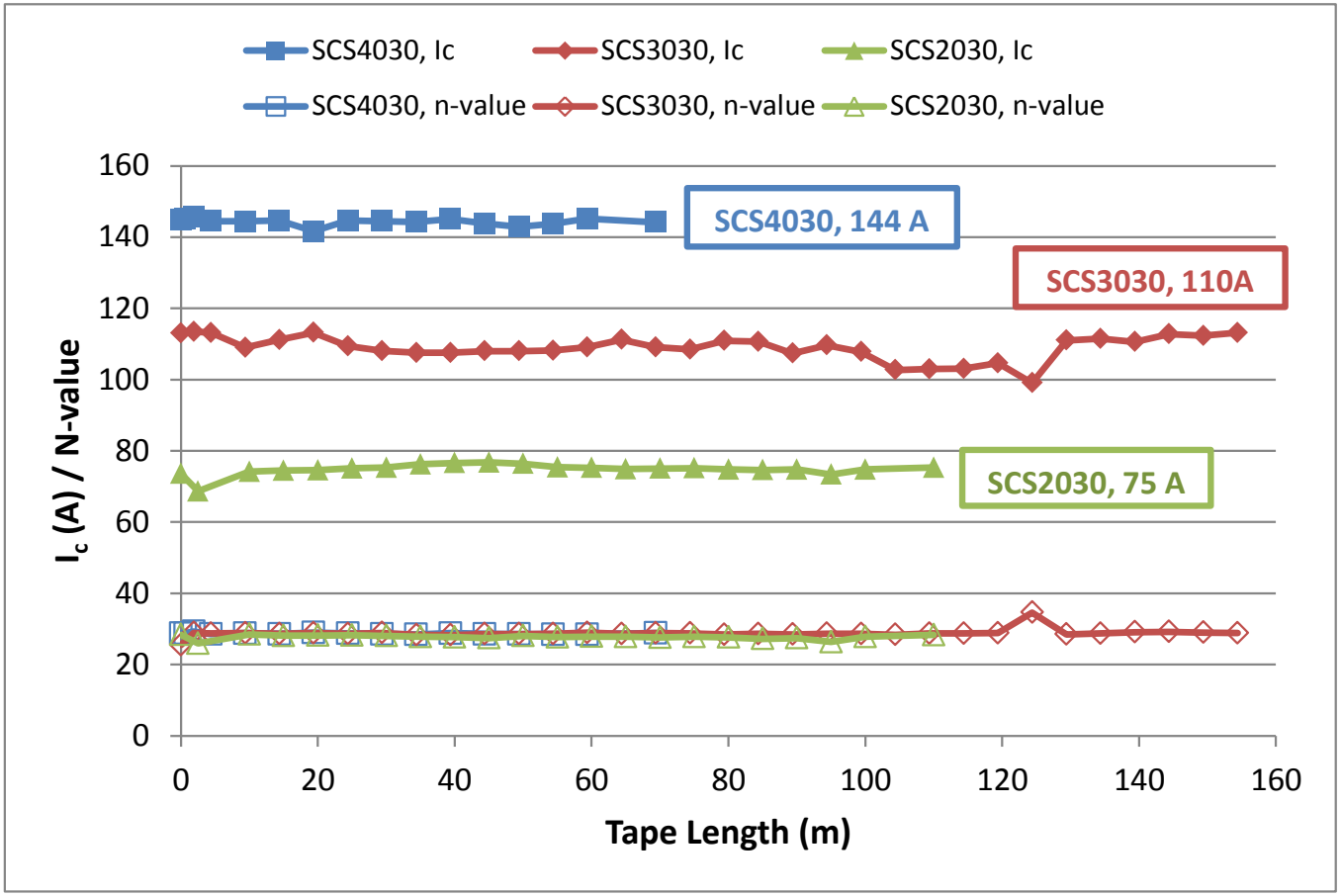

- Base performance of 30µm substrates are comparable to 50µm.

Electropolishing parameters of 30 μm Hastelloy C276 substrate developed

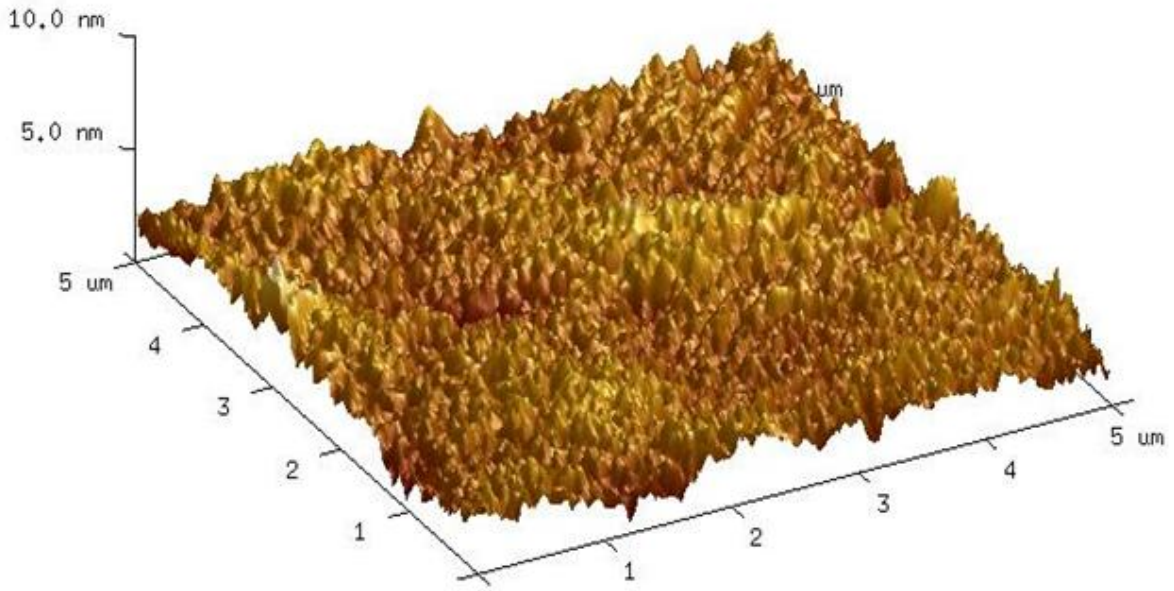

AFM 5 x 5 um scan obtained from 30 um thick electropolished Hastelloy C-276.

Buffer stack deposition parameters of 30 μm tapes developed

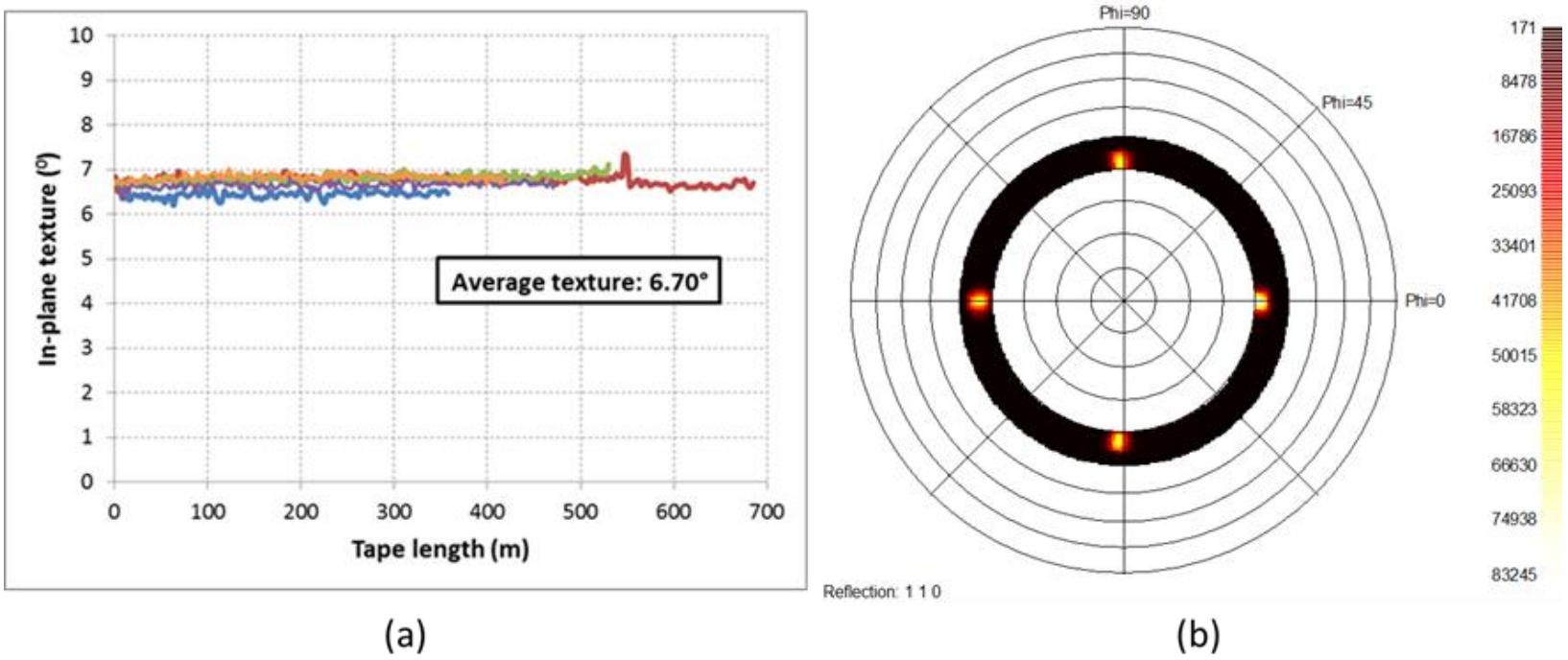

(a) In-plane texture and (b) (110) pole figure of LMO buffered IBAD MgO template on 30 um substrate.

MOCVD deposition parameters for 30 μm tapes established

(103) Pole figure of REBCO film with 7.5% Zr deposited on IBAD MgO template on 30 μm substrate.

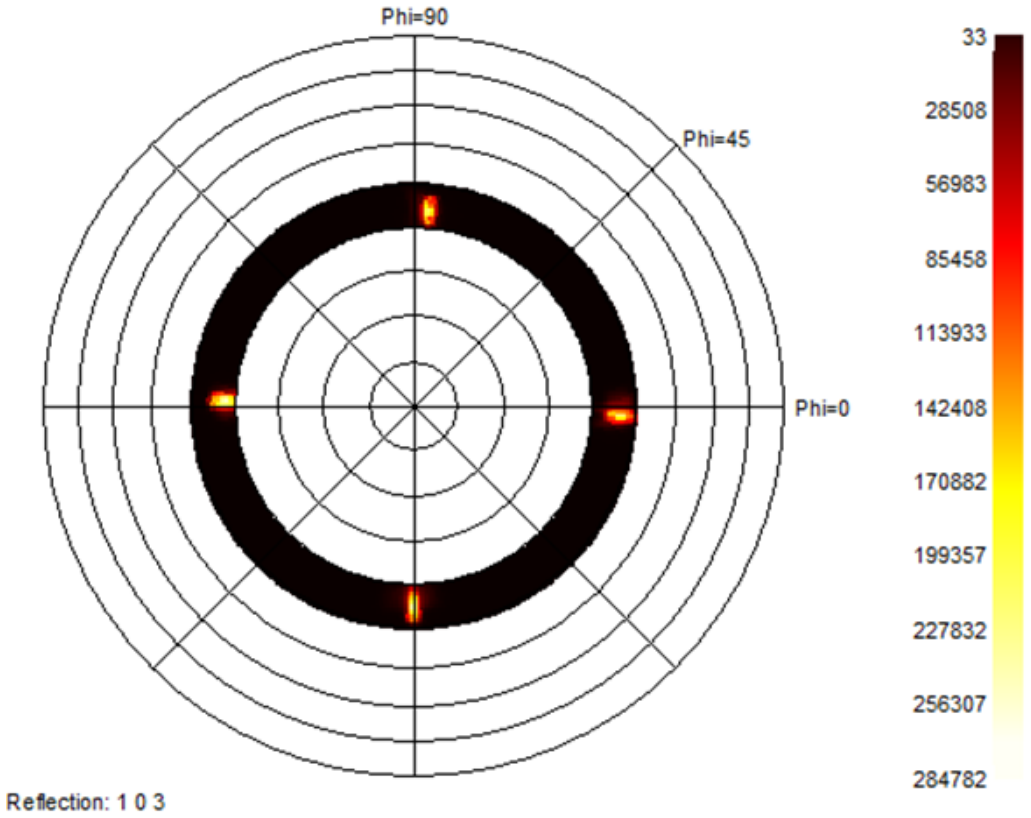

Improved Je demonstrated with 30 μm tapes

Engineering current density at 4.2 K vs. applied field for 30 um and 50 um ReBCO tapes with 7.5% Zr

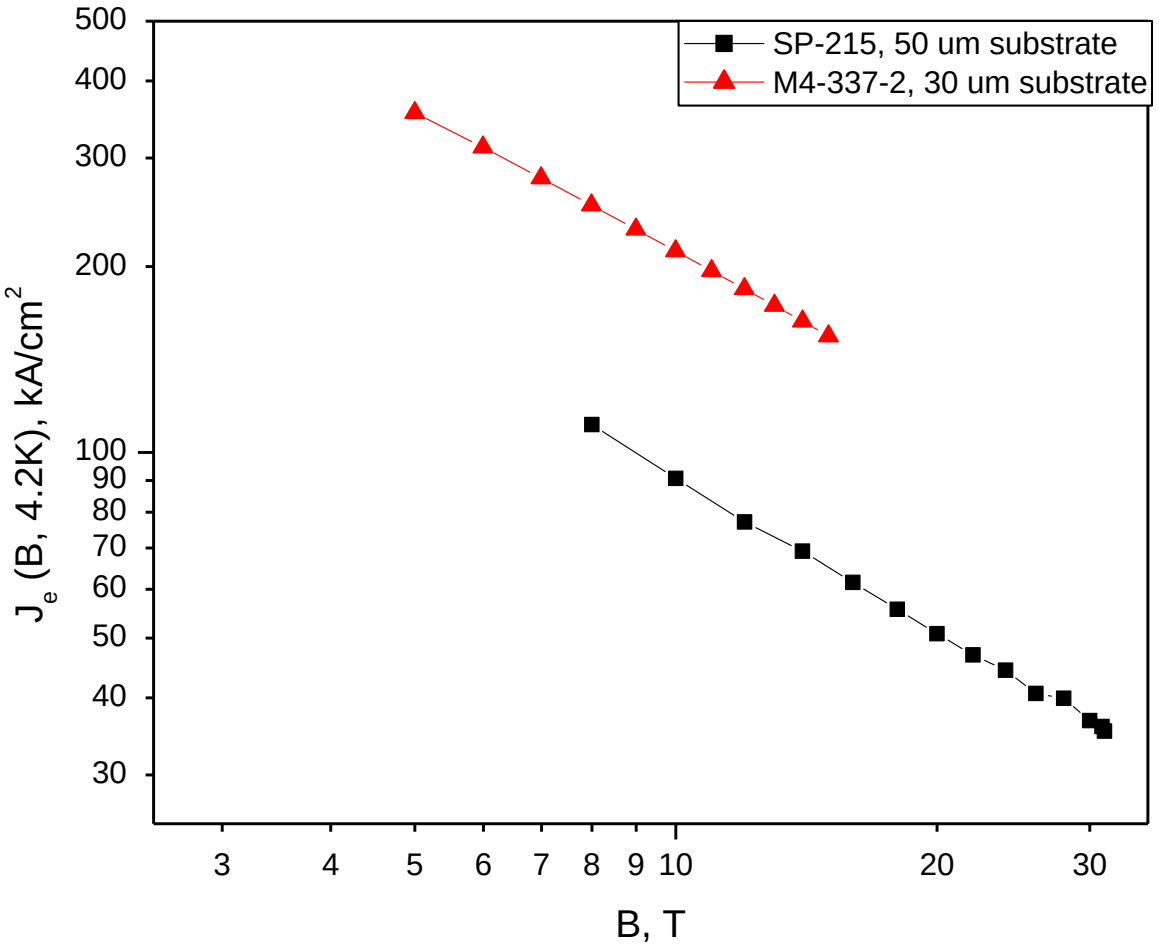

Measured at NHMFL

CORC® wires using SuperPower tapes

16 superpower tapes wound helically

- Copper core: 2.2 mm diameter
- 2 mm wide tapes with 30 µm substrate
- 6 mm twist pitch with partially transposed tapes for low AC loss
- Wire outer diameter: 3 mm
- Terminal diameter: 6.35 mm
- Nominal wire I_c: > 1,000 A (77 K)

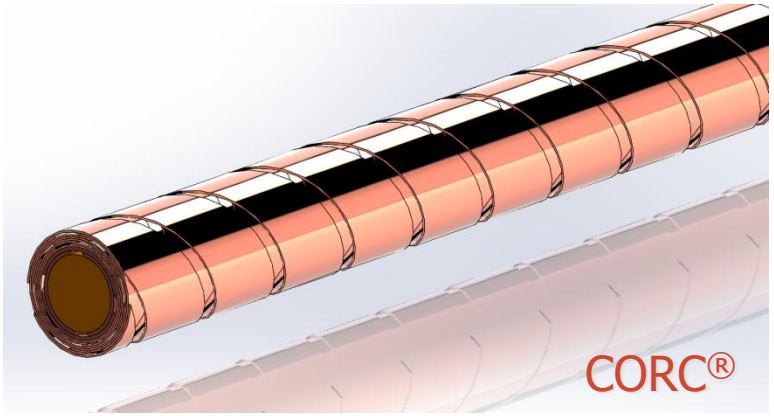

Applications

- High field magnets
- Accelerator magnets
- Fusion magnets
- High power density transmission

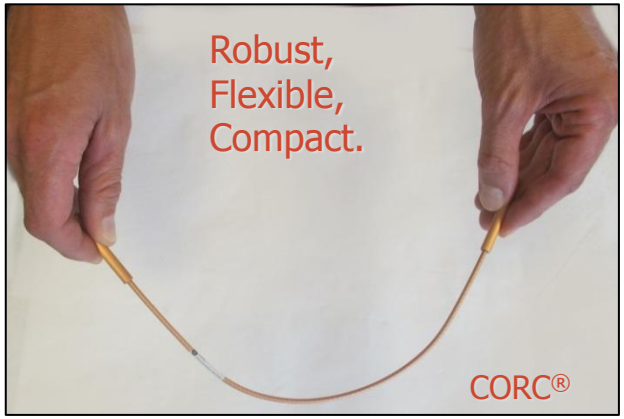

High magnetic field critical current density obtainable by increasing wire diameter and decreasing substrate thickness

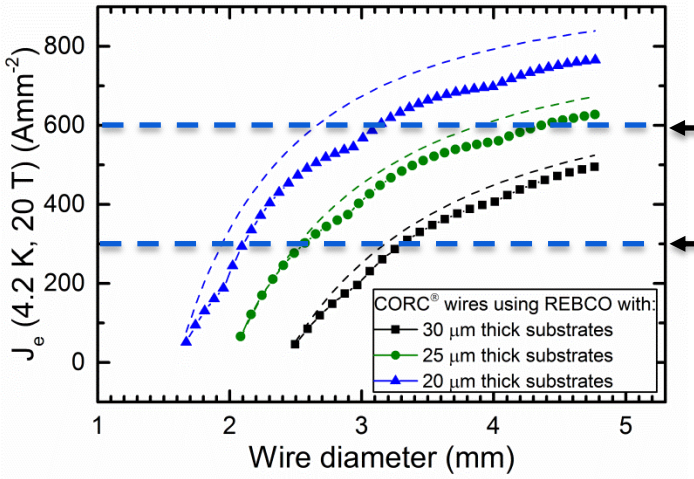

Bonding line developed for clad conductors

Feed Reel Stand-Superconductor	Feed Reel-Laminate	Main controller Tension and heater	Pre-Clean	Pre-heat, Bond, edge & cool	Hot wire deburr	Post clean	Quality: X-ray for voids Laser check for burrs voids, dimensions	Drive system	Take up reel stand

6 layers of “PPLP” insulation

1 mm x 14 mm C715 CuNi substrate

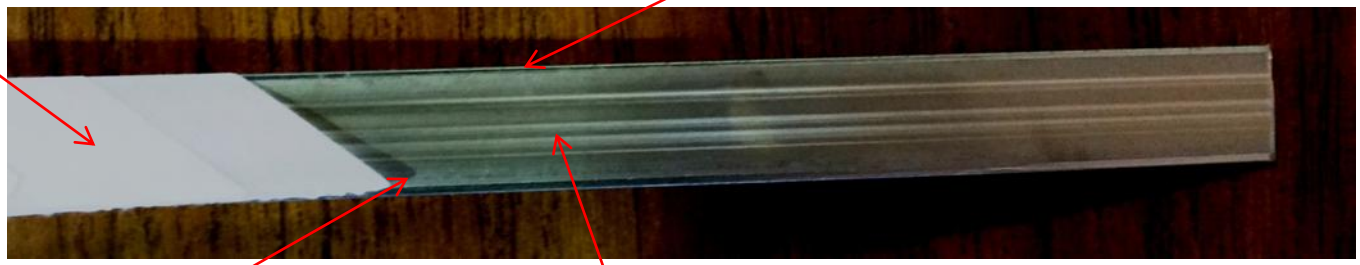

Solder interface layer

Modified SF12050 conductor - Ag alloy vs. Ag w/ bonding interface layer on back of conductor

Prototype HV windings fabricated

- Winding AC loss / FCL test coil
- Scaled version of HV coil module-using transformer winding technique

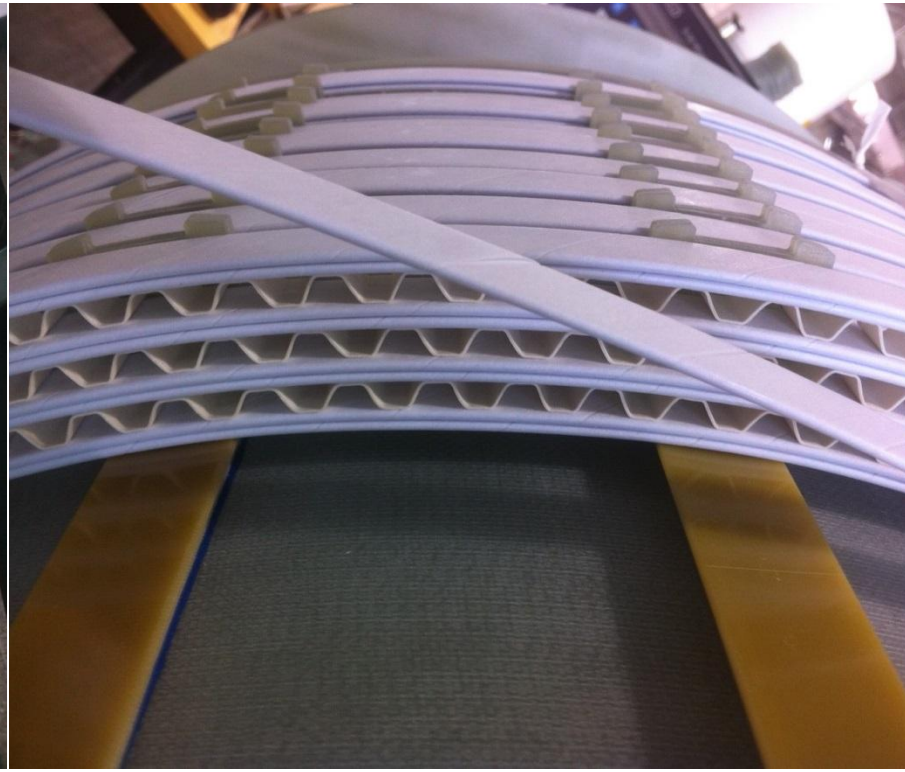

FCL functionality confirmed

FCL transformer module testing at CAPS(FSU)

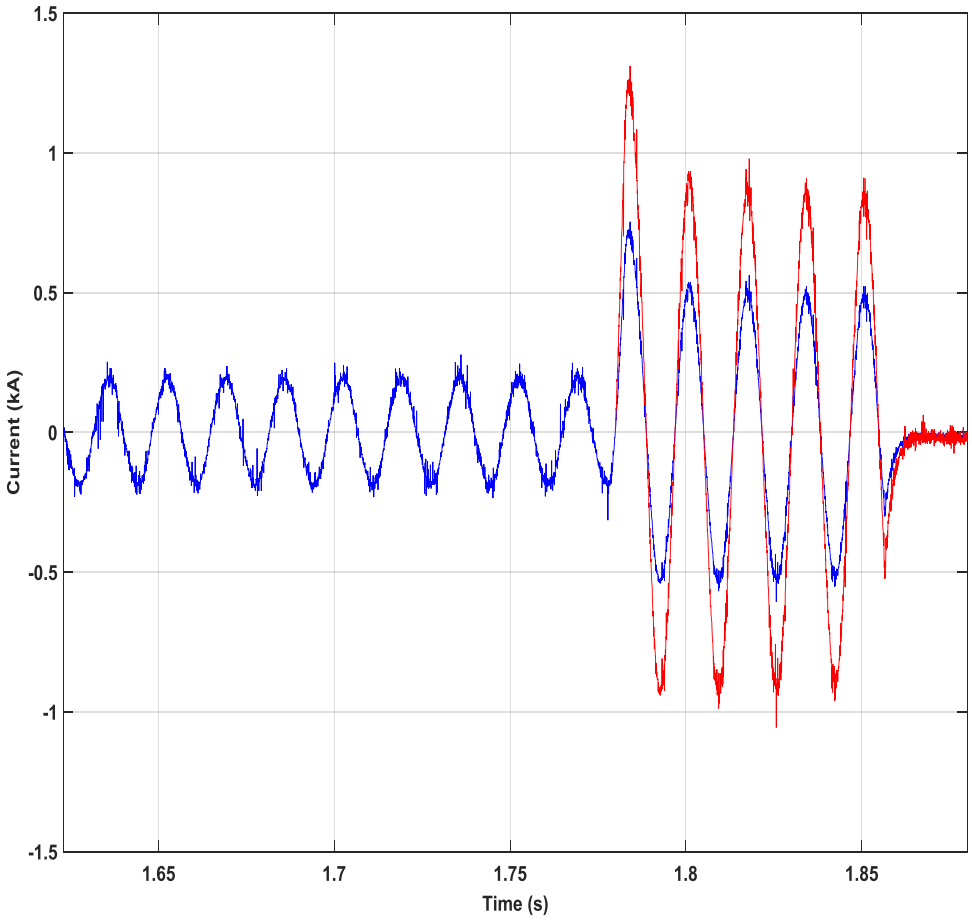

Red trace is calculated prospective current, based on empirical device impedance before current limiting effect

Alternative bonded conductors under evaluation

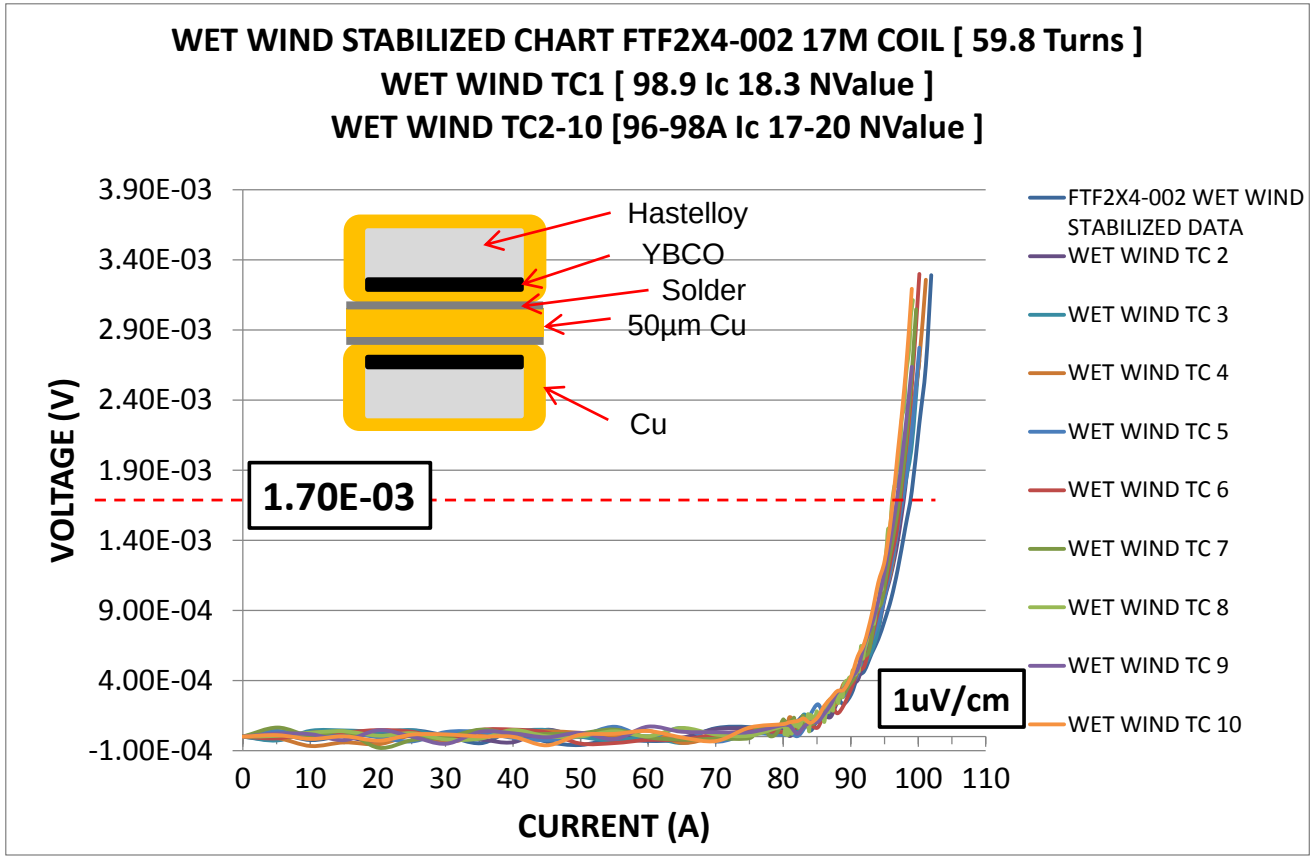

- Bonding conductor : Face to Face, 2 x 4mm, total thickness ~200µm
- No degradation after 10 times thermal cycles

Low heat leak 2G HTS tapes available for current lead application

- 2G HTS offers low heat leak options for current lead applications
- Standard 2G HTS tapes offer better performance than 1G HTS based leads
- Alloyed Ag w/ 2G HTS leads offers best low heat leak option

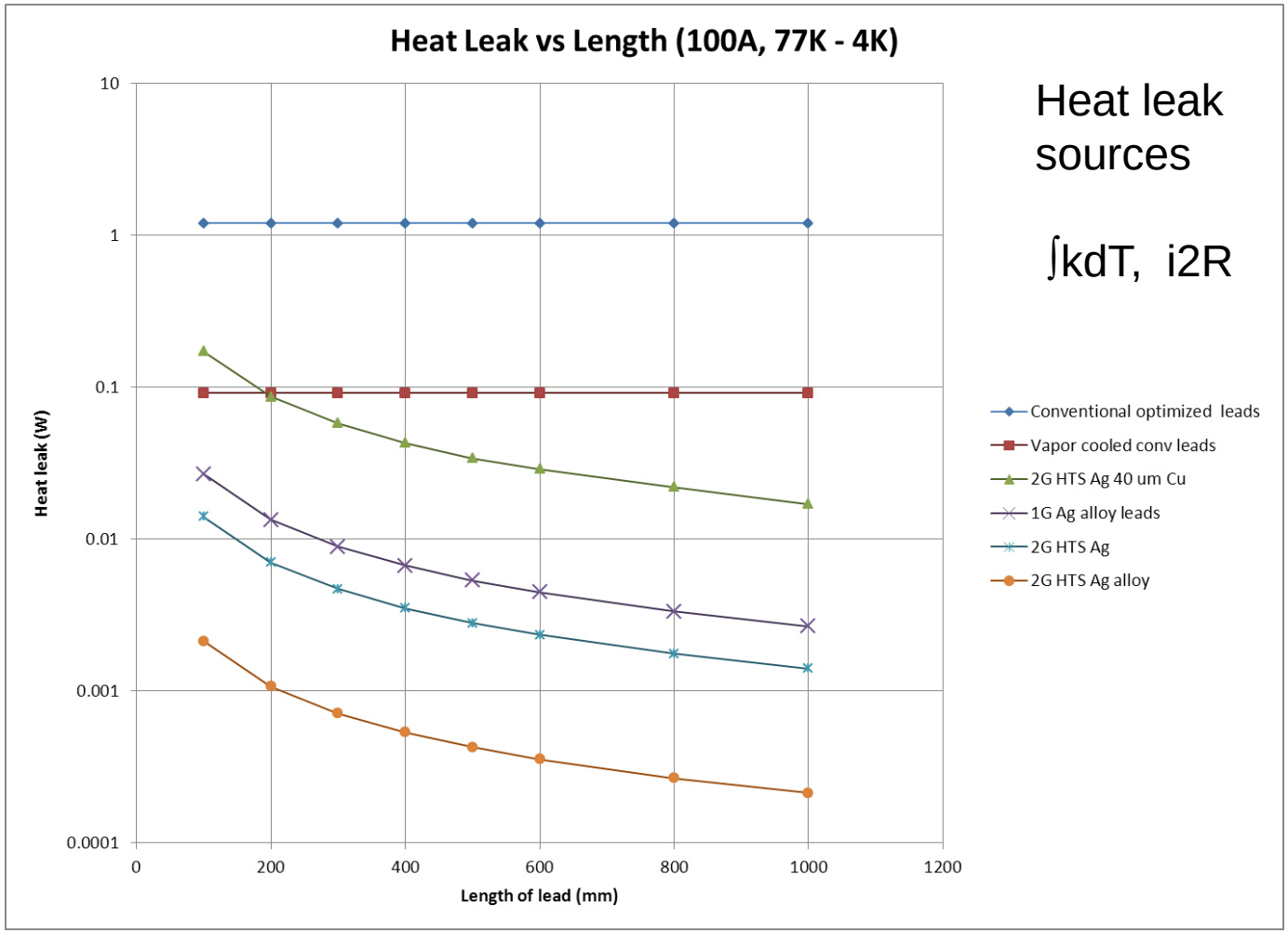

Heat leak sources

∫kdT, i2R

Summary

- Focus on processing to improve uniformity, repeatability, piece lengths and yield.
- Maximize current capacity while developing next generation equipment
  - When is the time to pull the trigger?
- Enhance performance parameters for developing operating spaces
  - Thinner substrates
  - Thicker films
  - Optimized pinning
- Continue to improve mechanical properties
  - Delamination mitigation
  - Ic (ε)

Thank you for your attention

superior performance. powerful technology.

http://www.superpower-inc.com/

SuperPower Inc. 450 Duane Ave. Schenectady, NY 12304 USA
Tel: (518) 346-1414
Fax: (518) 346-6080